UNIVERSITY OF CALIFORNIA,
IRVINE

Macroscopic modeling and analysis of urban vehicular traffic

DISSERTATION

submitted in partial satisfaction of the requirements
for the degree of

DOCTOR OF PHILOSOPHY

in Civil Engineering

by

Qi-Jian Gan

Dissertation Committee:
Professor Wen-Long Jin, Chair
Professor Will Recker
Professor R. Jayakrishnan

2014

DEDICATION

To my family in China, for their love, support and sacrifice

TABLE OF CONTENTS

LIST OF FIGURES

LIST OF TABLES

ACKNOWLEDGMENTS

Foremost, I would like to express my great gratitude to my advisor, Dr. Wen-long Jin, for his academic guidance and financial support in these five years. I know Dr. Jin since I was a sophomore. He is the first one who inspires me and leads me into this interesting field, Transportation Systems Engineering. I feel so lucky that I can continue my graduate study under his guidance. He teaches me not only how to solve research problems but also the importance of being a rigorous researcher. His attitude and passion on research inspire me to continue with my academic research.

Besides my advisor, I would like to thank my other two committee members, Dr. Will Recker and Dr. R. Jayakrishnan. They are excellent professors, and I have learned a lot from the courses they taught. They also provided me very helpful suggestions on how to improve this dissertation.

I would like to thank my best friends, Jielin Sun, Hao Yang, Wei Li, Xiaoling Ling, Shan Jiang, Yue sun, and Biling Liu. Thanks for their selfless help when I was in trouble. Without them, my Ph.D. life in Irvine would be very boring.

My sincere thanks also go to Dr. Vikash Gayah. I have learned a lot from him, especially in the modeling of Macroscopic Fundamental Diagrams.

I would also like to thank my colleagues, Zhe Sun, Lianyu Chu, Anupam Srivastava, Daji Yuan, and Sarah Hernandez for the research discussions.

Last but not the least, I would like to thank many other colleagues who are not mentioned above but also have contributions to this dissertation in various aspects.

CURRICULUM VITAE

Qi-Jian Gan

EDUCATION

Doctor of Philosophy in Civil Engineering **2014**
University of California, Irvine *Irvine, CA*

Master of Science in Civil Engineering **2010**
University of California, Irvine *Irvine, CA*

Bachelor of Science in Automatic Control **2009**
University of Science and Technology of China *Hefei, Anhui*

RESEARCH EXPERIENCE

Graduate Student Researcher **2009–2013**
University of California, Irvine *Irvine, California*

TEACHING EXPERIENCE

Teaching Assistant **Spring 2013 & Winter 2014 & Spring 2014**
University of California, Irvine *Irvine, CA*

REFEREED JOURNAL PUBLICATIONS

A kinematic wave approach to traffic statics and dynamics in a double-ring network **2013**
Transportation Research Part B

Validation of a macroscopic lane-changing model **2013**
Transportation Research Record: Journal of the Transportation Research Board

A kinematic wave theory of capacity drop **2013**
Transportation Research Part B (under review, `http://arxiv.org/abs/1310.2660`)

REFEREED CONFERENCE PUBLICATIONS

Invariant continuous approximate models for a signalized road link — **January 2015**
Transportation Research Board 94th Annual Meeting

Estimation of the number of left lane changes in laterally unbalanced traffic using lane-based loop detector data — **January 2015**
Transportation Research Board 94th Annual Meeting

A link queue approach to traffic statics and dynamics in signalized networks — **January 2014**
Transportation Research Board 93rd Annual Meeting

Calibration of the cell transmission model for a freeway network — **January 2014**
Transportation Research Board 93rd Annual Meeting

ABSTRACT OF THE DISSERTATION

Macroscopic modeling and analysis of urban vehicular traffic

By

Qi-Jian Gan

Doctor of Philosophy in Civil Engineering

University of California, Irvine, 2014

Professor Wen-Long Jin, Chair

A macroscopic relation between the network-level average flow-rate and density, which is known as the macroscopic fundamental diagram (MFD), has been shown to exist in urban networks in stationary states. In the literature, however, most existing studies have considered the MFD as a phenomenon of urban networks, and few have tried to derive it analytically from signal settings, route choice behaviors, or demand patterns. Furthermore, it is still not clear about the definition or existence of stationary traffic states in urban networks and their stability properties. This dissertation research aims to fill this gap.

I start to study the stationary traffic states in a signalized double-ring network. A kinematic wave approach is used to formulate the traffic dynamics, and periodic traffic patterns are found using simulations and defined as stationary states. Furthermore, traffic dynamics are aggregated at the link level using the link queue model, and a Poincaré map approach is introduced to analytically define and solve possible stationary states. Further results show that a stationary state can be Lyapunov stable, asymptotically stable, or unstable. Moreover, MFDs are explicitly derived such that the network flow-rate is a function of the network density, signal settings, and route choice behaviors. Also the time for the network to be gridlocked is analytically derived.

Even with the link queue model, traffic dynamics are still difficult to solve due to the discrete

control at signalized junctions. Therefore, efforts are also devoted to deriving invariant continuous approximate models for a signalized road link and analyzing their properties under different capacity constraints, traffic conditions, traffic flow fundamental diagrams, signal settings, and traffic flow models. Analytical and simulation results show that the derived invariant continuous approximate model can fully capture the capacity constraints at the signalized junction and is a good approximation to the discrete signal control under different traffic conditions and traffic flow fundamental diagrams. Further analysis shows that non-invariant continuous approximate models cannot be used in the link transmission model since they can yield no solution to the traffic statics problem under certain traffic conditions.

For a signalized grid network, simulations with the link queue model confirm that important insights obtained for double-ring networks indeed apply to more general networks.

Chapter 1

Introduction

1.1 Background

1.1.1 Urban traffic congestion

Nowadays traffic is getting more and more congested in urban road networks. Traffic congestion arising during peak periods has wasted travelers a tremendous amount of money and time and has caused various environmental and health problems. In the 2012 Urban Mobility Report [71], congestion has caused a total loss of $121 billion in 2011 in 498 urban areas nationwide, including 5.5 billion hours of extra time and 2.9 billion gallons of fuel. Meanwhile, 56 billion pounds of additional carbon dioxide (CO_2) greenhouse gas have been released into the atmosphere in 2011 because of urban congestion. In addition, unreliable travel times caused by congestion make it difficult for travelers to plan their trips. However, this is not the worst. The bad news is that congestion is likely to grow worse in the coming decades due to the fact that travel demand continues to rise while significant road expansion is unlikely [72].

In fact, traffic congestion can be either recurrent or non-recurrent. Events such as vehicle breakdowns, crashes, severe weather, special events, temporarily lane closure for construction or maintenance activities can cause non-recurrent traffic congestion. For recurrent traffic congestion, it is often seen as a capacity problem that the limited physical infrastructure can not meet the increasing travel demand, especially during peak hours. To relieve traffic congestion, one of the primary recommendations [72] is to upgrade signal timing and control strategies at intersections where the current technology is deficient.

In urban networks, traffic signal has been installed at numerous intersections to regulate traffic movements. A number of traffic signal control strategies have been proposed since one of the earliest attempts in [75]. According to [65], prevailing traffic signal control strategies can be categorized by the following characteristics: fixed-time versus traffic-responsive, isolated versus coordinated, and under-saturated versus over-saturated. However, most of them are only applicable to under-saturated traffic conditions, and few can work under over-saturated traffic conditions [65]. Therefore, as traffic is getting more and more congested in urban networks, there is a need to develop effective and efficient traffic signal control strategies that can work under various traffic conditions.

1.1.2 Importance of understanding traffic statics and dynamics in urban networks

In Figure 1.1, the framework of traffic studies on urban networks is provided. For an urban network, its inputs include many aspects such as weather conditions, vehicle types, driver behaviors, route choice behaviors, and travel demands. Given certain inputs, control and management strategies can be applied to determine the signal settings and manage the facility for automobile parking and other transportation modes such as transit, bus, and bike.

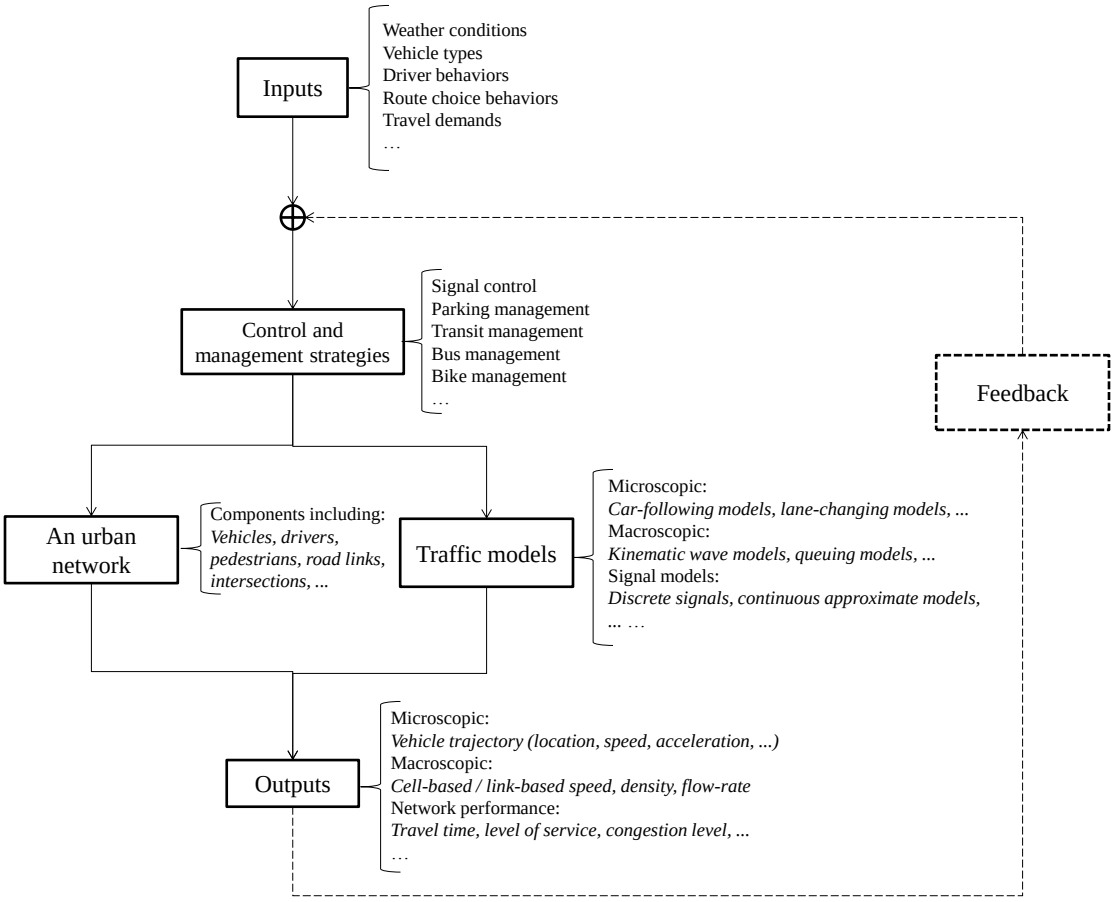

Figure 1.1: The framework of traffic studies on urban networks

However, urban networks are complex systems which involve a lot of components such as vehicles, drivers, pedestrians, road links, and intersections and the interactions among them. In order to understand the traffic dynamics in an urban network, traffic models are needed. At the microscopic level, car-following and lane-changing models are used to describe drivers' driving behaviors. At the macroscopic level, traffic flow models such as kinematic wave models and queuing models are used to describe the evolution pattern of traffic inside a road link. Since the road links are connected with each other at intersections, signal models, either discrete or continuous, are used to describe the evolution and route choice patterns of traffic at intersections. For network outputs, vehicle trajectories can be obtained if traffic models at the microscopic-level are used. For macroscopic models, information such as speed, density, and flow-rate can be obtained. Given these outputs, network performance such as travel time, level of service, and congestion level can be determined. Nowadays, with advanced detection techniques, these outputs can also be detected in real-time from the field. To improve the network performance, these outputs can serve as feedback to help engineers and planners modify the control and management strategies accordingly.

Before developing effective and efficient network control and management strategies, a fundamental challenge is to understand impacts of network inputs such as signal settings, route choice behaviors, and demand patterns on the static and dynamic characteristics of urban traffic. Under given network inputs, what the final states will be and how the transition process would look like are the questions needed to be answered first. But in the literature, very limited efforts [36, 12, 35, 11, 49] have been devoted to this area. And also, while developing traffic signal control strategies, optimization is performed with given objective functions such as maximizing the total throughput or minimizing the total travel delay. But such optimization problems are challenging to solve when the network gets larger due to the fact that the discrete signal control at intersections introduces many discrete variables. In the literature, there have been studies [26, 25, 34] proposing continuous models to approximate the junction flux at the intersections. However, some of them [26, 25] can only

apply to congested traffic conditions, while some others [34] were directly proposed without a general approach. To the best of our knowledge, there is a lack of a general method to derive continuous approximate models that can work under different traffic conditions with different types of traffic flow models.

1.2 Motivation of the dissertation research

The motivation of this dissertation research is to provide a comprehensive study on the static and dynamic properties of traffic flow in signalized urban networks and to provide a systematic method to derive invariant continuous approximate models for signalized intersections. In Figure 1.2, the research outline of this dissertation is provided. Instead of working on large-scale urban networks, e.g., the signalized grid network, we focus on the traffic statics and dynamics in a signalized double-ring network, which retains the most important feature of urban networks, the signalized intersection. In this dissertation, we try to understand possible stationary states in the signalized double-ring network under different frameworks of traffic flow models, e.g., the cell transmission model (CTM)[9] and the link queue model (LQM)[43]. Due to infinite-dimensional state variables introduced by the kinematic wave model, CTM simulations are used to find the possible stationary states. Periodic traffic pattens are found in the signalized double-ring network and defined as stationary states. To analyze the existence and the property of the stationary states, we use the link-queue model to aggregate the traffic dynamics at the link level, and thus, each link only has one state variable, its average density. Furthermore, the signalized double-ring network is formulated as a switched affine system by using the triangular traffic flow fundamental diagram [33]. Periodic density evolution orbits are found when the system reaches stationary states, and therefore, the Poincaré map approach in [76, 74] is used to analyze the static and dynamic properties of these periodic orbits. With the analytical tools of the link queue model, the

switched affine system, and the Poincaré map, we can obtain a more complete picture of possible stationary states inside the signalized double-ring network than other existing studies. Macroscopic fundamental diagrams (MFDs) [12, 27] and gridlock times can be analytically derived under different combinations of signal settings, route choice behaviors, and traffic demands.

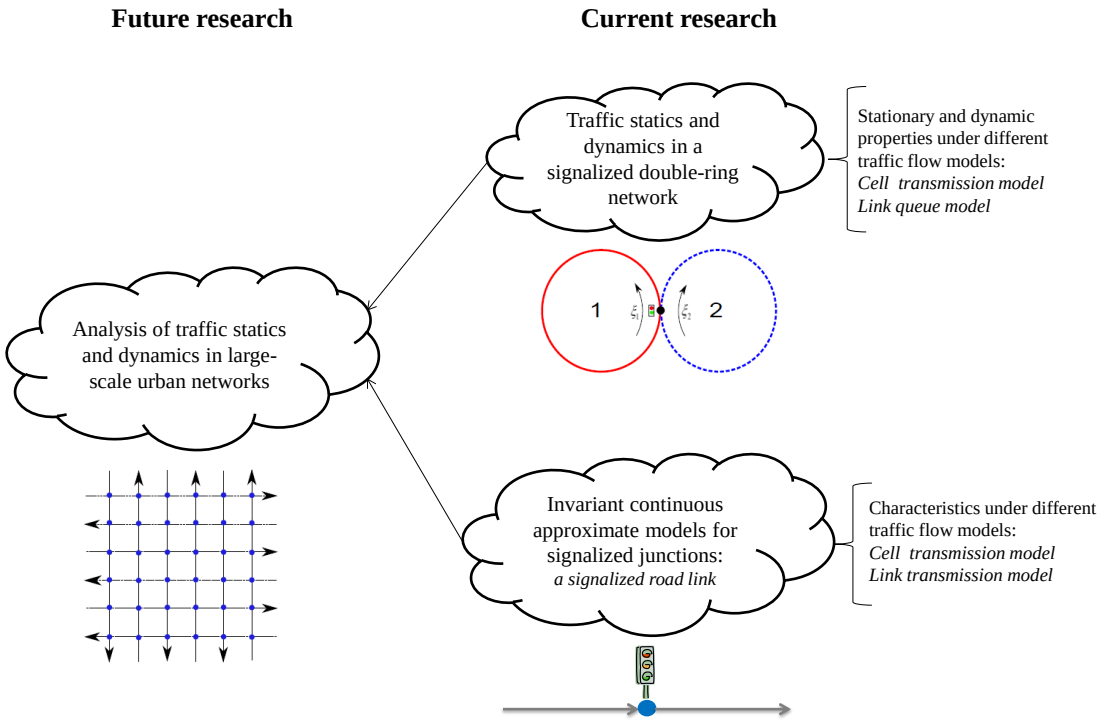

Figure 1.2: The dissertation research outline

In urban networks, traffic signal is one of the most important components. Even with the link queue model, traffic dynamics are still difficult to solve analytically due to the existence of signals at intersections. Therefore, in this dissertation, we introduce the analytical framework in [48, 41] to derive invariant continuous approximate models for a signalized road link. We also evaluate the approximation performance of the invariant continuous approximate models

under different cycle lengths, demand patterns, and traffic flow fundamental diagrams. In addition, we show the importance of invariance continuous approximate models in the link transmission model [78, 47].

Insights from this dissertation research can provide a deeper understanding of how the network inputs such as signal settings, route choice behaviors and traffic demands can impact the performance of urban networks. The analytical tools such as the link queue model, the switch affine system, and the Poincaré map and the invariant continuous approximate models can be applied to the analysis of large-scale urban networks, which definitely will yield more interesting and practical results. The organization of this dissertation research is provided as follows. In Chapter 2, we provide a brief literature review on signal control strategies, continuous approximate models, traffic flow models, and traffic flow fundamental diagrams. In Chapter 3, we provide a kinematic wave approach to formulate the traffic dynamics in a signalized double-ring network and use CTM simulations to find the stationary traffic states. In Chapter 4, we provide a Poincaré map approach to analyze the static and dynamic properties of traffic in the signalized double-ring network. In Chapter 5, we provide a comprehensive study on deriving and analyzing invariant continuous approximate models for a signalized road link. In Chapter 6, we use LQM simulations to study the traffic statics and dynamics in a signalized grid network. In Chapter 7, we summarize our research findings and provide some future research directions.

Chapter 2

Literature review

2.1 Control strategies at signalized intersections

In the literature, a number of signal control strategies have been proposed to improve the traffic performance since one of the earliest attempts in [75]. According to [65], signal control strategies can be classified into two types: isolated strategies for a single intersection and coordinated strategies that consider an urban arterial or even an urban network with many intersections. In the following subsections, we provide some examples of control strategies in these two types.

2.1.1 For isolated intersections

Fixed-time control strategies for a single intersection can be stage-based or phase-based [65]. Under given stage settings, stage-based strategies try to find optimal splits and cycle lengths by minimizing the total delay or maximizing the total throughput at the intersection. To calculate vehicles' average delay, the delay formulation proposed by Webster [75] has

been widely used. In his delay formulation, average delay for a vehicle consists of three parts: uniform delay, random delay, and empirical adjustments. Optimal cycle lengths were obtained by minimizing the total delay at the intersection under given arrival flow-rates [75]. Optimal settings of splits and cycle lengths were obtained in [60] by considering the impact of various arrival patterns in the calculation of random delay. In [1, 2], SIGSET was proposed to take into account the case that approaches have right of way in more than one stage within a cycle. Webster's delay formula was still used in the delay estimation. Optimal settings of cycle length and effective green time for each stage were obtained by minimizing the total delay with capacity, cycle length, and minimum green time constraints. Different from SIGSET, another program, SIGCAP, was proposed in [3, 4] to maximize the practical capacity at the signalized intersection under similar constraints as those in SIGSET. For phase-based control strategies, they are extended to further consider optimal stage settings. For example, the constraint of fixed staging was released in [39]. Incompatibility of traffic streams at the intersection was considered as a constraint in the optimization problem. Optimal settings of splits, cycle length, and stage settings were obtained by minimizing the total delay or maximizing the intersection capacity. The optimization problem was formulated as a binary-mixed-integer-linear-programming (BMILP) problem, and solutions were obtained using a branch-and-bound method. However, the aforementioned studies are only applicable to under-saturated traffic conditions, and their performance deteriorates as traffic gets congested. In addition, they are fixed-time strategies and fail to utilize real-time traffic information at the intersection.

Due to the installation of vehicle detectors at signalized intersections, traffic-responsive control strategies that utilize real-time flow and occupancy information have been proposed. Examples such as the Vehicle Interval strategy, the Volume Density strategy, and Miller's algorithm were provided in [14]. In the Vehicle Interval strategy, minimum and maximum green times are prespecified for each stage. A critical interval (CI) is used to extend the green time to allow detected vehicles cross the intersection. The control logic in the Vol-

ume Density strategy is similar to that in the Vehicle Interval strategy. But it also takes into account queue lengths and vehicles' waiting time during the red phase in deciding the switching time instants. In Miller's algorithm [59], at every time step, the computer program determines whether to switch the signal immediately or to delay the switch for $k \times h$ seconds, e.g., $h = 2$s and $k = 1, 2, ..., 5$. The evaluation is based on the time gain in postponing the switch. If the time gain is negative, the signal is switched immediately. Otherwise it remains unchanged for the next time step.

2.1.2 For coordinated intersections

When traffic signals are close enough, vehicles arrive the downstream intersections in platoons. For an arterial, traffic signals can be synchronized so that a vehicle can travel from the beginning to the end without stopping. The time difference between the first and the last vehicles which satisfy such a condition is defined as bandwidth for that direction. MAXBAND was introduced in [55] to specify the offset settings so as to maximize the total bandwidths of a two-way arterial within given cycle and speed ranges. The optimization problem was formulated as a mixed-integer-linear-programing problem, and a branch-and-bound method was used to solve it. Later in [22], MULTI-BAND was proposed to consider new features such as determination of left-turn phases and different bandwidths among the links in the optimization problem. Different from MAXBAND or MULTI-BAND [55, 22], TRANSYT (TRAffic Network StudY Tool)[69], was proposed to find multi-directional green waves by minimizing the total delay. The model consists of two parts: a traffic flow model and an optimization procedure. In the traffic flow model, network information such as road geometries, constant and known turning ratios at intersections, and constant and known demands is needed. A platoon dispersion model is used to describe vehicles' progressions inside a link. In the optimization procedure, a 'hill-climbing' method is used. The program generates small changes in the decision variables such as offsets and serves them as new inputs in the traffic model.

A so-called Performance Index is used to evaluate the improvements at each optimization step, and the process stops when a (local) minimum is found. However, the aforementioned studies are fixed-time control strategies and only applicable to under-saturated conditions [65].

In reality, demands and turning movements at intersections are not constant and can vary in different days or even within a time of day. Therefore, several traffic-responsive coordinated strategies have been proposed. In [38, 37], a traffic-responsive version of TRANSYT, SCOOT (Split, Cycle and Offset Optimization Technique) , was developed. Different from TRANSYT, which is 'off-line' and predicts delay and stops based on specified average flows, SCOOT predicts delay and stops using real-time measurements of flows and occupancies from vehicle loop detectors. The optimization structure in SCOOT is similar to that in TRANSYT, which also consists of a traffic model and a signal optimizer. But the SCOOT signal optimizer works in read time, and new signal settings are implemented directly on the street. As mentioned in [65], SCOOT cannot work properly under saturated traffic conditions. Besides SCOOT, model-based traffic-responsive strategies such as OPAC (Optimization Policies for Adaptive Control) [21] have been proposed. Different from SCOOT, splits, offsets, and cycles are not explicitly considered in OPAC. For real-time applications, a rolling horizon approach is used in OPAC. Given observed traffic data in the time period $[t-h, t]$, the optimization method calculates an optimal switching scheme for the whole time period $[t-h, t+H-h]$, where $H > h$. But the optimal switching scheme is only applied to the time period $[t, t+h]$. When the real-time traffic data in the time period $[t, t+h]$ are collected, the optimization method will generate a new optimal switching scheme for the time period $[t, t+H]$ and apply it to the time period $[t+h, t+2h]$. However, OPAC employs complete enumeration in the optimization of switching schemes, and thus, it is not real-time feasible for multiple intersections [65]. In [56], the cell transmission model in [9, 10] was used to describe traffic dynamics inside a link. The optimization problem was formulated as a mixed-integer-programing problem, and optimal signal settings were obtained by minimizing

the total network delay of queued vehicles inside the cells. Later in [57], the signal control framework was extended to the network level, and a genetic algorithm approach was introduced to obtain the optimal signal settings. Results showed that compared with TRANSYT, the proposed control strategy improves the network performance by as much as 33 % under a wide range of demand patterns.

2.2 Continuous approximate models at signalized intersections

At urban intersections, the operation of traffic signal follows a discrete pattern: vehicles are allowed to move when the traffic light is green, while they have to stop when it turns red. Such a discrete control pattern introduces difficulties in optimizing signal control parameters such as green splits, especially when the network size increases. Therefore, continuous approximate models have been proposed in some studies.

2.2.1 The store-and-forward method

For an intersection of two one-way streets, the arrival rates are denoted as $a_1(t)$ and $a_2(t)$, respectively. During the peak period, a queue is likely to develop in one or both directions when the following condition is satisfied:

$$a_1(t)/s_1 + a_2(t)/s_2 > 1 - (T_l/T_c), \tag{2.1}$$

where s_1 and s_2 are the saturation flow-rates in the downstream of the intersection, T_l the total lost time, and T_c the cycle length. The cumulative arrival rates of the two upstream

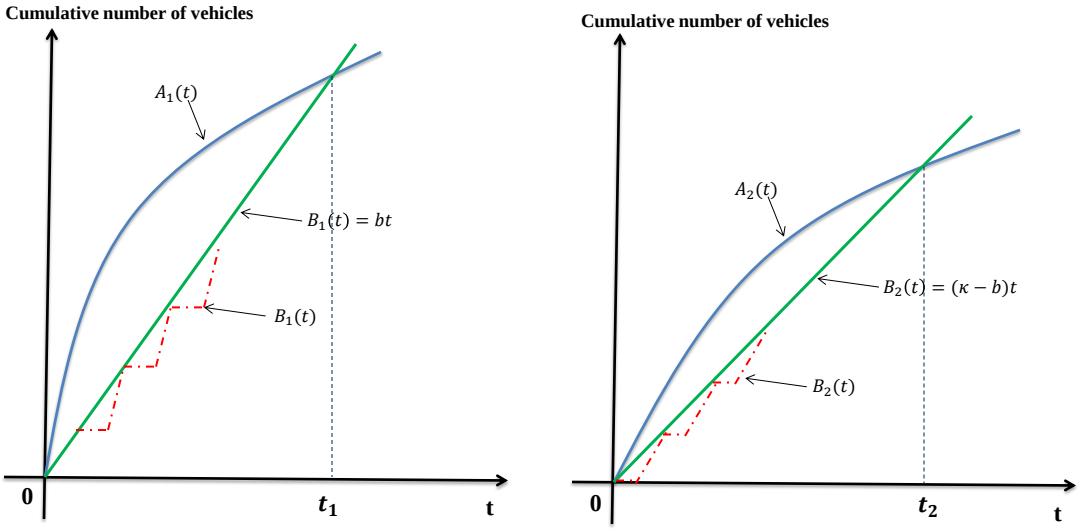

(a) Upstream approach 1

(b) Upstream approach 2

Figure 2.1: Arrival and discharging patterns at an intersection with two upstream approaches under congested conditions.

approaches are given by

$$A_i(t) = A_i(0) + \int_0^t a_i(\tau)d\tau, \qquad i = 1, 2 \tag{2.2}$$

where $A_i(0)$ is the initial queue at the onset of the rush period ($t = 0$). The cumulative arrival rates are provided in Figure 2.1. Since traffic demands are high at both directions, the green times are fully used, and thus, the discharging flow-rates are equal to the saturation flow-rates. The saw-toothed patterns of the service curves $B_i(t)$, $i = \{1, 2\}$, are also provided in Figure 2.1. In [26, 25], considering large delays are caused by queueing, the addition delay due to this pattern is neglected and the service curves are smoothed using continuous functions. If the saturation flow-rates are the same in both directions, i.e., $s_1 = s_2$, the total throughput at the intersection remains constant regardless of the signal settings. For a fixed

signal setting, the service curves can be calculated as

$$B_1(t) = bt, \tag{2.3a}$$

$$B_2(t) = (\kappa - b)t, \tag{2.3b}$$

where b and κ are constants and the ratio of the effective green times of the two approaches is $\frac{b}{\kappa - b}$. The delays in both directions are calculated as

$$T_{d1} = \int_0^{t_1} [A_1(t) - bt]dt, \tag{2.4a}$$

$$T_{d2} = \int_0^{t_2} [A_2(t) - (\kappa - b)t]dt, \tag{2.4b}$$

where t_1 and t_2 satisfy the following relations:

$$A_1(t_1) = bt_1, \tag{2.5a}$$

$$A_2(t_2) = (\kappa - b)t_2. \tag{2.5b}$$

The total delay at the intersection is given by

$$T_{tot} = T_{d1} + T_{d2}. \tag{2.6}$$

To minimize the total delay, the optimum split can be found when the queues in both directions are dissolved simultaneously. It is also shown that the minimization of the total delay doesn't necessarily guarantee the minimization of the maximum individual delay [26, 25].

2.2.2 A continuum model for a signalized merging junction

For a signalized merging junction, let's consider the traffic signal is installed at $x = 0$. The two upstream links are denoted as links 1 and 2, respectively, and the downstream link as link 3. Each cycle is a combination of two phases for the two upstream links, respectively. The cycle length is T with zero lost times. The green ratio is denoted as π_1 for link 1, and thus $1-\pi_1$ for link 2. Then the discrete signal control at the merging junction can be written as

$$\delta_1(t;T,\pi_1) = \begin{cases} 1, & t \in [nT, nT+\pi_1 T), \\ 0, & otherwise, \end{cases} \qquad n \in \mathbb{N}_0 \tag{2.7a}$$

$$\delta_2(t;T,\pi_1) = \begin{cases} 1, & t \in [nT+\pi_1 T, (n+1)T), \\ 0, & otherwise, \end{cases} \qquad n \in \mathbb{N}_0 \tag{2.7b}$$

The junction fluxes at the merging junction can be calculated as

$$f_1(k_1(t,0^-)) = \min\{D_1(0^-,t), \delta_1(t)C_1, \delta_1(t)S_3(0^+,t)\}, \tag{2.8a}$$

$$f_2(k_2(t,0^-)) = \min\{D_2(0^-,t), \delta_2(t)C_2, \delta_2(t)S_3(0^+,t)\}, \tag{2.8b}$$

$$f_2(k_3(t,0^+)) = f_1(k_1(t,0^-)) + f_2(k_2(t,0^-)). \tag{2.8c}$$

Here $k_1(t,0^-)$ and $k_2(t,0^-)$ are the densities of links 1 and 2 at $x = 0^-$, respectively, and $k_3(t,0^+)$ is the density of link 3 at $x = 0^+$. $D_1(0^-,t)$ and $D_2(0^-,t)$ are the link demands at $x = 0^-$ for links 1 and 2, respectively, while $S_3(0^+,t)$ is the link supply at $x = 0^+$ for link 3 [10, 53]. In [34], a continuum model was proposed to approximate the discrete junction fluxes in Equation (2.8) by averaging the periodic signal control parameters $\delta_1(t)$ and $\delta_2(t)$

over time. The model can be written as

$$f_1(k_1(t,0^-)) = \min\{D_1(0^-,t), \pi_1 C_1, \pi_1 S_3(0^+,t)\}, \tag{2.9a}$$

$$f_2(k_2(t,0^-)) = \min\{D_2(0^-,t), (1-\pi_1) C_2, (1-\pi_1) S_3(0^+,t)\}, \tag{2.9b}$$

$$f_2(k_3(t,0^+)) = f_1(k_1(t,0^-)) + f_2(k_2(t,0^-)). \tag{2.9c}$$

2.3 Traffic flow models

For a general road network, we denote the set of normal links as A, the set of normal junctions as J, the set of origins as O, and the set of destinations as R. To describe traffic dynamics inside a link, different traffic flow models have been proposed. In this section, we only review three types of traffic flow models that will be used in the following chapters.

2.3.1 The cell transmission model

In kinematic wave models, traffic on link $a \in A$ is considered as a continuous media. At time t, traffic at point $x_a \in [0, L_a]$ can be described by the following three location-and-time dependent parameters: flow-rate $q_a(x_a, t)$, density $k_a(x_a, t)$, and speed $v_a(x_a, t)$, where L_a is the length of link a. Hereafter, we omit (x_a, t) in these three variables unless necessary. For a road section without internal entrances and exits, e.g., a freeway section without on-/off-ramps, the following traffic conservation law holds:

$$\frac{\partial q_a}{\partial x_a} + \frac{\partial k_a}{\partial t} = 0. \tag{2.10}$$

In [54, 68], it was assumed there is a functional relation between speed and density, e.g., $v_a = V_a(k_a)$, which is known as the traffic flow fundamental diagram. Since we have $q_a = k_a v_a$, Equation (2.10) can be rewritten as

$$\frac{\partial k_a V_a(k_a)}{\partial x_a} + \frac{\partial k_a}{\partial t} = 0, \tag{2.11}$$

which is known as the LWR model.

For simulation studies, a discrete version of Equation (2.11) is needed. Therefore, the Godunov method [30] is used to numerically solve Equation (2.11). In the Godunov method, a link is divided into N cells, and the time is partitioned into K steps. For a cell i, we define the the average density at time step j as $k_{a,i}^j$, and the one at time step $j+1$ as $k_{a,i}^{j+1}$. During the time duration at time step j, we define $f_{a,i-1/2}^j$ and $f_{a,i+1/2}^j$ as fluxes at the upstream and downstream boundaries of cell i, respectively. Then the Godunov-type finite difference equation of Equation (2.11) can be written as

$$\frac{k_{a,i}^{j+1} - k_{a,i}^j}{\Delta t} - \frac{f_{a,i-1/2}^j - f_{a,i+1/2}^j}{\Delta x} = 0, \tag{2.12}$$

where Δx is the cell length, and Δt is the time duration at time step j. Here, the choice of $\frac{\Delta t}{\Delta x}$ should follow the CFL condition [8], which requires vehicles can not travel across more than one cell during Δt. Given the initial and the boundary conditions at time step j, the corresponding density at time step $j+1$ can be updated by

$$k_{a,i}^{j+1} = k_{a,i}^j + \frac{\Delta t}{\Delta x}(f_{a,i-1/2}^j - f_{a,i+1/2}^j). \tag{2.13}$$

In order to uniquely determine the boundary flux between cells $i-1$ and i, the supply and demand concept in [18] was used in [9, 53]. Suppose the fundamental diagram on a link is $q_a = Q_a(k_a) = k_a V_a(k_a)$, then the demand $D_{a,i}$ and the supply $S_{a,i}$ for cell i are calculated

as

$$D_{a,i} = \mathbb{D}_a(k_{a,i}) = Q_a(\min\{k_{a,c}, k_{a,i}\}), \tag{2.14a}$$

$$S_{a,i} = \mathbb{S}_a(k_{a,i}) = Q_a(\max\{k_{a,c}, k_{a,i}\}), \tag{2.14b}$$

where $k_{a,c}$ and $k_{a,i}$ are the critical density and the density in cell i, respectively. In [9, 10], the boundary flux $f^j_{a,i-1/2}$ entering cell i is taken as the minimum of cell i's supply and its upstream cell $(i-1)$'s demand, which is

$$f^j_{a,i-1/2} = \min\{D_{a,i-1}, S_{a,i}\}. \tag{2.15}$$

Equations (2.13) to (2.15) are known as the cell transmission model (CTM) proposed in [9, 10].

However, it is hard to obtain analytical insights from simulations with the discrete version of CTM. Therefore, a continuous version of CTM was recently proposed in [48, 41, 46, 42]. Traditionally, density is used as a state variable, which determines the corresponding speed and flow-rate from the fundamental diagram. However, the supply and demand are considered as state variables in [48, 41, 46, 42]. At point (a, x_a), if the demand D_a and the supply S_a are known, the corresponding flow-rate, density, and capacity can be calculated as

$$q_a = \min\{D_a, S_a\}, \tag{2.16a}$$

$$C_a = \max\{D_a, S_a\}, \tag{2.16b}$$

$$k_a = R_a(D_a/S_a) = \begin{cases} \mathbb{D}_a^{-1}(C_a D_a/S_a), & D_a \le S_a \\ \mathbb{S}_a^{-1}(C_a S_a/D_a), & D_a \ge S_a \end{cases} \tag{2.16c}$$

To calculate the traffic flux through point (a, x_a), the following equation is used:

$$q_a(x_a, t) = \min\{D_a(x_a^-, t), S_a(x_a^+, t)\}, \tag{2.17}$$

where x_a^- and x_a^+ are the upstream and downstream points of (a, x_a), respectively.

The aforementioned discrete and continuous versions of CTM can only be applied to study the traffic dynamics inside a link. For network traffic simulations and analysis, junctions models are needed to determine links' in-/out-fluxes from the demand information of the upstream links and the supply information of the downstream links. In the literature, many different types of junction models have been proposed, such as the merging models in [10, 53, 50, 41], the diverging models in [10, 46], and the general junction model in [42].

2.3.2 The link transmission model

At point (a, x_a), the evolution of density k_a, speed v_a, and flow-rate q_a is described based on the flow conservation equation, $\frac{\partial k_a}{\partial t} + \frac{\partial q_a}{\partial x} = 0$, and a fundamental diagram $q_a = Q_a(k_a)$ in the LWR model. However, in the link transmission model (LTM) [78], the cumulative flow $A_a(x_a, t)$, which is known as the Moskovitz function [61], is used. Since we have $k_a = -\frac{\partial A_a}{\partial x}$ and $q_a = \frac{\partial A_a}{\partial t}$, the flow conservation equation is automatically satisfied if we have $\frac{\partial^2 A_a}{\partial x \partial t} = \frac{\partial^2 A_a}{\partial t \partial x}$. Then with the fundamental diagram $q_a = Q_a(k_a)$, to solve the LWR model in Equation (2.11) is equivalent to solve the following Hamilton-Jacobi equation:

$$\frac{\partial A_a}{\partial t} - Q_a(-\frac{\partial A_a}{\partial x}) = 0, \tag{2.18}$$

with the Hamiltonian $\mathbf{H}(\frac{\partial A_a}{\partial x}) = -Q_a(-\frac{\partial A_a}{\partial x})$. In [78], a discrete version of LTM was proposed to numerically solve Equation (2.18). Recently, a continuous formulation of LTM was provided in [47].

Here, the following triangular traffic flow fundamental diagram [33] is used:

$$q = Q(k) = \min\{v_f k, w(k_j - k)\}, \tag{2.19}$$

where v_f is the free-flow speed, and w is the shock-wave speed. The initial cumulative flow at $x_a \in [0, L_a]$ is denoted as $N_a(x_a)$. At the upstream boundary, the cumulative in-flow and the in-flux are denoted as $F_a(t)$ and $f_a(t)$, respectively. Similarly, at the downstream boundary, the cumulative out-flow and the out-flux are denoted as $G_a(t)$ and $g_a(t)$, respectively. Inside link a, the link queue size $\alpha_a(t)$ and the link vacancy size $\beta_a(t)$ are calculated as

$$\alpha_a(t) = \begin{cases} N_a(L_a - v_{a,f}t) - G_a(t), & t \le \frac{L_a}{v_{a,f}} \\ F_a(t - \frac{L_a}{v_{a,f}}) - G_a(t), & t > \frac{L_a}{v_{a,f}} \end{cases} \tag{2.20a}$$

$$\beta_a(t) = \begin{cases} N_a(w_a t) + k_{a,j} w_a t - F_a(t), & t \le \frac{L_a}{w_a} \\ G_a(t - \frac{L_a}{w_a}) + k_{a,j} L_a - F_a(t), & t > \frac{L_a}{w_a} \end{cases} \tag{2.20b}$$

where $k_{a,j}$, $v_{a,f}$, and w_a are the jam density, the free-flow speed, and the shock-wave speed of link a, respectively. When $t = 0$, we have $\alpha_a(0) = 0$ and $\beta_a(0) = 0$. We first define an indicator function $H(y)$ for $y \ge 0$ as follows:

$$H(y) = \lim_{\Delta t \to 0^+} \frac{y}{\Delta t} = \begin{cases} 0, & y = 0 \\ +\infty, & y > 0 \end{cases} \tag{2.21}$$

Then the link demand $d_a(t)$ and supply $s_a(t)$ are defined as

$$d_a(t) = \begin{cases} \min\{k_a(L_a - v_{a,f}t, 0)v_{a,f} + H(\alpha_a(t)), C_a\}, & t \le \frac{L_a}{v_{a,f}} \\ \min\{f_a(t - \frac{L_a}{v_{a,f}}) + H(\alpha_a(t)), C_a\}, & t > \frac{L_a}{v_{a,f}} \end{cases} \tag{2.22a}$$

$$s_a(t) = \begin{cases} \min\{k_{a,j} w_a - k_a(w_a t, 0)w_a + H(\beta_a(t)), C_a\}, & t \le \frac{L_a}{w_a} \\ \min\{g_a(t - \frac{L_a}{w_a}) + H(\beta_a(t)), C_a\}, & t \le \frac{L_a}{w_a} \end{cases} \tag{2.22b}$$

At a junction j, macroscopic junction models are needed to uniquely determine the boundary fluxes from the upstream demands, downstream supplies, and turning proportions, which can be written as

$$(\mathbf{g}_j(t), \mathbf{f}_j(t)) = \mathcal{F}(\mathbf{d}_j(t), \mathbf{s}_j(t), \xi_j(t)). \tag{2.23}$$

Here, $\mathbf{d}_j(t)$ is the set of demands of the upstream links, and $\mathbf{s}_j(t)$ is the set of supplies of the downstream links. $\xi_j(t)$ is the matrix of turning proportions from the upstream links to the downstream links. $\mathbf{g}_j(t)$ is the set of out-fluxes from the upstream links, and $\mathbf{f}_j(t)$ is the set of in-fluxes to the downstream links. As proved in [47], non-invariant junction models should not be used in LTM, and examples of invariant junction models can be found in [48, 41, 46, 42].

In LTM, either cumulative flows or link queue and vacancy sizes can be used as state variables. If the cumulative flow, i.e., $F_a(t)$ and $G_a(t)$, are used, we have the following evolution equations:

$$\frac{d}{dt}F_a(t) = f_a(t), \tag{2.24a}$$
$$\frac{d}{dt}G_a(t) = g_a(t). \tag{2.24b}$$

However, if the link queue and vacancy sizes, i.e., $\alpha_a(t)$ and $\beta_a(t)$, are used, we have the

following evolution equations:

$$\frac{d\alpha_a(t)}{dt} = \begin{cases} k_a(L_a - v_{a,f}t, 0)v_{a,f} - g_a(t), & t \leq \frac{L_a}{v_{a,f}} \\ f_a(t - \frac{L_a}{v_{a,f}}) - g_a(t), & t > \frac{L_a}{v_{a,f}} \end{cases} \tag{2.25a}$$

$$\frac{d\beta_a(t)}{dt} = \begin{cases} -k_a(w_a t, 0)w_a + k_{a,j}w_a - f_a(t), & t \leq \frac{L_a}{w_a} \\ g_a(t - \frac{L_a}{w_a}) - f_a(t), & t > \frac{L_a}{w_a} \end{cases} \tag{2.25b}$$

As shown in Equation (2.22), link demands and supplies depend on historical states, and therefore, Equations (2.24) and (2.25) are systems of ordinary differential equations with delays. Once $F_a(t)$ and $G_a(t)$ are found, traffic states inside link a can be obtained [47].

2.3.3 The link queue model

In the link queue model (LQM) [43], traffic on a link is considered as a single queue, and therefore, the average density of link $a \in A$, or the link volume of origin $o \in O$, is used as the state variable. For a regular link $a \in A$, the demand and supply are defined as

$$D_a(t) = Q_a(\min\{k_a(t), k_{a,c}\}) = \begin{cases} Q_a(k_a(t)), & k_a(t) \in [0, k_{a,c}] \\ C_a, & k_a(t) \in (k_{a,c}, k_{a,j}] \end{cases} \tag{2.26a}$$

$$S_a(t) = Q_a(\max\{k_a(t), k_{a,c}\}) = \begin{cases} C_a, & k_a(t) \in [0, k_{a,c}] \\ Q_a(k_a(t)), & k_a(t) \in (k_{a,c}, k_{a,j}] \end{cases} \tag{2.26b}$$

Here $k_a(t)$ is the average density of link a, and $Q_a(k_a(t))$ is the corresponding fundamental diagram with the capacity C_a attained at the critical density $k_{a,c}$. The flow-rate is zero when $k_a(t) = 0$ or $k_a(t) = k_{a,j}$, where $k_{a,j}$ is the jam density. For an origin $o \in O$, the demand is

defined as

$$D_o(t) = f_o(t) + I_{K_o(t)\geq 0} = \begin{cases} +\infty, & K_o(t) > 0 \\ f_o(t), & K_o(t) = 0 \end{cases} \tag{2.27}$$

where $f_o(t)$ is the arrival rate and $K_o(t)$ is the queue length at the origin o. Equation (2.27) means that the demand is infinite when there is a queue at the origin or the same as the arrival rate when no queue exists. For a destination $r \in R$, its supply is defined as $S_r(t)$ and serves as boundary conditions. But if the downstream is not blocked, we can have $S_r(t) = +\infty$.

At a junction j, a junction flux function is needed to calculate the in-/out-fluxes from the upstream demands and downstream supplies, which can be formulated in the following general form:

$$(\mathbb{G}_j(t), \mathbb{F}_j(t)) = \mathbb{FF}(\mathbb{D}_j(t), \mathbb{S}_j(t), \xi_j(t)), \tag{2.28}$$

where $\mathbb{G}_j(t)$ is the set of out-fluxes, $\mathbb{F}_j(t)$ the set of in-fluxes, $\mathbb{D}_j(t)$ the set of upstream demands, $\mathbb{S}_j(t)$ the set of downstream supplies, and $\xi_j(t)$ the matrix of turning proportions from the upstream links to the downstream links at junction j.

With the demand and supply definitions in Equations (2.26) and (2.27) and the flux function in Equation (2.28), the link queue model of network traffic flow can be formulated as

$$\frac{dk_a(t)}{dt} = \frac{1}{L_a}(f_a(t) - g_a(t)), \qquad a \in A \tag{2.29a}$$

$$\frac{dK_o(t)}{dt} = f_o(t) - g_o(t), \qquad o \in O \tag{2.29b}$$

where L_a is the link length, $f_a(t)$ the influx, and $g_a(t)$ the outflux of link a. $f_o(t)$ is the arrival rate, and $g_o(t)$ is outflux at origin o.

The link queue model in Equation (2.29) cannot be solved under general initial and boundary conditions, numerical methods should be used to obtain its approximate solutions. In [43], an explicit Euler method is used to obtain the discrete version of Equation (2.29). The simulation time period is equally discretized into M time steps with a duration of Δt. At time step i, the density of link a is denoted as k_a^i, and the queue at origin o is denoted as K_o^i. During the time period $[i\Delta t, (i+1)\Delta t]$, the boundary fluxes for link a are denoted as f_a^i and g_a^i, respectively. To calculate the demand D_a^i and the supply S_a^i, Equation (2.26) still can be used. But for the demand at origin o, it is now computed as

$$D_o^i = \frac{K_o^i}{\Delta t} + f_o^i. \tag{2.30}$$

Then the density and queue length at time step $i+1$ can be updated by

$$k_a^{i+1} = k_a^i + \frac{\Delta t}{L_a}(f_a^i - g_a^i), \tag{2.31a}$$

$$K_a^{i+1} = K_a^i + (f_o^i - g_o^i)\Delta t. \tag{2.31b}$$

2.3.4 Comparisons among these three models

In network simulations, CTM needs to calculate the demands and supplies for all cells, determine the fluxes through the cell boundaries and junctions, and update the cell densities at each time step. However, LQM only needs to calculate the demand and supply for a whole link and then calculate the fluxes and cumulative vehicle numbers at the link boundaries. Therefore, LTM is computationally more efficient than CTM. Moreover, CTM introduces errors into the calculation due to the numerical diffusion when a shock wave occurs inside a link. However, in LTM, numerical diffusion only occurs once when the shock wave crosses

the link boundary. Therefore, LTM is more accurate than CTM. In addition, since there are delays in Equations (2.24) and (2.25), LTM requires more memory storage to store historical information of cumulative numbers of vehicles at the link boundaries. In CTM, only the most recent cell densities are stored.

However, LQM is different from CTM and LTM. This model has two important features. First, the fundamental diagram on each link is used to calculate its supply and demand based on its average link density. Second, network junction models are used to determine the in-/out-fluxes from the supply and demand information at the junction. Therefore, LQM can be considered as an approximation to the network kinematic wave models, e.g., CTM and LQM. However, LQM is not equivalent to CTM. In the discrete version of LQM, the solutions are more accurate with a smaller Δt. However, in the discrete version of CTM, the relation between Δx and Δt is governed by the CFL condition [8]. There is a trade-off in the selection of Δt and Δx: Δt should be as big as possible to improve the simulation speed, while Δx should be as small as possible to improve the simulation accuracy. In addition, in CTM the maximum Δt can not exceed the minimum link traverse time under free-flow conditions in a network. However, there is no constraint on Δt in LQM.

2.4 Traffic flow fundamental diagrams

2.4.1 Link-based

To evaluate traffic conditions on a link, one practical approach is via the traffic flow fundamental diagram which describes the functional relations among flow-rate, speed, and density. In the literature, many types of fundamental diagrams have been proposed since one of the earliest attempts in [32]. Examples can be found in [32, 31, 63, 15, 67, 33, 7] and are also provided in Table 2.1. Among the proposed fundamental diagrams, the triangular one in

[33] is widely used because it is not only simple but also consistent with field observations. In the triangular fundamental diagram, traffic states are divided into two regimes: free-flow and congested. It assumes that drivers tend to drive at a free-flow speed when traffic is not congested, but they need to follow their leaders' driving patterns when traffic gets congested.

Table 2.1: Examples of speed-density relations

Models	$v = V(k)$	Parameters
Greenshields (1935)	$v = v_f(1 - \frac{k}{k_j})$	v_f, k_j
Greenberg (1959)	$v = v_m \ln(k_j/k)$	v_m, k_j
Newell (1961)	$v = v_f[1 - e^{\frac{-\lambda}{v_f}(\frac{1}{k} - \frac{1}{k_j})}]$	v_f, k_j
Drake (1967)	$v = v_f e^{-\frac{1}{2}(\frac{k}{k_j})^2}$	v_f, k_j
Pipes (1967)	$v = v_f[1 - (\frac{k}{k_j})^n]$	v_f, k_j
Haberman (1977)	$v = \min\{v_f, \frac{v_f k_c}{k_j - k_c}(\frac{k_j}{k} - 1)\}$	v_f, k_c, k_j
Del Castillo (1995)	$v = v_f[1 - e^{\frac{\lvert c_j \rvert}{v_f}(1 - \frac{k_j}{k})}]$	v_f, k_j, c_j

Here c_j is the shock-wave speed at the jam density k_j, and v_m is the optimum speed for a particular roadway.

Actually, under steady traffic conditions, the congested regime in the triangular fundamental diagram can be derived from some car-following models, such as Pipes' model [66], the Optimal Velocity model [5], and Newell's model [62]. Suppose the leading and the following vehicles are labeled as $n-1$ and n, respectively. At time t, the location and speed are denoted as $x_n(t)$ and $v_n(t)$ for the follower, and $x_{n-1}(t)$ and $v_{n-1}(t)$ for the leader, respectively. In Pipes' model [66], the follower's speed at time t is determined by

$$v_n(t) = \frac{1}{\tau}(x_{n-1}(t) - x_n(t) - s_j), \tag{2.32}$$

where τ and s_j are the time gap and the jam spacing, respectively. We know that the spacing between the follower and the leader at time t is $s_n(t) = x_{n-1}(t) - x_n(t)$. Under steady traffic conditions, vehicle's spacing and speeds remain constant over time. Therefore, we have $s_n(t) = s = 1/k$, $s_j = 1/k_j$, and $v_n(t) = v$, where k, k_j, and v are the density, the jam density, and the speed under steady traffic conditions, respectively. So Equation (2.32)

can be written as

$$v = \frac{1}{\tau}(\frac{1}{k} - \frac{1}{k_j}), \tag{2.33}$$

which is the congested part in the triangular fundamental diagram [33] with $\tau = \frac{1}{v_f}(\frac{1}{k_c} - \frac{1}{k_j})$.

2.4.2 Network-based

Fundamental diagrams in Section 2.4.1 are link specific and can not represent traffic characteristics at the network level. In the literature, efforts have been devoted to finding a macroscopic relation between the network-level flow-rate and density. An earlier attempt was made in [29] by considering the town center, Ipswich, as a complex system. The collected data showed that a monotonic decreasing relationship exists between density (concentration) and journey speed. The decreasing trend was further observed in field observations [16, 64] as well as simulations [58]. Recently, using more thorough data (loop detector and taxi GPS data) in Yokohama, Japan, studies in [27] showed that such a network-level functional relation, which is known as the macroscopic or network fundamental diagram (MFD or NFD), exists in urban networks.

In the literature, efforts have been devoted to deriving or approximating the shape of MFDs. Earlier in [36], a two-fluid model was introduced to town traffic by splitting vehicles into two groups: moving and stopped vehicles. Relations among flow, density, and speed were derived by assuming the average speed in an urban network is a function of the fraction of stopped vehicles at any given time. In [12], variational theory was used to approximate the MFD for any multi-block, signal-controlled streets without turning movements. In [35], a utilization-based approach was used to derive the MFD for urban traffic flow. A link-based urban fundamental diagram was derived first and then transfered to an area-based one by assuming all links have the same parameter settings. In [11], a two-bin model was used to

study the possible stationary states in a double-ring network. Multivaluedness and gridlock phenomena were observed in the network flow-density relations. In [49], stationary states were analytically solved in an uninterrupted (i.e., unsignalized) double-ring network within the framework of kinematic wave models. It was found that infinitely many stable states with zero-speed shock waves (ZS) could arise for the same network density in the congested regime, so the corresponding network flow-rates could vary a lot and MFDs would be expected to be very scattered. The aforementioned analytical studies have their limitations. Signal settings and turning movements at intersections are not explicitly considered in [36]. The MFDs in [12, 35] fail to capture the multivaluedness and gridlock phenomena since turning movements at the signalized intersections are not explicitly modeled. The ones in [11, 49] fail to capture the capacity constraints at the signalized intersection since traffic signals are not explicitly modeled. Furthermore, the network flow-rate in the derived or approximated MFDs in the aforementioned studies is only a function of the network density. However, many recent simulation and empirical studies have shown that the MFD is related to many factors, such as spatial variability in congestion and density distributions [6, 40, 28], route choice behaviors [51], signal settings and turning movements [77, 23, 20], and loading and unloading processes [24].

Chapter 3

Traffic statics and dynamics in a signalized double-ring network, part I: A kinematic wave approach

3.1 Introduction

In order to develop effective control and management strategies for urban networks, a fundamental challenge is to understand the static and dynamic properties of urban traffic under various conditions, e.g., different combinations of demand patterns, signal settings, and route choice behaviors. To evaluate the impact of changes (e.g., re-timing the signals) on urban networks, one practical approach is via the macroscopic fundamental diagram (MFD)[12], which is a network-level average flow and density relation under stationary states. However, existing analytical studies on MFDs have their limitations: (i) route choice behaviors were not explicitly modeled in [36, 12, 35]; (ii) signal settings were not explicitly modeled in [36, 11]; and (iii) the study network in [49] is not signalized. Furthermore, the definition of

stationary states in signalized networks is not clear.

In this chapter, we are trying to fill this gap. Both route choice behaviors and signal settings are considered in analyzing the signalized networks. Instead of studying general urban networks, we focus on the signalized 2×2 junction shown in Figure 3.1(a). If exiting vehicles in the downstream are immediately added into the corresponding upstream entrances, the signalized 2×2 junction is further changed into a signalized double-ring network with periodic boundary conditions, which is shown in Figure 3.1(b). In the signalized double-ring network, traffic statics and dynamics are easier to analyze because we only need to keep track of traffic states on the two links. The tangent point represents the signalized junction. The retaining ratios ξ_1 and ξ_2 at the junction are the proportions of vehicles remaining in the same link and closely related to vehicles' route choice behaviors. To describe the traffic dynamics, a continuous kinematic wave approach is used. CTM simulations are used to analyze the existence of stationary states and the impacts of cycle lengths and retaining ratios in the network traffic flow.

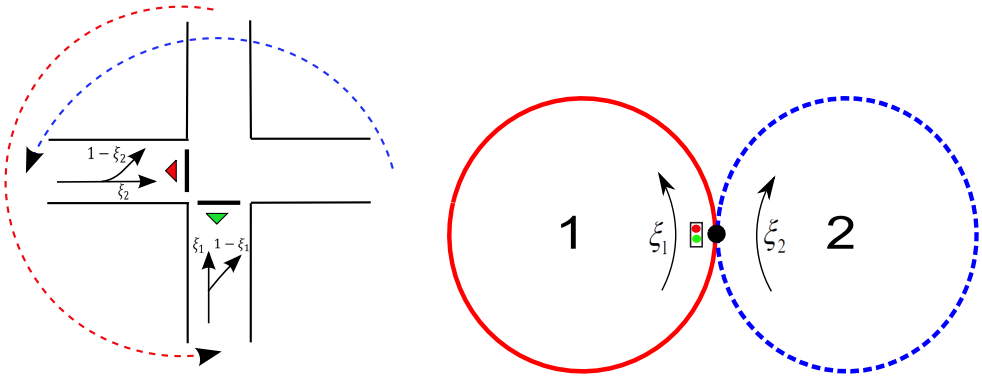

(a) A signalized 2×2 junction (b) An abstract network

Figure 3.1: A signalized double-ring network.

The rest of this chapter is organized as follows. In Section 3.2, we provide a kinematic wave formulation of traffic dynamics in the signalized double-ring network. In Section 3.3, we show periodic traffic patterns in the signalized double-ring network and the impacts of cycle

lengths and retaining ratios on the average network flow-rates using CTM simulations. In Section 3.4, we provide the MFD in asymptotically periodic states. Finally, we draw our conclusions in Section 3.5.

3.2 A kinematic wave formulation of traffic dynamics

In Figure 3.1(b), the left and the right rings are denoted as rings 1 and 2, respectively. We assume both links have the same length L, and the same location-and-time independent fundamental diagram $q_a = Q(k_a), a \in \{1, 2\}$, for $k_a \in [0, k_j]$, where k_j is the jam density. Generally speaking, $Q(k_a)$ is a concave function with its capacity C obtained at the critical density k_c, i.e., $C = Q(k_c)$. For each ring $a \in \{1, 2\}$, the point connecting to the upstream branch of the intersection is denoted as L^-, while the point connecting to the downstream branch is denoted as 0^+. For a point $x_a \in (0, L)$ on ring $a \in \{1, 2\}$ at time t, we have the following variables as functions of (x_a, t): density $k_a(x_a, t)$, speed $v_a(x_a, t)$, flow-rate $q_a(x_a, t)$, demand $d_a(x_a, t)$, and supply $s_a(x_a, t)$. Hereafter, we omit (x_a, t) in these variables unless necessary. Then the local demand and supply are defined as

$$d_a = Q(\min\{k_a, k_c\}) = \begin{cases} Q(k_a), & k_a \in [0, k_c], \\ C, & k_a \in (k_c, k_j], \end{cases} \qquad a = 1, 2 \tag{3.1a}$$

$$s_a = Q(\max\{k_a, k_c\}) = \begin{cases} C, & k_a \in [0, k_c], \\ Q(k_a), & k_a \in (k_c, k_j], \end{cases} \qquad a = 1, 2 \tag{3.1b}$$

Inside link $a \in \{1, 2\}$, the traffic flux function through a point $x_a \in (0, L)$ is given by

$$q_a(x_a, t) = \min\{d_a(x_a^-, t), s_a(x_a^+, t)\}, \tag{3.2}$$

where x_a^- and x_a^+ are the upstream and downstream points of x_a, respectively. At the junction, vehicles in the two upstream approaches move alternately, and therefore, there are two phases in each cycle. Without loss of generality, we assign phase 1 to vehicles in ring 1 and phase 2 to vehicles in ring 2. We assume the cycle length is T with zero lost times and equally split between two rings. Therefore, the signal regulation can be described by the following indicator function:

$$\pi(t) = \begin{cases} 1, & t \in [nT, (n+\frac{1}{2})T), \\ 0, & \text{otherwise}, \end{cases} \qquad n \in \mathbb{N}_0 \tag{3.3}$$

where $\mathbb{N}_0 = \{0, 1, 2, 3, ...\}$.

Due to the signal regulations, the signalized 2×2 junction is equivalent to two alternating diverging junctions, and the invariant first-in-first-out (FIFO) diverging model [10] is used. The retaining ratio is denoted as $\xi_1(t) \in (0, 1)$ for ring 1 and $\xi_2(t) \in (0, 1)$ for ring 2, which means the turning ratio is $1 - \xi_1(t)$ from ring 1 to ring 2 and $1 - \xi_2(t)$ from ring 2 to ring 1. If we assume the retaining ratios at both rings are the same and time independent, i.e., $\xi_1(t) = \xi_2(t) = \xi$, the out-fluxes $g_1(t)$, $g_2(t)$, and the in-fluxes $f_1(t)$, $f_2(t)$ can be calculated as

$$g_1(t) = \pi(t) \min\{d_1(L^-, t), \frac{s_1(0^+, t)}{\xi}, \frac{s_2(0^+, t)}{1-\xi}\}, \tag{3.4a}$$

$$g_2(t) = (1 - \pi(t)) \min\{d_2(L^-, t), \frac{s_2(0^+, t)}{\xi}, \frac{s_1(0^+, t)}{1-\xi}\}, \tag{3.4b}$$

$$f_1(t) = g_1(t)\xi + g_2(t)(1 - \xi), \tag{3.4c}$$

$$f_2(t) = g_1(t)(1 - \xi) + g_2(t)\xi. \tag{3.4d}$$

Traffic dynamics in the double-ring network can be described by the following kinematic

wave model, comprising two LWR models [54, 68]:

$$\frac{\partial k_1}{\partial t} + \frac{\partial Q(k_1)}{\partial x_1} = 0, \tag{3.5a}$$

$$\frac{\partial k_2}{\partial t} + \frac{\partial Q(k_2)}{\partial x_2} = 0. \tag{3.5b}$$

Note that Equation (3.5) is a partial differential equation with periodic forces and thus very difficult to solve analytically. Instead, in the following sections, the cell transmission model (CTM) [9, 10], which is the discrete version of Equation (3.5), will be used to study the static and dynamic properties of traffic in the signalized double-ring network.

3.3 Asymptotically periodic solutions and impacts of cycle lengths and retaining ratios

First, we consider solutions to the kinematic wave model when the retaining ratio is $\xi = 0.85$, and initially two rings have the same constant density of 15 vpm. With $\Delta t = 0.5$ s, we apply the CTM with Equation (3.4) to simulate traffic dynamics in the network for two hours, when traffic dynamics converge to a stable pattern. Figure 3.2 shows the traffic patterns for the last four cycles when $T = 60$ s and $T = 120$ s. In Figures 3.2(a) and 3.2(c), the solid lines are for the normalized out-flux of ring 1, $f_1(t)/C$, and the dashed lines are for the normalized asymptotic network flow-rate, q/C. From the figure, we can see that traffic patterns become periodic after a long time, and the period is the same as the signal's period (Note that the period may not be the same as the cycle length under other conditions). Therefore it is reasonable to consider such asymptotically periodic solutions as stationary states in a signalized network [29]. We also define the asymptotic average fluxes as $\hat{f}_1 = \frac{1}{T}\int_{s=t-T}^{t} f_1(s)ds$, and $\hat{f}_2 = \frac{1}{T}\int_{s=t-T}^{t} f_2(s)ds$, where t is a large time. In this case, the

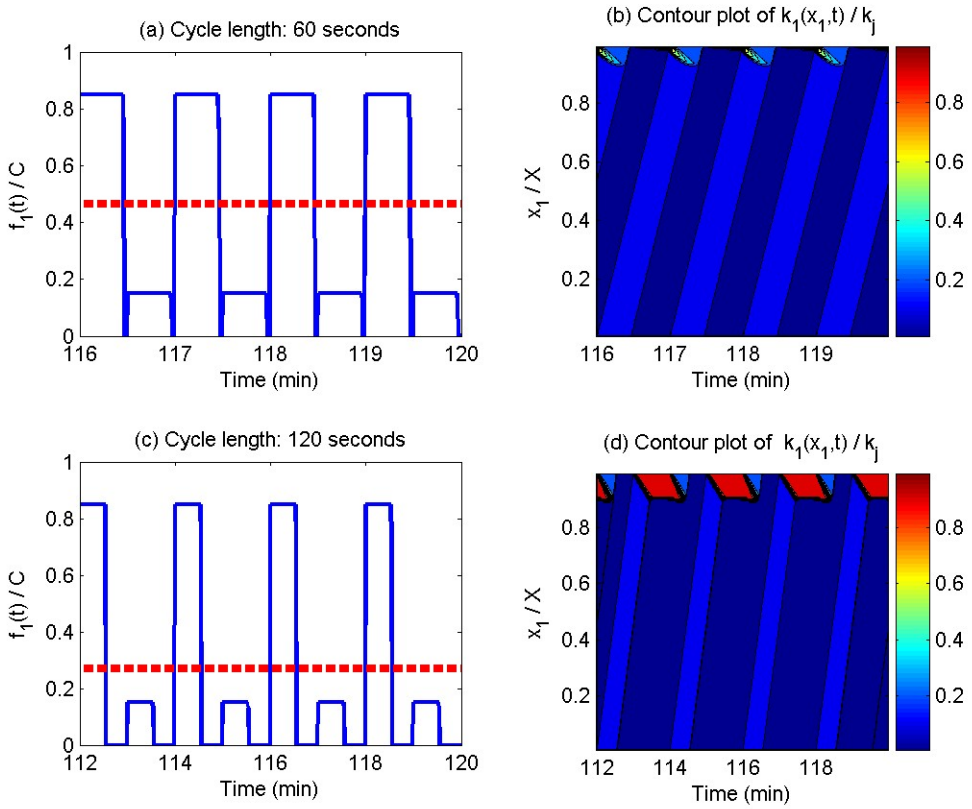

Figure 3.2: Asymptotically periodic traffic patterns in the signalized double-ring network.

asymptotic (stationary) network flow-rate is given by

$$q = \frac{\hat{f}_1 + \hat{f}_2}{2}. \tag{3.6}$$

From Figure 3.2 we can tell that different cycle lengths can lead to totally different traffic patterns and different asymptotic network flow-rate. In Figure 3.3, we demonstrate the relationships between the asymptotic network flow-rate, q, and the cycle length, T, for four densities: 15, 50, 85, and 120 vpm. Here the retaining ratio is 0.85. As expected, the maximum q equals 900 vph, half of the road capacity. However, except for 50 vpm, when the asymptotic network flow-rate is always 900 vph, the relationship between cycle lengths and network flow-rates is quite complicated.

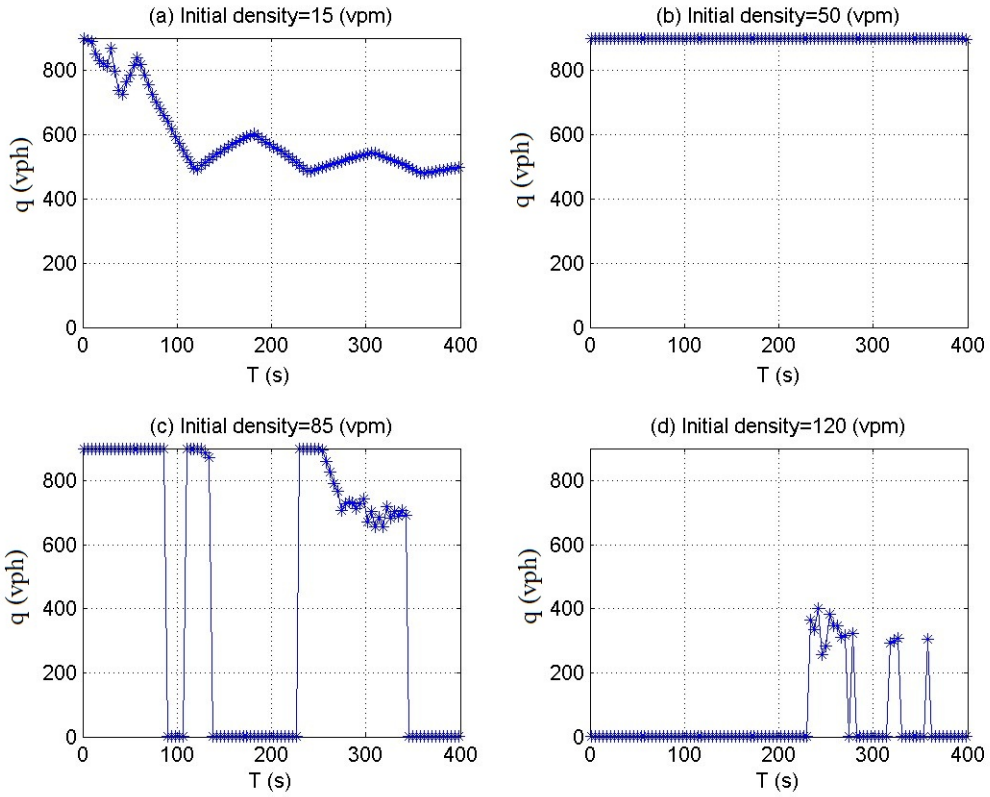

Figure 3.3: Impacts of the cycle length on asymptotic network flow-rates.

In Figure 3.4, we demonstrate the relationships between the asymptotic network flow-rate, q, and the retaining ratio, ξ, for four densities: 15, 50, 85, and 120 vpm. Here the cycle length is 100 s. Except for 50 vpm, when the asymptotic network flow-rate is always 900 vph, generally network flow-rates decrease in retaining ratios. That is, with higher turning proportions (lower retaining ratios), the network operates more efficiently (higher flow-rates). In addition, when $k = 85$ and 120 vpm, the network becomes totally gridlocked with $q = 0$ when the retaining ratio is high. Note that, however, we can have very different patterns for different cycle lengths, as can be expected, including patterns in which network-flow rates increase with retaining ratios.

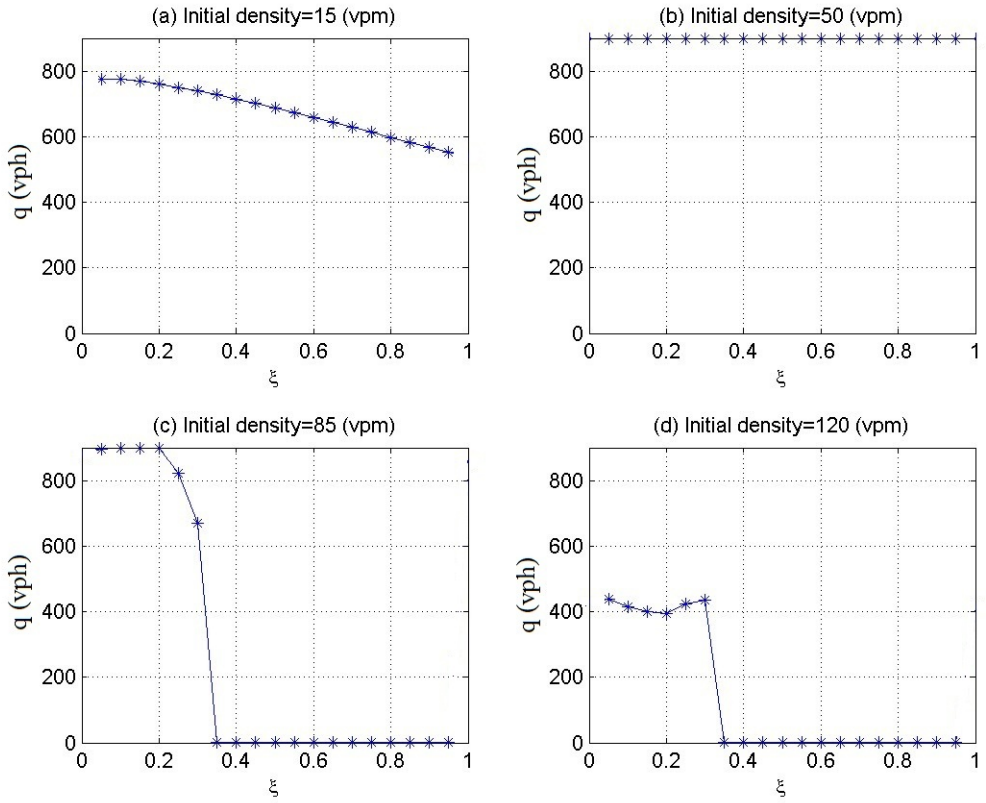

Figure 3.4: Impacts of retaining ratios on asymptotic network flow-rates.

3.4 Macroscopic fundamental diagrams in asymptotically periodic states

When a signalized double-ring network reaches a stationary state, i.e., with asymptotically periodic traffic patterns, we can define the relationship between the asymptotic network flow-rate, q, and the traffic density, k, as the corresponding macroscopic fundamental diagram of the signalized network.

In Figure 3.5, we present the macroscopic fundamental diagram when the retaining ratio is $\xi = 0.85$ and the cycle length is $T = 100$ sec. For the same traffic density, we use different combinations of initial densities, k_1 and k_2, on the two rings. Note that gridlock states

can be considered as special cases of asymptotically periodic states, but in the figure we separate gridlock states from non-gridlock, periodic states. Also plotted on Figure 3.5(a) is the theoretical MFD expected from this system using the variational theory method from [12] for comparison with the kinematic wave results. Note that the variational theory in [12] was proposed for a ring road with multiple signals and cannot capture the interactions among traffic streams at the junction. This can explain why the variational theory cannot capture the asymmetric traffic patterns, including the gridlock states occurring at a density smaller than the jam density.

From Figure 3.5(a) we have the following observations: (i) the MFD is well defined for a signalized network; (ii) the $q - k$ relation is unique for $k \leq 52.5$ vpm and $k \geq 82$ vpm, but has two branches between the two values; (iii) the network can be easily gridlocked when $k \geq k_j/2$. This MFD is significantly different from the MFD for uninterrupted network in [49]: the flow-rates in the signalized network are lower and can only reach half of the capacity in the uninterrupted cases, as would be expected. For low densities, a single stationary state exists where average flows are non-decreasing with density. However, for higher densities a bifurcation occurs. For densities greater than this bifurcation, two unique branches exist on the MFD. In one branch, high flows (of 900 vph) can be maintained for a small range of densities. In the other branch, flow declines with density until the network eventually gridlocks. In both cases, there is a critical density for which gridlock is the only stationary state that exists. Also note that for low densities the average flows are close to but not exactly equal to the flows predicted by the variational theory methodology in [12], because turning maneuvers and conflicting traffic streams were ignored. These results highlight the importance of properly accounting for traffic dynamics at the junction, as it can influence the functional form of the MFD.

In Figure 3.5(b), where the arrows show the convergence directions of traffic densities, we demonstrate the convergence patterns of the stationary states under different initial con-

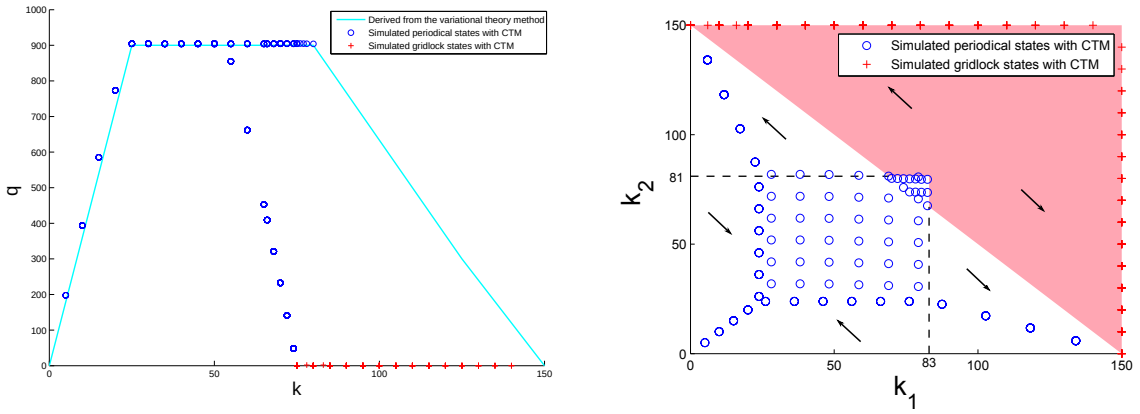

(a) $q - k$ relation

(b) Convergence patterns

Figure 3.5: The macroscopic fundamental diagram with $\xi = 0.85$ and $T = 100$ secs.

ditions: (i) when the average network density $k < k_j/2$, all initial states will converge to periodical states after some time; and (ii) when $k \geq k_j/2$, all initial states inside the shaded region will finally converge to gridlock states while the rest of them will converge to periodical states. For example, with the interactive simulator available at `http://www.ce.berkeley.edu/~daganzo/Simulations/two_ring_sim.html`, if we set $N = 62$, $P_T = 0.15$ (the turning proportion equals 1-ξ), and $T = 100$ s, periodic traffic patterns can be observed after a long time (e.g., more than 1000 minutes). In addition, we can see that the gridlock states are asymptotically stable in a signalized network. These results further validate the kinematic wave approach developed in this study and also illustrates the analytical and computational advantage of the new approach, which can provide us a more complete picture of traffic dynamics with a higher efficiency.

As discussed in the preceding section, different retaining ratios and cycle lengths would lead to different MFDs, but they share the same qualitative properties as those in Figure 3.5.

3.5 Conclusions

In this chapter, we formulated the traffic dynamics in a signalized double-ring network using the kinematic wave approach. Asymptotic periodic traffic patterns were found using CTM simulations and thus defined as stationary states. Simulation results also revealed that cycle lengths and retaining ratios play an important role in the signalized double-ring network: different retaining ratios (or cycle lengths) can yield different average network flow-rates even starting with the same initial densities and cycle lengths (or retaining ratios). The MFD of the signalized double-ring network was obtained using simulations and compared with the one obtained from the variational theory method. The comparison showed that more stationary traffic states can be observed using the kinematic wave model: multivaluedness and gridlock phenomena in the MFD can be observed.

However, due to infinite-dimensional state variables introduced by the kinematic wave model, it is very difficult to analytically solve the static and dynamic properties of traffic flow in the signalized double-ring network with the existence of traffic signals. Therefore, in the next chapter, we will provide an analytical framework to aggregate the traffic dynamics at the link level and solve possible stationary states and their stability properties under different combinations of cycle lengths, retaining ratios, and demand patterns.

Chapter 4

Traffic statics and dynamics in a signalized double-ring network, part II: A Poincaré map approach

4.1 Introduction

In this chapter, instead of using the kinematic wave model to describe detailed traffic dynamics inside a link, we use the link queue model in [43] to aggregate the traffic dynamics at the link level. With the assumption of a triangular traffic flow fundamental diagram [33], the signalized double-ring network is further formulated as a switched affine system. The switching rule is governed by three sets of parameters: initial densities, route choice behaviors, and signal settings. Periodic density evolution orbits are found and defined as stationary states. A Poincaré map approach [76, 74] is used to study the properties of such stationary states. Poincaré map was originally used to study the movements of celestial bodies and is a very important tool in analyzing periodic orbits: each periodic orbit corresponds to a fixed point

on the Poincaré map, and its stability is directly related to the stability of the fixed point. In [45], Poincaré map has been applied to study the stability and bifurcation of network traffic flow in diverge-merge networks. With short cycle lengths, closed-form Poincaré maps are derived, and stationary states and the corresponding stabilities are obtained by solving and analyzing the fixed points on the Poincaré maps. The impacts of retaining ratios and initial densities on the MFDs and the gridlock times are analyzed. With long cycle lengths, closed-form Poincaré maps are hard to obtain, and thus, the corresponding fixed points are numerically solved using the secant method [19].

The rest of this chapter is organized as follows. In Section 4.2, we aggregate the traffic dynamics in the signalized double-ring network using the link queue model. We further change the network as a switched affine system when the triangular traffic flow fundamental diagram is used. In Section 4.3, we derive the Poincaré maps from the density evolution orbits in the switched affine system. Stationary states and their stability properties are defined in terms of the fixed points and their stability properties on the Poincaré maps. In Section 4.4, we solve the stationary states and the corresponding stability properties with short cycle lengths. In Section 4.5, we discuss the impacts of retaining ratios and initial densities on the MFDs and the gridlock times. In Section 4.6, we provide numerical solutions to the fixed points on the Poincaré maps when the cycle lengths are long. Finally, we draw our conclusions in Section 4.7.

4.2 A link queue formulation and a switched affine system

4.2.1 A link queue formulation

According to the link queue model (LQM) [43], vehicles on a link is considered as a queue, and therefore, each link has only one state variable, the average link density. The left and the right rings in Figure 3.1 are denoted as rings 1 and 2 with average densities $k_1(t)$ and $k_2(t)$, respectively. We assume both rings have the same length L. Since it is a closed network, we have $k_1(t) + k_2(t) = 2k$, where k is the average network density. In addition, we assume both rings have the same location-and-time independent fundamental diagram, $q_a = Q(k_a)$, $a = 1, 2$, for $k_a \in [0, k_j]$, where k_j is the jam density. Generally speaking, $Q_a(k_a)$ is a concave function with its capacity C obtained at the critical density k_c, i.e., $C = Q(k_c)$. Then the local demand and supply are defined as

$$D_a(t) = Q(\min\{k_a(t), k_c\}) = \begin{cases} Q(k_a(t)), & k_a(t) \in [0, k_c], \\ C, & k_a(t) \in (k_c, k_j], \end{cases} \qquad a = 1, 2 \tag{4.1a}$$

$$S_a(t) = Q(\max\{k_a(t), k_c\}) = \begin{cases} C, & k_a(t) \in [0, k_c], \\ Q(k_a(t)), & k_a(t) \in (k_c, k_j], \end{cases} \qquad a = 1, 2 \tag{4.1b}$$

At the junction, vehicles in the two upstream approaches move alternately, and therefore, there are two phases in each cycle. Without loss of generality, we assign phase 1 to vehicles in ring 1 and phase 2 to vehicles in ring 2. The cycle length is T with a lost time Δ for each phase. The green ratio is denoted as π_1 for ring 1 and π_2 for ring 2. We assume the yellow and all red period in each phase is the same as the lost time, and therefore, the effective green time is $\pi_1 T$ for ring 1 and $\pi_2 T$ for ring 2, and $(\pi_1 + \pi_2)T = T - 2\Delta$. Then the signal

regulation can be described by the following two indicator functions:

$$\delta_1(t;T,\Delta,\pi_1) = \begin{cases} 1, & t \in [nT, nT+\pi_1 T), \\ 0, & \text{otherwise}, \end{cases} \qquad n \in \mathbb{N}_0 \tag{4.2a}$$

$$\delta_2(t;T,\Delta,\pi_1) = \begin{cases} 1, & t \in [nT+\Delta+\pi_1 T, (n+1)T-\Delta), \\ 0, & \text{otherwise}, \end{cases} \qquad n \in \mathbb{N}_0 \tag{4.2b}$$

where $\mathbb{N}_0 = \{0, 1, 2, 3, ...\}$. According to Equation (4.2), we have three different combinations of $(\delta_1(t), \delta_2(t))$ within one cycle: (i) $(1, 0)$ stands for the effective green time period in phase 1; (ii) $(0, 1)$ stands for the effective green time period in phase 2; (iii) $(0, 0)$ stands for the lost time period in either of the phases.

Due to the signal regulations, the signalized 2×2 junction is equivalent to two alternating diverging junctions, and the invariant first-in-first-out (FIFO) diverging model [10] is used. The retaining ratio is denoted as $\xi_1(t) \in (0, 1)$ for ring 1 and $\xi_2(t) \in (0, 1)$ for ring 2, which means the turning ratio is $1 - \xi_1(t)$ from ring 1 to ring 2 and $1 - \xi_2(t)$ from ring 2 to ring 1. Then the out-fluxes $g_1(t)$, $g_2(t)$, and the in-fluxes $f_1(t)$, $f_2(t)$ can be calculated as

$$g_1(t) = \delta_1(t) \min\{D_1(t), \frac{S_1(t)}{\xi_1(t)}, \frac{S_2(t)}{1-\xi_1(t)}\}, \tag{4.3a}$$

$$g_2(t) = \delta_2(t) \min\{D_2(t), \frac{S_2(t)}{\xi_2(t)}, \frac{S_1(t)}{1-\xi_2(t)}\}, \tag{4.3b}$$

$$f_1(t) = g_1(t)\xi_1(t) + g_2(t)(1-\xi_2(t)), \tag{4.3c}$$

$$f_2(t) = g_1(t)(1-\xi_1(t)) + g_2(t)\xi_2(t). \tag{4.3d}$$

Since it is a closed network, we only need to focus on the traffic dynamics in one of the rings,

e.g., ring 1. According to the traffic conservation in ring 1, the following equation holds:

$$\frac{dk_1(t)}{dt} = \frac{1}{L}(f_1(t) - g_1(t)) = \frac{-(1-\xi_1(t))}{L}g_1(t) + \frac{(1-\xi_2(t))}{L}g_2(t). \tag{4.4}$$

With Equations (4.1) to (4.4), the system equation can be written as

$$\frac{dk_1(t)}{dt} = F(k_1(t); k, \delta_1(t), \delta_2(t), \xi_1(t), \xi_2(t)), \tag{4.5}$$

which is closely related to the average network density k, the signal settings $(\delta_1(t), \delta_2(t))$, and the route choice behaviors $(\xi_1(t), \xi_2(t))$. Note that Equation (4.5) is a nonlinear ordinary differential equation (ODE) with periodic forces. It is simpler than the kinematic wave model (Equation (3) in [49]), which is a partial differential equation (PDE), but still quite challenging to solve.

4.2.2 A switched affine system

In this chapter, the following triangular traffic flow fundamental diagram [33] is used.

$$Q(k_a) = \min\{v_f k_a, w(k_j - k_a)\}, \qquad a = 1, 2, \tag{4.6}$$

where v_f and w are the free-flow speed and the shock-wave speed, respectively. Then the signalized double-ring network can be further formulated as a switched affine system [17, 73], and the traffic dynamics in Equation (4.5) can be rewritten as

$$\frac{dk_1(t)}{dt} = A_i k_1(t) + B_i, \qquad i \in I = \{1, ..., N\}, \tag{4.7}$$

where N is the number of possible combinations of (A_i, B_i). In Equation (4.7), the switching rule for coefficients (A_i, B_i) is governed by three sets of parameters: the initial densities

$(k_1(t), k)$, the signal settings $(\delta_1(t), \delta_2(t))$, and the route choice behaviors $(\xi_1(t), \xi_2(t))$.

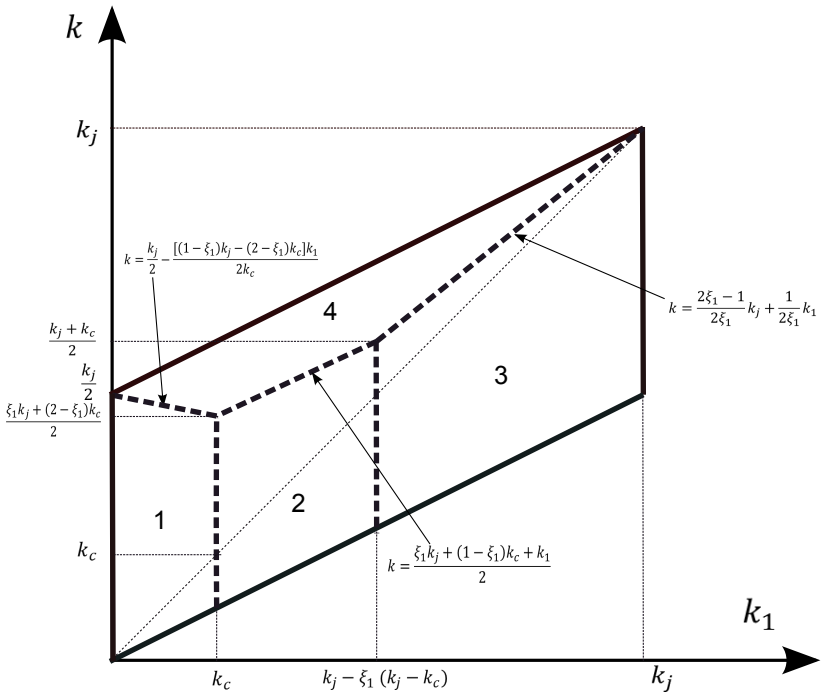

(a) $(\delta_1(t), \delta_2(t)) = (1, 0)$

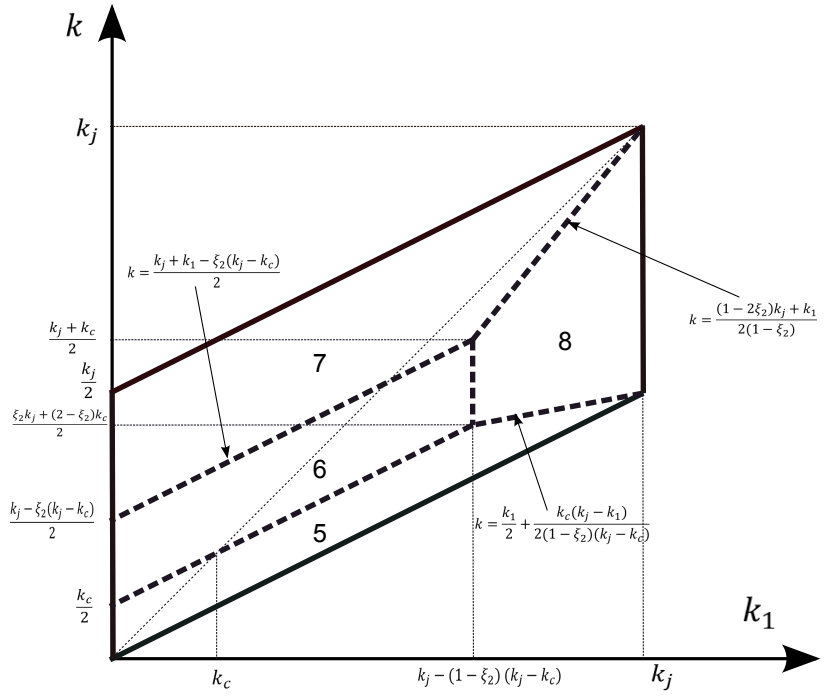

(b) $(\delta_1(t), \delta_2(t)) = (0, 1)$

Figure 4.1: Regions in the (k_1, k) space.

Since densities in both rings vary during the effective green times, the (k_1, k) space can be divided into different regions, in which the coefficients (A_i, B_i) remain the same. According to Equations (4.1), (4.3), and (4.6), the (k_1, k) space can be divided into four regions when $(\delta_1(t), \delta_2(t)) = (1, 0)$, which are provided in Figure 4.1(a). The meanings of the bold dashed lines in Figure 4.1(a) are explained as follows:

(i) the line $k = \frac{k_j}{2} - \frac{[(1-\xi_1)k_j-(2-\xi_1)k_c]k_1}{2k_c}$ stands for the case when $D_1 = \frac{S_2}{1-\xi_1} < C < \frac{S_1}{\xi_1}$;

(ii) the line $k = \frac{\xi_1 k_j+(1-\xi_1)k_c+k_1}{2}$ stands for the case when $D_1 = \frac{S_2}{1-\xi_1} = C < \frac{S_1}{\xi_1}$;

(iii) the line $k = \frac{2\xi_1-1}{2\xi_1}k_j + \frac{1}{2\xi_1}k_1$ stands for the case when $\frac{S_1}{\xi_1} = \frac{S_2}{1-\xi_1} < D_1 = C$;

(iv) the line $k_1 = k_j - \xi_1(k_j - k_c)$ stands for the case when $D_1 = \frac{S_1}{\xi_1} = C < \frac{S_2}{1-\xi_1}$.

Similarly, the (k_1, k) space can be divided into another four regions when $(\delta_1(t), \delta_2(t)) = (0, 1)$, which are provided in Figure 4.1(b). The meanings of the bold dashed lines in Figure 4.1(b) are provided below:

(i) the line $k = \frac{k_j+k_1-\xi_2(k_j-k_c)}{2}$ stands for the case when $D_2 = \frac{S_2}{\xi_2} = C < \frac{S_1}{1-\xi_2}$;

(ii) the line $k = \frac{(1-2\xi_2)k_j+k_1}{2(1-\xi_2)}$ stands for the case when $\frac{S_2}{\xi_2} = \frac{S_1}{1-\xi_2} < D_2 = C$;

(iii) the line $k = \frac{k_1}{2} + \frac{k_c(k_j-k_1)}{2(1-\xi_2)(k_j-k_c)}$ stands for the case when $D_2 = \frac{S_1}{1-\xi_2} < C < \frac{S_2}{\xi_2}$;

(iv) the line $k_1 = k_j - (1 - \xi_2)(k_j - k_c)$ stands for the case when $D_2 = \frac{S_1}{(1-\xi_2)} = C < \frac{S_2}{\xi_2}$.

In addition, for each cycle, we have two lost time periods (i.e., $(\delta_1(t), \delta_2(t)) = (0, 0)$), which have the same coefficients in Equation (4.7) (i.e., $(A_i, B_i) = (0, 0)$). But these two periods are physically different since one is the transition period from $(1, 0)$ to $(0, 1)$, while the other is from $(0, 1)$ to $(1, 0)$. So we consider they belong to two different regions, in which the densities remain unchanged. Then, we have $N = 10$. The possible values of A_i and B_i and the corresponding conditions are provided in Table 4.1.

Table 4.1: Possible values of A_i and B_i and the corresponding conditions

Region (i)	A_i	B_i	Conditions
1	$-\gamma_1$	0	$(\delta_1(t),\delta_2(t))=(1,0)$, $0<k_1<k_c$, $\frac{k_1}{2}\le k\le \frac{k_j}{2}-\frac{((1-\xi_1)k_j-(2-\xi_1)k_c)k_1}{2k_c}$
2	0	$-\gamma_1 k_c$	$(\delta_1(t),\delta_2(t))=(1,0)$, $k_c\le k_1<k_j-\xi_1(k_j-k_c)$, $\frac{k_1}{2}\le k\le \frac{\xi_1 k_j+(1-\xi_1)k_c+k_1}{2}$
3	γ_2	$-\gamma_2 k_j$	$(\delta_1(t),\delta_2(t))=(1,0)$, $k_j-\xi_1(k_j-k_c)\le k_1\le k_j$, $\frac{k_1}{2}\le k\le \frac{2\xi_1-1}{2\xi_1}k_j+\frac{1}{2\xi_1}k_1$
4	$-\gamma_3$	$-\gamma_3(k_j-2k)$	$(\delta_1(t),\delta_2(t))=(1,0)$, $0<k_1<k_j$ $\max\{\frac{k_j}{2}-\frac{[(1-\xi_1)k_j-(2-\xi_1)k_c]k_1}{2k_c},\frac{\xi_1 k_j+(1-\xi_1)k_c+k_1}{2},\frac{2\xi_1-1}{2\xi_1}k_j+\frac{1}{2\xi_1}k_1\}<k\le\frac{k_j+k_1}{2}$
5	-γ_4	$2k\gamma_4$	$(\delta_1(t),\delta_2(t))=(0,1)$, $0\le k_1\le k_j$, $\frac{k_1}{2}\le k\le \min\{\frac{k_1+k_c}{2},\frac{k_1}{2}+\frac{k_c(k_j-k_1)}{2(1-\xi_2)(k_j-k_c)}\}$
6	0	$\gamma_4 k_c$	$(\delta_1(t),\delta_2(t))=(0,1)$, $0\le k_1\le k_j-(1-\xi_2)(k_j-k_c)$, $\frac{k_1+k_c}{2}<k\le\frac{k_j+k_1-\xi_2(k_j-k_c)}{2}$
7	γ_5	$\gamma_5(k_j-2k)$	$(\delta_1(t),\delta_2(t))=(0,1)$, $0\le k_1\le k_j$, $\max\{\frac{k_j+k_1-\xi_2(k_j-k_c)}{2},\frac{(1-2\xi_2)k_j+k_1}{2(1-\xi_2)}\}<k\le\frac{k_1+k_j}{2}$
8	$-\gamma_3$	$\gamma_3 k_j$	$(\delta_1(t),\delta_2(t))=(0,1)$, $k_j-(1-\xi_2)(k_j-k_c)<k_1\le k_j$ $\frac{k_1}{2}+\frac{k_c(k_j-k_1)}{2(1-\xi_2)(k_j-k_c)}<k<\frac{(1-2\xi_2)k_j+k_1}{2(1-\xi_2)}$
9	0	0	$(\delta_1(t),\delta_2(t))=(0,0)$, and transition from $(\delta_1(t),\delta_2(t))=(1,0)$
10	0	0	$(\delta_1(t),\delta_2(t))=(0,0)$, and transition from $(\delta_1(t),\delta_2(t))=(0,1)$

where $\gamma_1=\frac{(1-\xi_1)v_f}{L}$, $\gamma_2=\frac{(1-\xi_1)v_f k_c}{L\xi_1(k_j-k_c)}$, $\gamma_3=\frac{v_f k_c}{L(k_j-k_c)}$, $\gamma_4=\frac{(1-\xi_2)v_f}{L}$, and $\gamma_5=\frac{(1-\xi_2)v_f k_c}{L\xi_2(k_j-k_c)}$.

4.3 Periodic density evolution orbits and derivation of Poincaré maps

4.3.1 Periodic density evolution orbits

Due to the periodic signal regulations, the switched affine system periodically visits the (k_1, k) space in Figure 4.1, and therefore, density evolution orbits are formed. The circulating period is fixed, which is the cycle length T. In Figure 4.2(a), we provide the density evolution orbit within one cycle in the (k_1, k) space. And also, since it is a closed network (i.e., k is fixed once it is given), we can map the density evolution orbit to the k_1 axis, which is shown in Figure 4.2(b). The evolution process can be described as follows:

(1) At the beginning of the cycle at time t, the initial densities are denoted as $(k_1(t), k)$. During $[t, t + \pi_1 T)$, we have $(\delta_1, \delta_2) = (1, 0)$. The density k_1 decreases as time elapses since vehicles in ring 1 can diverge to either of the rings while vehicles in ring 2 have to wait. The density evolution may cross multiple regions during this time period, i.e., $i \in [1, 4]$ in Table 4.1.

(2) At time $t + \pi_1 T$, the system switches to region 9. During $[t + \pi_1 T, t + \pi_1 T + \Delta)$, we have $(\delta_1, \delta_2) = (0, 0)$. The densities in both rings remain the same since no vehicles can move to the downstream approaches.

(3) At time $t + \pi_1 T + \Delta$, the system switches to phase 2. During $[t + \pi_1 T + \Delta, t + T - \Delta)$, we have $(\delta_1, \delta_2) = (0, 1)$. The density k_1 increases as time elapses since vehicles in ring 2 are allowed to diverge to either of the rings while vehicles in ring 1 have to wait. Similarly, the density evolution may cross multiple regions during this time period, i.e., $i \in [5, 8]$ in Table 4.1.

(4) At time $t + T - \Delta$, the system switches to region 10. During $[t + T - \Delta, t + T)$,

$(\delta_1, \delta_2) = (0, 0)$ and the density in ring 1 remains the same.

(5) At $t + T$, the system switches back to Step (1) with $(\delta_1, \delta_2) = (1, 0)$. The densities become $(k_1(t + T), k)$ and serve as new initial densities in the next cycle.

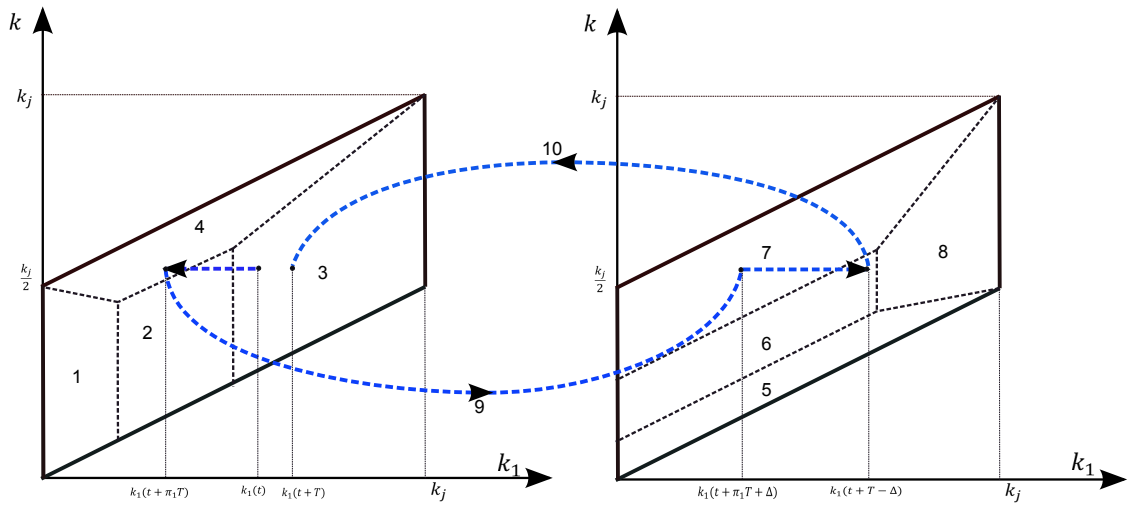

(a) In the (k_1, k) space

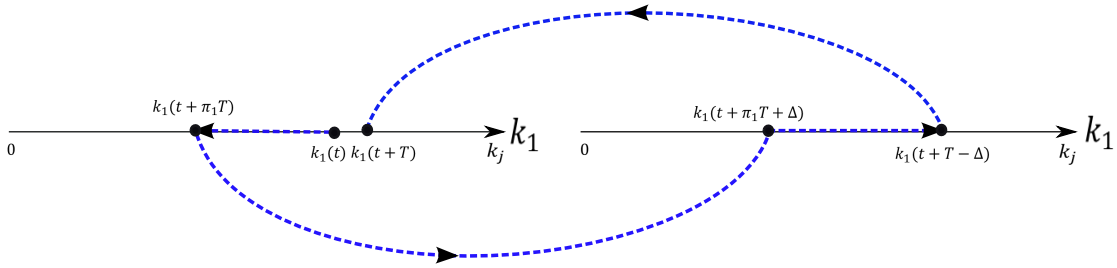

(b) In the mapping of k_1

Figure 4.2: The density evolution orbit within one cycle.

Based on the above description, it is possible for the signalized double-ring network to have periodic density evolution orbits if $k_1(t+T) = k_1(t)$. Such periodic patterns were observed in the simulations in [49] and defined as stationary states. To calculate the asymptotic average

network flow-rate, the following equation was used in [49]:

$$q(t) = \frac{\hat{g}_1(t) + \hat{g}_2(t)}{2} = \frac{\int_{s=t-T}^{t} g_1(s)ds + \int_{s=t-T}^{t} g_2(s)ds}{2T}. \tag{4.8}$$

When the system reaches a stationary state, $q(t)$ becomes a constant value, which depends on the average network density; i.e., $q(t)|_{t\to+\infty} = q(k)$. Then the relation between $q(k)$ and k is the MFD for the signalized double-ring network.

4.3.2 Derivation of Poincaré maps

In the following we study the static and dynamic properties associated with the density evolution orbits in terms of Poincaré maps. According to the discussion in Section 4.3.1, the density evolution orbit for each cycle is combined with the following four local maps, P_i, $i = 1, 2, 3, 4$:

$$k_1(t + \pi_1 T) = P_1 k_1(t), \tag{4.9a}$$

$$k_1(t + \pi_1 T + \Delta) = P_2 k_1(t + \pi_1 T), \tag{4.9b}$$

$$k_1(t + T - \Delta) = P_3 k_1(t + \pi_1 T + \Delta), \tag{4.9c}$$

$$k_1(t + T) = P_4 k_1(t + T - \Delta). \tag{4.9d}$$

If we define the Poincaré section as the time instant when the system first visits the (k_1, k) space in Figure 4.2(a) in each cycle, i.e., the beginning of each cycle, the Poincaré map can be derived as the composition of the four local maps.

$$k_1(t + T) = P k_1(t) = P_4 \circ P_3 \circ P_2 \circ P_1 k_1(t). \tag{4.10}$$

The Poincaré map in Equation (4.10) is well defined and can be analytically derived if initial densities, retaining ratios, and signal settings are given. Then we can have the following definition of stationary states:

Definition 4.1 (Stationary states)**.** *The signalized double-ring network is in a stationary state when there exists a fixed point k_1^* on the Poincaré map $Pk_1(t)$ satisfying $k_1^* = Pk_1^*$.*

Due to the existence of noise in transportation networks, it is necessary to understand the stability properties of stationary states. Suppose at the beginning of one cycle, there exists a perturbation that drives the density in link 1 from k_1^* to $k_1(t) = k_1^* + \epsilon(t)$, where $\epsilon(t)$ is a small error term. Then after n cycles, the density in ring 1 and the error term become

$$k_1(t + nT) = P^n k_1(t), \qquad n \in \mathbb{N}_0 \tag{4.11a}$$

$$\epsilon(t + nT) = P^n k_1(t) - k_1^* = (\partial P)^n \epsilon(t), \qquad n \in \mathbb{N}_0 \tag{4.11b}$$

According to [52, 74], we have the following definition of stability for the fixed points on the Poincaré maps:

Definition 4.2 (Local stability)**.** *The fixed point k_1^* is: (i) Lyapunov stable if for any given $\beta > 0$, there exists an $\omega \leq \beta$ such that $|\epsilon(t + nT)| < \beta$ for any $|\epsilon(t)| < \omega$ and $n \in \mathbb{N}_0$; (ii) unstable otherwise. Furthermore, k_1^* is asymptotically stable if it is stable and $\epsilon(t+nT) \to 0$ as $n \to +\infty$.*

4.4 Stationary states and their stability properties with short cycle lengths

In this section, we are going to consider the case with short cycle lengths, as we will be able to derive closed-form Poincaré maps. For simplicity, we consider the following homogeneous

settings in the rest of the chapter: both rings have the same effective green times, i.e., $\pi_2 = \pi_1 = \pi$, and the same time-independent retaining ratios, i.e., $\xi_1 = \xi_2 = \xi$.

4.4.1 Possible stationary states

With short cycle lengths, the density evolution orbit will stay in region $i \in \{1, 2, 3, 4\}$ when $(\delta_1, \delta_2) = (1, 0)$, and in region $j \in \{5, 6, 7, 8\}$ when $(\delta_1, \delta_2) = (0, 1)$. Under different retaining ratios, e.g., $\xi > 0.5$ and $\xi < 0.5$, we have 11 different combinations of regions in one cycle, which are provided in Table 4.2. Here, we define the sum of the coefficients (A_i, B_i) and (A_j, B_j) as

$$\lambda(k_1, k) = A_j k_1 + B_j + A_i k_1 + B_i. \tag{4.12}$$

When traffic is not jammed, if $\lambda(k_1, k)$ is always greater or smaller than zero, k_1 will keep increasing or decreasing, which means it is impossible to have stationary states with the combination of regions (i, j). But if $\lambda(k_1, k)$ can take both positive and negative values or is always zero, it is possible to have stationary states inside the combination of regions (i, j). In Table 4.2, we provide possible values of $\lambda(k_1, k)$ and the corresponding conditions for different combinations of regions under different retaining ratios. Specifically, when $\xi = 0.5$, we only have the following combinations of regions (i, j): $(1, 5)$, $(1, 6)$, $(1, 7)$, $(2, 5)$, $(2, 6)$, $(4, 7)$, $(3, 5)$, and $(3, 8)$. The values of $\lambda(k_1, k)$ and the corresponding conditions in regions $(1, 5)$, $(1, 6)$, $(1, 7)$, $(2, 5)$, $(2, 6)$, and $(3, 5)$ are the same as those with $\xi < 0.5$ in Table 4.2. However, the values of $\lambda(k_1, k)$ in regions $(4, 7)$ and $(3, 8)$ are always zero with $\xi = 0.5$. Therefore, we have the following lemma:

Lemma 4.1 (Possible regions having stationary states)**.** *When traffic is not jammed, it is only possible for the following combinations of regions (i, j) to have stationary states:*

Table 4.2: Possible values of $\lambda(k_1, k)$ in the 11 combinations of regions

$0.5 < \xi < 1$			$0 < \xi < 0.5$		
Regions	$\lambda(k_1,k)$	Condition	Regions	$\lambda(k_1,k)$	Condition
$(1,5)$	> 0	$k_1 < k$	$(1,5)$	> 0	$k_1 < k$
	$= 0$	$k_1 = k$		$= 0$	$k_1 = k$
	< 0	$k_1 > k$		< 0	$k_1 > k$
$(1,6)$	> 0		$(1,6)$	> 0	
$(1,7)$	> 0	$\gamma_1 < \gamma_5$ or $\gamma_1 > \gamma_5$ and $k_1 < \frac{\gamma_5(k_j-2k)}{\gamma_1-\gamma_5}$	$(1,7)$	> 0	
	$= 0$	$\gamma_1 > \gamma_5$ and $k_1 = \frac{\gamma_5(k_j-2k)}{\gamma_1-\gamma_5}$			
	< 0	$\gamma_1 > \gamma_5$ and $k_1 > \frac{\gamma_5(k_j-2k)}{\gamma_1-\gamma_5}$			
$(2,5)$	< 0		$(2,5)$	< 0	
$(2,6)$	$= 0$		$(2,6)$	$= 0$	
$(2,7)$	< 0		$(4,6)$	> 0	
$(4,7)$	< 0		$(4,7)$	> 0	
$(3,5)$	> 0	$\gamma_2 < \gamma_4$ and $k_1 < \frac{2k\frac{\xi(k_j-k_c)}{k_c}-k_j}{\frac{\xi(k_j-k_c)}{k_c}-1}$	$(3,5)$	< 0	
	$= 0$	$\gamma_2 < \gamma_4$ and $k_1 = \frac{2k\frac{\xi(k_j-k_c)}{k_c}-k_j}{\frac{\xi(k_j-k_c)}{k_c}-1}$			
	< 0	$\gamma_2 < \gamma_4$ and $k_1 > \frac{2k\frac{\xi(k_j-k_c)}{k_c}-k_j}{\frac{\xi(k_j-k_c)}{k_c}-1}$ or $\gamma_2 > \gamma_4$			
$(3,6)$	> 0		$(2,8)$	< 0	
$(3,7)$	> 0	$k_1 > k$	$(4,8)$	> 0	$k_1 < k$
	$= 0$	$k_1 = k$		$= 0$	$k_1 = k$
	< 0	$k_1 < k$		< 0	$k_1 > k$
$(3,8)$	> 0		$(3,8)$	< 0	

(i) $(1,5)$, $(1,7)$, $(2,6)$, $(3,5)$, *and* $(3,7)$ *for* $0.5 < \xi < 1$*;*

(ii) $(1,5)$, $(2,6)$, *and* $(4,8)$ *for* $0 < \xi < 0.5$*;*

(iii) $(1,5)$, $(2,6)$, $(4,7)$, *and* $(3,8)$ *for* $\xi = 0.5$.

However, when traffic is jammed, it is only possible for the combinations of regions $(4,7)$ *and* $(3,8)$ *to have stationary states with any* $\xi \in (0,1)$.

The proof is simple and thus omitted here. Note that when the network is gridlocked with at least one ring jammed, the gridlock states are stationary states since they satisfy Definition

4.1. It is easy to identify that these stationary states are inside the combinations of regions $(4, 7)$ and $(3, 8)$.

After identifying the possible combinations of regions having stationary states, we can analytically derive the closed-form Poincaré maps. The corresponding fixed points are the stationary states we are interested in. Therefore, we have the following theorem:

Theorem 4.1 (Possible stationary states)**.** *According to Equation (4.7) and Table 4.1, the Poincaré maps and the corresponding fixed points in the possible regions having stationary states are derived and provided in Table 4.3.*

Table 4.3: Poincaré maps and fixed points in the possible regions having stationary states

Regions	Poincaré map $Pk_1(t)$ with $0.5 < \xi < 1$	Fixed points k_1^*
$(1, 5)$	$2k(1 - e^{-\gamma_1 \pi T}) + k_1(t)e^{-2\gamma_1 \pi T}$	$\frac{2k}{1+e^{-\gamma_1 \pi T}}$
$(1, 7)$	$(k_j - 2k)(e^{\gamma_5 \pi T} - 1) + k_1(t)e^{(\gamma_5 - \gamma_1)\pi T}$	$\frac{(k_j - 2k)(e^{\gamma_5 \pi T} - 1)}{1-e^{(\gamma_5 - \gamma_1)\pi T}}$
$(2, 6)$	$k_1(t)$	$k_1(t)$
$(4, 7)$	$(k_j - 2k)(e^{(\gamma_5 - \gamma_3)\pi T} - 1) + k_1(t)e^{(\gamma_5 - \gamma_3)\pi T}$	$2k - k_j$
$(3, 5)$	$k_j(1 - e^{\gamma_2 \pi T})e^{-\gamma_4 \pi T} + 2k(1 - e^{-\gamma_4 \pi T}) + k_1(t)e^{(\gamma_2 - \gamma_4)\pi T}$	$\frac{2k(1-e^{-\gamma_4 \pi T}) - k_j(e^{\gamma_2 \pi T} - 1)e^{-\gamma_4 \pi T}}{1-e^{(\gamma_2 - \gamma_4)\pi T}}$
$(3, 7)$	$k_j(2e^{\gamma_2 \pi T} - e^{2\gamma_2 \pi T} - 1) - 2k(e^{\gamma_2 \pi T} - 1) + k_1(t)e^{2\gamma_2 \pi T}$	$\frac{2k + k_j(e^{\gamma_2 \pi T} - 1)}{e^{\gamma_2 \pi T} + 1}$
$(3, 8)$	$k_j(1 - e^{(\gamma_2 - \gamma_3)\pi T}) + k_1(t)e^{(\gamma_2 - \gamma_3)\pi T}$	k_j

Regions	Poincaré map $Pk_1(t)$ with $0 < \xi < 0.5$	Fixed points k_1^*
$(1, 5)$	$2k(1 - e^{-\gamma_1 \pi T}) + k_1(t)e^{-2\gamma_1 \pi T}$	$\frac{2k}{1+e^{-\gamma_1 \pi T}}$
$(2, 6)$	$k_1(t)$	$k_1(t)$
$(4, 7)$	$(k_j - 2k)(e^{(\gamma_5 - \gamma_3)\pi T} - 1) + k_1(t)e^{(\gamma_5 - \gamma_3)\pi T}$	$2k - k_j$
$(4, 8)$	$k_j(e^{-2\gamma_3 \pi T} - 2e^{-\gamma_3 \pi T} + 1) - 2k(e^{-2\gamma_3 \pi T} - e^{-\gamma_3 \pi T}) + k_1(t)e^{-2\gamma_3 \pi T}$	$\frac{k_j(1-e^{-\gamma_3 \pi T}) + 2ke^{-\gamma_3 \pi T}}{1+e^{-\gamma_3 \pi T}}$
$(3, 8)$	$k_j(1 - e^{(\gamma_2 - \gamma_3)\pi T}) + k_1(t)e^{(\gamma_2 - \gamma_3)\pi T}$	k_j

Regions	Poincaré map $Pk_1(t)$ with $\xi = 0.5$	Fixed points k_1^*
$(1, 5)$	$k_1(2k(1 - e^{-\gamma_1 \pi T}) + k_1(t)e^{-2\gamma_1 \pi T})$	$\frac{2k}{1+e^{-\gamma_1 \pi T}}$
$(2, 6)$	$k_1(t)$	$k_1(t)$
$(4, 7)$	$k_1(t)$	$k_1(t)$
$(3, 8)$	$k_1(t)$	$k_1(t)$

4.4.2 Stability properties

In this subsection, we are going to analyze the stability properties of the stationary states provided in Table 4.3, especially the gridlock states. According to Equation (4.11b), the

error term is changed to $\epsilon(t+T) = \partial P \epsilon(t)$ after one cycle. In Table 4.4, we provide the error term $\epsilon(t+T)$ in different combinations of regions under different retaining ratios. According to Definition 4.2, we have the following theorem.

Table 4.4: Changes in the error term after one cycle

Regions	$\epsilon(t+T)$ with $0.5 < \xi < 1$
$(1,5)$	$\epsilon(t)e^{-2\gamma_1\pi T}$
$(1,7)$	$\epsilon(t)e^{(\gamma_5-\gamma_1)\pi T}$
$(2,6)$	$\epsilon(t)$
$(4,7)$	$\epsilon(t)e^{(\gamma_5-\gamma_3)\pi T}$
$(3,5)$	$\epsilon(t)e^{(\gamma_2-\gamma_4)\pi T}$
$(3,7)$	$\epsilon(t)e^{2\gamma_2\pi T}$
$(3,8)$	$\epsilon(t)e^{(\gamma_2-\gamma_3)\pi T}$
Regions	$\epsilon(t+T)$ with $0 < \xi < 0.5$
$(1,5)$	$\epsilon(t)e^{-2\gamma_1\pi T}$
$(2,6)$	$\epsilon(t)$
$(4,7)$	$\epsilon(t)e^{(\gamma_5-\gamma_3)\pi T}$
$(4,8)$	$\epsilon(t)e^{-2\gamma_3\pi T}$
$(3,8)$	$\epsilon(t)e^{(\gamma_2-\gamma_3)\pi T}$
Regions	$\epsilon(t+T)$ with $\xi = 0.5$
$(1,5)$	$\epsilon(t)e^{-2\gamma_1\pi T}$
$(2,6)$	$\epsilon(t)$
$(4,7)$	$\epsilon(t)$
$(3,8)$	$\epsilon(t)$

Theorem 4.2 (Stability properties of the stationary states)**.** *When $\xi > 0.5$, the stationary states are: (i) asymptotically stable in the combinations of regions $(1,5)$, $(1,7)$, $(4,7)$, $(3,5)$ and $(3,8)$; (ii) Lyapunov stable in the combination of regions $(2,6)$; (iii) unstable in the combination of regions $(3,7)$. When $\xi < 0.5$, the stationary states are: (i) asymptotically stable in the combinations of regions $(1,5)$ and $(4,8)$; (ii) Lyapunov stable in the combination of regions $(2,6)$; (iii) unstable in the combinations of regions $(4,7)$ and $(3,8)$. When $\xi = 0.5$, the stationary states are: (i) asymptotically stable in the combination of regions $(1,5)$; (ii) Lyapunov stable in the combinations of regions $(2,6)$, $(4,7)$ and $(3,8)$.*

Proof: From Table 4.4, the error term $\epsilon(t+T)$ can be written as $\epsilon(t+T) = \epsilon(t)e^c$, where c is the coefficient. To obtain the stability properties, we only need to identify the values of

the coefficient c. The fixed point is unstable if $c > 0$, while it is stable if $c \leq 0$. Furthermore, the fixed point is asymptotically stable if $c < 0$. Since $\xi_1 = \xi_2 = \xi$, we can have $\gamma_1 = \gamma_4$, $\gamma_2 = \gamma_5$. Normally, we assume $k_j \approx 5k_c$, so we have $\gamma_1 > \gamma_5$ when $\xi > 0.5$. In addition, we have $\gamma_3 > \gamma_5$ when $\xi > 0.5$, and $\gamma_3 \leq \gamma_5$ when $\xi \leq 0.5$. Then the derivation of stability properties for the fixed points is easy and thus omitted here. ■

4.5 Analysis of macroscopic fundamental diagrams and gridlock times

4.5.1 Macroscopic fundamental diagrams

Once the stationary states under different retaining ratios are obtained, the MFD can be analytically derived. However, the calculation of the average network flow-rate in Equation (4.8) involves the integral of out-fluxes $g_1(t)$ and $g_2(t)$, which is difficult to solve. Therefore, we use the following approximation when the signalized double-ring network has reached a stationary state, i.e., $k_1(nT) = k_1^*$, $n \in \mathbb{N}_0$.

$$\begin{aligned} q(k) = & \frac{\int_{s=nT}^{(n+1)T} g_1(s)ds + \int_{s=nT}^{(n+1)T} g_2(s)ds}{2T} = \frac{2\int_{s=nT}^{(n+1)T} g_1(s)ds}{2T} \\ \approx & \frac{\pi T(g_1(nT)+g_1(nT+\pi T))}{2T} = \pi \frac{g_1(k_1^*)+g_1(k_1(nT+\pi T))}{2}. \end{aligned} \tag{4.13}$$

According to Equation (4.13), we have the following MFD when $0.5 < \xi < 1$:

$$q(k;\pi,\xi) \approx \begin{cases} \pi v_f k, & k \in [0, k_c] \\ \pi C, & k \in (k_c, k_j - \xi(k_j - k_c)] \\ \pi C \frac{k_j - 2k}{\xi(k_j - k_c) - k_c}, & k \in (\frac{(1-\xi)k_j + (1+\xi)k_c}{2}, k_j/2] \\ \pi C \frac{k_j - k}{\xi(k_j - k_c)}, & k \in (k_j - \xi(k_j - k_c), k_j) \\ 0, & k \in (k_j/2, k_j] \end{cases} \tag{4.14}$$

The proof is provided in Appendix A. The MFD in Equation (4.14) is shown in Figure 4.3(a). From the figure, we find that: (i) multivaluedness exists in the network flow-density relation when $k \in (\frac{(1-\xi)k_j + (1+\xi)k_c}{2}, k_j)$; (ii) for $k \geq \frac{k_j}{2}$, the network can have stationary states with non-zero flow-rates, but these stationary states are either Lyapunov stable or unstable; (iii) the gridlock states exist for $k \geq \frac{k_j}{2}$ and are asymptotically stable.

Similarly, when $0 < \xi < 0.5$, we have the following MFD:

$$q(k;\pi,\xi) \approx \begin{cases} \pi v_f k, & k \in [0, k_c] \\ \pi C, & k \in (k_c, k_j - (1-\xi)(k_j - k_c)] \\ \pi C \frac{k_j - k}{(1-\xi)(k_j - k_c)}, & k \in (k_j - (1-\xi)(k_j - k_c), k_j) \\ 0, & k \in (k_j/2, k_j] \end{cases} \tag{4.15}$$

The proof is similar to Appendix A and thus omitted here. The MFD in Equation (4.15) is provided in Figure 4.3(b). From the figure, we find that: (i) the signalized double-ring network can maintain higher average network flow-rates when the retaining ratios are small; (ii) multivaluedness also exists when $k \geq k_j/2$; (iii) the gridlock states are unstable with small retaining ratios.

However, when $\xi = 0.5$, we find that the initial densities in the combination of regions $(2, 6)$, $(4, 7)$, and $(3, 8)$ are all stationary states. Therefore, the MFD is very different from those

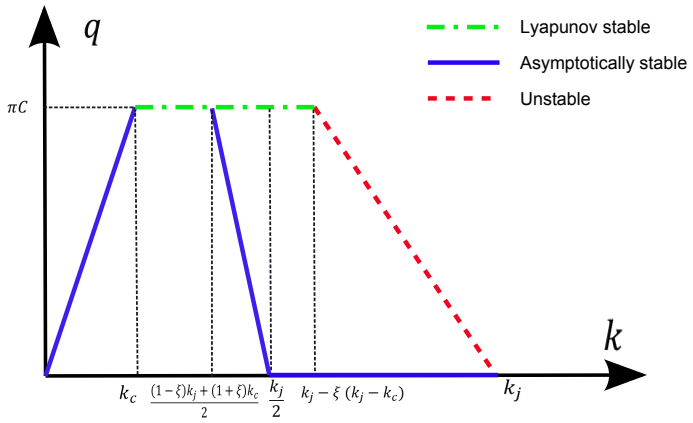

(a) $0.5 < \xi < 1$

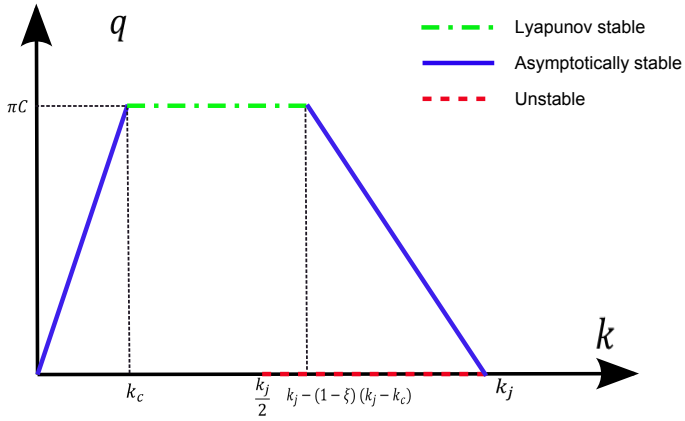

(b) $0 < \xi < 0.5$

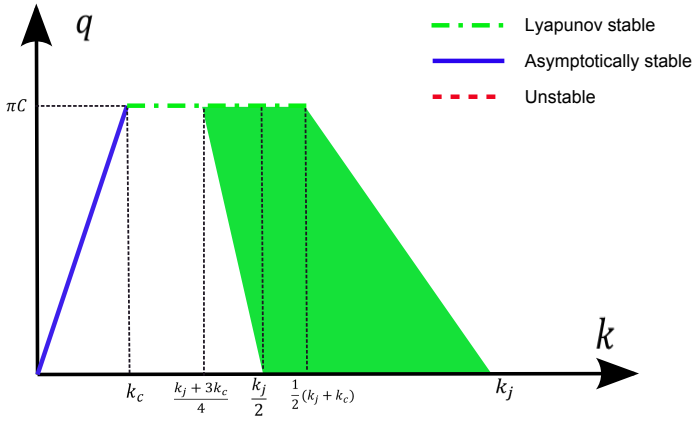

(c) $\xi = 0.5$

Figure 4.3: Macroscopic fundamental diagrams for the signalized double-ring network with different retaining ratios.

in Equations (4.14) and (4.15) and is provided below:

$$q(k;k_1,\pi,\xi)\approx\begin{cases}\pi v_f k, & k\in[0,k_c]\\ \pi C, & k\in(k_c,\frac{k_j+3k_c}{4}]\\ \pi C\frac{k_j-2k+k_1}{(k_j-k_c)/2}, & k\in(\frac{k_j+3k_c}{4},k_j] \text{ and}\\ & k_1\in[\max\{\frac{k_c(k_j-2k)}{k_j/2-3k_c/2},2k-k_j\},\max\{2k-\frac{k_j+k_c}{2},k\}]\end{cases} \tag{4.16}$$

The proof is similar to Appendix A and thus omitted here. The MFD in Equation (4.16) is provided in Figure 4.3(c). From the figure, we find that: (i) there are infinitely many stationary states when $k>\frac{k_j+3k_c}{4}$, and thus, the corresponding average network flow-rate covers the whole green region shown in the figure; (ii) the gridlock states are Lyapunov stable; (iii) there are no unstable stationary states.

4.5.2 Gridlock times

In Theorem 4.1, we find that stationary states in the combinations of regions $(4,7)$ and $(3,8)$ are stable gridlock states when $\xi>0.5$. That means starting from any initial conditions in these regions, traffic in the signalized double-ring network will finally converge to gridlock. The gridlock times can be analytically calculated from the Poincaré maps. For example, in the combination of regions $(3,8)$, we have the Poincaré map $k_1(t+T)=Pk_1(t)=k_j(1-e^{(\gamma_2-\gamma_3)\pi T})+k_1(t)e^{(\gamma_2-\gamma_3)\pi T}$. For an initial state $(k_1(0),k)$, we have

$$k_1(T)=k_j(1-e^{(\gamma_2-\gamma_3)\pi T})+k_1(0)e^{(\gamma_2-\gamma_3)\pi T}. \tag{4.17}$$

Then after n cycles, we have

$$k_1(nT)=k_j-(k_j-k_1(0))e^{(\gamma_2-\gamma_3)n\pi T}. \tag{4.18}$$

Since $\gamma_2 < \gamma_3$, $k_1(nT)$ will converge to k_j as $n \to +\infty$. If we define the gridlock time T_g as the time when $k_1(T_g) \approx (1-\sigma)k_j$, where σ is very small, we have

$$T_g \approx \frac{1}{\pi(\gamma_3 - \gamma_2)} \ln\{\frac{k_j - k_1(0)}{\sigma k_j}\}. \tag{4.19}$$

In Figure 4.4, we provide the gridlock patterns with different retaining ratios and initial densities in the combination of regions $(3, 8)$. In the figure, the horizontal dashed line is the threshold with $\sigma = 0.01$ for jammed conditions. The vertical dashed lines are the calculated gridlock times from Equation (4.19). The cycle length is 30s with a lost time of 2s for each phase. The updating time step Δt is 0.01s in LQM simulations. The following two trends can be observed from the figure and verified by taking the derivatives with respect to ξ and $k_1(0)$ in Equation (4.19): (i) given the same initial densities, the network is harder to get gridlocked with lower retaining ratios, which is shown in Figure 4.4(a); (ii) given the same retaining ratios, the network will get gridlocked earlier if link 1 is initially more congested, which is shown in Figure 4.4(b). The gridlock patterns obtained from CTM simulations with $\Delta t = 0.25$s are also provided in Figure 4.4. We find that the above two trends can also be found in CTM simulations, which indicates that they are the characteristics of the signalized double-ring network itself and not related to the simulation models. Interestingly, we also find that with the same initial settings in Figure 4.4, traffic tends to get jammed earlier in CTM simulations.

4.6 Numerical solutions to the Poincaré maps with long cycle lengths

With long cycle lengths, derivation of closed-form Poincaré maps is difficult since it is hard to track the time instants when the evolution orbit crosses the boundaries of different regions.

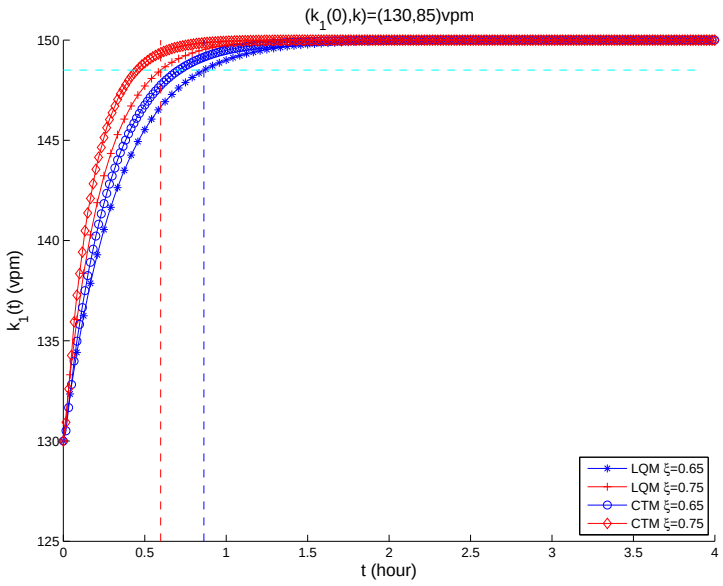

(a) With different retaining ratios

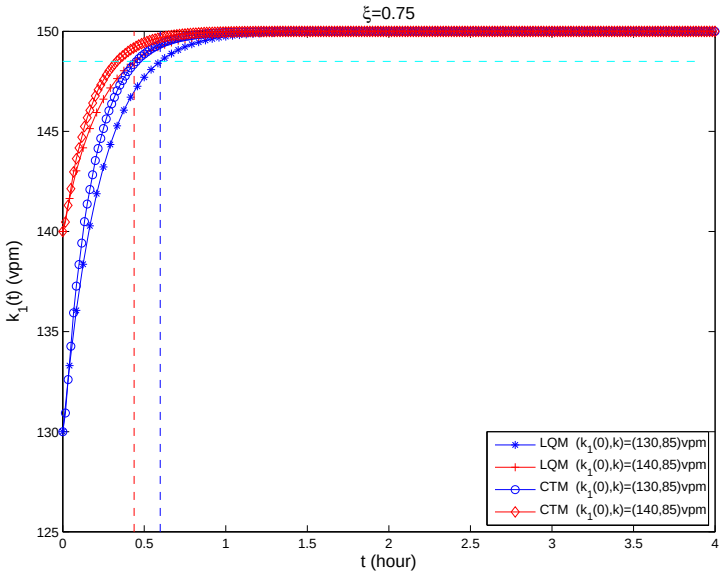

(b) With different initial densities

Figure 4.4: Gridlock patterns with different retaining ratios and initial densities.

However, since the system dynamic equation (Equation (4.7)) and the coefficients of different regions (Table 4.1) are known, it is possible to provide numerical methods to solve the Poincaré maps.

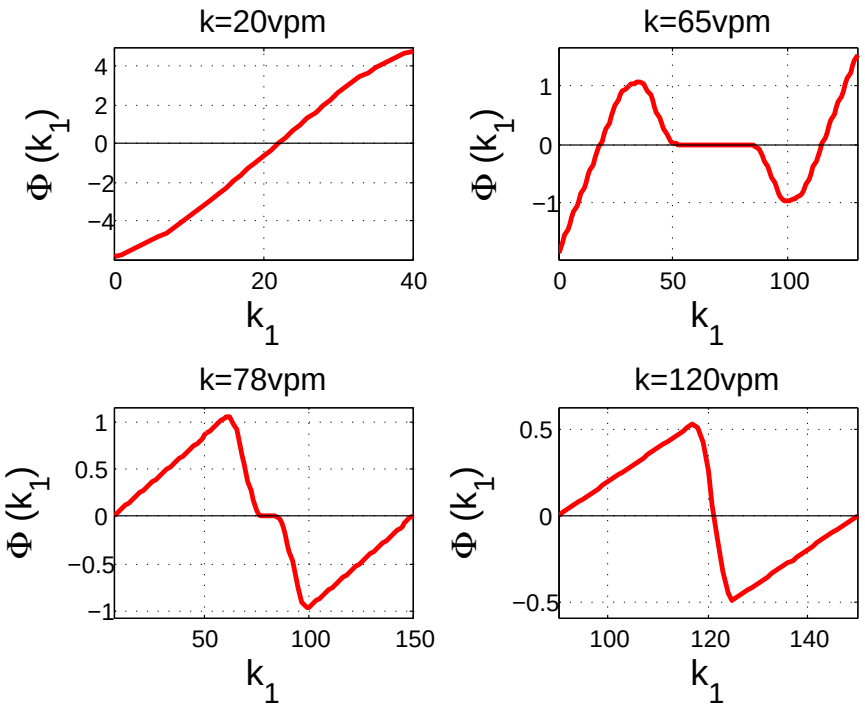

Figure 4.5: Relations between $\Phi(k_1)$ and k_1 under different average network densities when $\xi = 0.55$, $T = 60$s, and $\Delta = 4$s.

Here, we denote $\Phi(k_1) = k_1 - Pk_1$. For given average network density k, retaining ratio ξ, and signal settings $(\delta_1(t), \delta_2(t))$, finding the fixed points k_1^* is the same as finding the roots in $\Phi(k_1)$. Note that the right-hand side of Equation (4.7) is a piecewise linear function and is continuous at the boundaries, and thus, Pk_1 as well as $\Phi(k_1)$ is continuous. But since the derivative of $\Phi(k_1)$ is not available, the secant method [19] is used and provided below:

$$k_1^{n+1} = k_1^n - \Phi(k_1^n)[\frac{k_1^n - k_1^{n-1}}{\Phi(k_1^n) - \Phi(k_1^{n-1})}]. \tag{4.20}$$

k_1^{n+1} is the updated density in step $n+1$. k_1^n, k_1^{n-1}, $\Phi(k_1^n)$ and $\Phi(k_1^{n-1})$ are the densities and function values in steps n and $n-1$, respectively.

In Figure 4.5, we provide the relations between $\Phi(k_1)$ and k_1 under different average network densities when $\xi = 0.55$, $T = 60$s, and $\Delta = 4$s. From the figure, we know that $\Phi(k_1)$ can have one root, multiple roots, or infinite roots under different average network densi-

ties. That means starting from different k_1^0, we may get different roots in the end using numerical methods. Therefore, a brute-force search in k_1 is needed to obtain a full map of the stationary states. In addition, when $\Phi(k_1)$ has infinite roots (e.g., when $k = 65$vpm or 78vpm), judgements on the values of $\Phi(k_1^n)$ and $\Phi(k_1^{n-1})$ are needed to avoid zero values in the denominator in Equation (4.20). The algorithm of finding stationary states is provided in Appendix B.

In Figure 4.6(a), we provide the MFD in the signalized double-ring network with $\xi = 0.85$, $T = 100$s, and $\Delta = 0$s using Equation (4.20). As a comparison, we also provide the MFDs obtained from the variational theory method and CTM simulations [49] with the same settings in the same figure. From the figure, we find that the MFDs obtained from the three methods are different. The variational theory method fails to observe the multivaluedness and gridlock phenomena in the MFD. Even though such two phenomena are observed using CTM simulations, the congested branch is not observable since it is unstable. Using Equation (4.20), we can get a complete map of the MFD: the multivaluedness and gridlock phenomena as well as the congested branch are all observed. The obtained MFD is similar to the one in Figure 4.3(a) with small cycle lengths. Since detailed traffic dynamics inside a link are aggregated at the link level in the link queue model, it is not surprised to find that the flow-rates obtained from the Poincaré map method are systematically lower than or equal to those obtained from the variational theory method and CTM simulations.

In addition, in Figures 4.6(b) and 4.6(c), we provide the MFDs obtained from the Poincaré map methods with $\xi = 0.3$ and $\xi = 0.5$, respectively. From the two figures, we find that the MFDs with long cycle lengths are very similar to the ones with short cycle lengths in Figures 4.3(b) and 4.3(c).

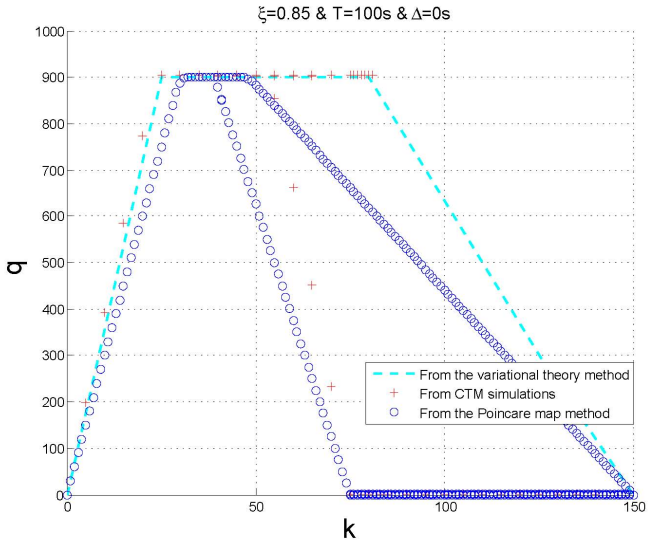

(a) $\xi = 0.85$

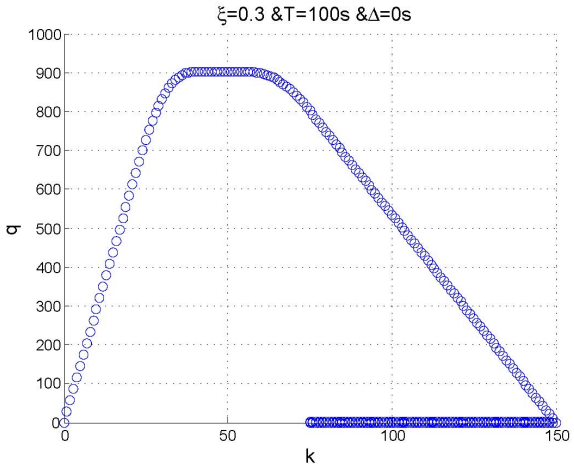

(b) $\xi = 0.3$

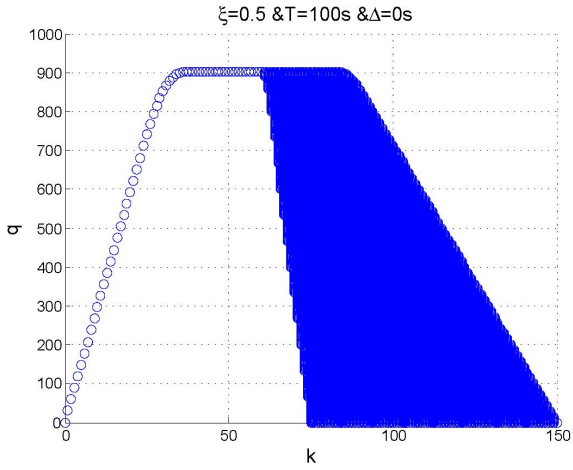

(c) $\xi = 0.5$

Figure 4.6: Macroscopic fundamental diagrams with $T = 100$s, $\Delta = 0$s, and different retaining ratios.

4.7 Conclusions

In this chapter, a signalized double-ring network was formulated as a switched affine system under the framework of the link queue model [43] and the assumption of a triangular traffic flow fundamental diagram [33]. Stationary states with periodic density evolution orbits were shown to exist as the switched affine system periodically visits the (k_1, k) space in Figure 4.2(a). Poincaré map was introduced to analyze the existence and the property of these stationary states. With short cycle lengths, closed-form Poincaré maps were obtained. Stationary states and their corresponding stability properties were derived and analyzed by finding and analyzing the fixed points on the Poincaré maps. It is found that under different combinations of signal settings, retaining ratios, and initial densities, stationary states can be Lyapunov stable, asymptotically stable, or unstable. Macroscopic fundamental diagrams were derived based on the stationary states, in which the network flow-rate is a function of the network density, route choice behaviors, and signal settings. In addition, the derived MFDs are more complete since the multivaluedness and gridlock phenomena as well as the unstable congested branch are all observed. Since the system will get gridlocked when $k \geq k_j/2$ and $\xi > 0.5$, the gridlock time was also analyzed under different retaining ratios and initial densities. It was found that the network is harder to get gridlocked with lower retaining ratios. However, the network will get gridlocked earlier if one ring is initially more congested. Since closed-form Poincaré maps are hard to obtain when the cycle lengths are long, the secant method was used to numerically find the fixed points on the Poincaré maps. It was found that the obtained stationary states and the MFDs are very similar to those with short cycle lengths.

Different from the kinematic wave model in Chapter 3 and the two bin model in [11, 24], the introduction of the link queue model and the switched affine system enables us to analytically study the traffic statics and dynamics in the double-ring network with general signal settings. The way of using Poincaré maps to find the stationary states is physically meaningful and

mathematically easier to solve. The findings in this chapter, e.g., stationary states, stability, macroscopic fundamental diagrams, and gridlock patterns, are consistent with those in earlier studies [11, 24, 49]. But the solutions in this chapter are more complete.

Even with the link queue model, we find that traffic statics and dynamics in the signalized double-ring network are still difficult to solve due to the discrete signal control at the junction. Therefore, in the following chapter, we try to derive invariant continuous approximate models to simplify the traffic dynamics at signalized junctions.

Chapter 5

Invariant continuous approximate models for a signalized road link

5.1 Introduction

In urban networks, traffic signal plays a vital role in regulating traffic movements. A number of signal control strategies have been proposed since one of the earliest attempts in [75]. The operation of traffic signals follows a discrete pattern: vehicles are allowed to move when the traffic light is green, while they have to stop and wait when it turns red. Such a discrete control pattern introduces binary variables in the optimization of signal settings, which leads to solving mixed integer mathematical problems [55, 39, 56]. However, solving such problems becomes difficult and requires a massive amount of time as the network gets larger [34]. Therefore, continuous models are needed to approximate the traffic dynamics at signalized intersections.

At a signalized intersection, when traffic demand is high enough for one approach, its discharging pattern is simple: the outflow equals to the saturation flow during the green time

period and zero during the red time period. Earlier in [26, 25, 13], a so-called store-and-forward method was proposed to average the junction outflow with a time-dependent linear function in optimizing the green splits in over-saturated road networks. However, this approach does not work when the network is not congested. In [34], a continuous approximate model was proposed for a signalized merging junction, and the approximation accuracy was analyzed using the variational theory under different traffic conditions, e.g., with/without queue spillback, and different traffic flow fundamental diagrams, e.g., the triangular fundamental diagram [33] and Greenshields' fundamental diagram [32]. However, this continuous approximate model was proposed directly without analyzing its property under different traffic flow models, e.g., the LWR model [54, 68] and the link transmission model [78, 47]. To the best of our knowledge, there is still a lack of a systematic and comprehensive study on deriving continuous approximate models for signalized intersections and analyzing their properties under different capacity constraints, traffic conditions, fundamental diagrams, and traffic flow models.

In this chapter, we want to fill this gap. We first propose three discrete control forms for a signalized road link in the LWR model [54, 68] and derive their corresponding continuous approximate models by averaging the periodic signal control parameter over time. Then we obtain their invariant forms by applying these continuous approximate models as entropy conditions at the signalized junction and solving the corresponding Riemann problems in the supply-demand framework [48]. Later we analyze the properties of these invariant continuous approximate models under different capacity constraints at the signalized junction. We also use simulations in a signalized ring road to analyze the approximation accuracy under different traffic conditions and fundamental diagrams. Furthermore, we analyze the properties of invariant and non-invariant models in the link transmission model [78, 47].

The rest of this chapter is organized as follows. We formulate the traffic dynamics on a signalized road link in the LWR model and provide three different forms of discrete signal

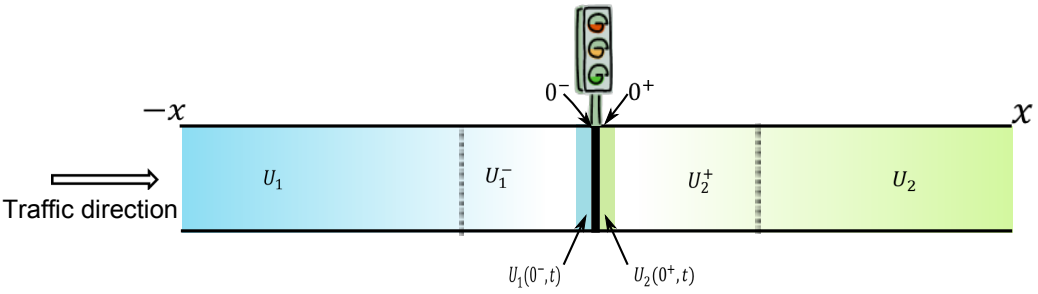

Figure 5.1: A signalized road link.

control at the signalized junction in Section 5.2. Next, we derive the invariant continuous approximate models from the three forms of discrete signal control in Section 5.3 and analyze their properties in Section 5.4. In Section 5.5, we analyze the approximation accuracy of the invariant continuous approximate model in a signalized ring road. In Section 5.6, we demonstrate the importance of invariant continuous approximate models in the link transmission model. In Section 5.7, we summarize our research findings.

5.2 Discrete signal control on a road link

5.2.1 Traffic dynamics on the road link

For a signalized road link shown in Figure 5.1, let's assume the traffic signal is installed at $x = 0$. The upstream section ($x < 0$) is denoted as link 1, while the downstream section ($x > 0$) is denoted as link 2. For link $a \in \{1, 2\}$, the flow-rate, density, and speed are denoted as $q_a(x,t)$, $k_a(x,t)$, and $v_a(x,t)$, respectively. The traffic flow fundamental diagram of each link is of the same type and denoted as $q_a(x,t) = Q(k_a(x,t))$, $a \in \{1, 2\}$, which is concave and attains its capacity C_a at the critical density $k_{a,c}$. The jam density of link a is denoted as $k_{a,j}$, at which the flow-rate is zero. Then the local supply and demand [53] are defined as

$$D_a(x,t) = Q(\min\{k_a(x,t), k_{a,c}\})$$
$$= \begin{cases} Q(k_a(x,t)), & k_a(x,t) \in [0, k_{a,c}], \\ C_a, & k_a(x,t) \in (k_{a,c}, k_{a,j}], \end{cases} \qquad a \in \{1,2\} \tag{5.1a}$$

$$S_a(x,t) = Q(\max\{k_a(x,t), k_{a,c}\})$$
$$= \begin{cases} C_a, & k_a(x,t) \in [0, k_{a,c}], \\ Q(k_a(x,t)), & k_a(x,t) \in (k_{a,c}, k_{a,j}], \end{cases} \qquad a \in \{1,2\} \tag{5.1b}$$

To describe traffic dynamics on the road link ($x \neq 0$), the LWR model [54, 68] is used, which can be formulated as

$$\frac{\partial k_a(x,t)}{\partial t} + \frac{\partial Q(k_a(x,t))}{\partial x} = 0, \qquad a \in \{1,2\}. \tag{5.2}$$

Suppose the initial condition is given by

$$k_a(x, t=0) = k_a, \qquad a \in \{1,2\}. \tag{5.3}$$

Under the supply-demand framework developed in [48], Equation (5.3) can be rewritten as

$$U_a(x, t=0) = U_a = (D_a, S_a), \qquad a \in \{1,2\} \tag{5.4}$$

where D_a and S_a are link a's demand and supply calculated from Equation (5.1) with the initial density k_a.

5.2.2 Discrete signal control

For the traffic signal at $x = 0$, the cycle length is T, and the effective green time is ηT with $\eta \in (0,1)$. An indicator function $\delta(t)$ is introduced to describe the discrete signal control,

which is formulated as

$$\delta(t) = \begin{cases} 1, & t \in [nT, nT + \eta T); \\ 0, & t \in [nT + \eta T, (n+1)T); \end{cases} \quad n = 0, 1, 2, ... \tag{5.5}$$

Then the junction flux q can be calculated using the following three forms:

$$q = f_1(D_1(0^-, t), S_2(0^+, t), \delta(t)) = \delta(t) \min\{D_1(0^-, t), S_2(0^+, t)\}; \tag{5.6a}$$

$$q = f_2(D_1(0^-, t), S_2(0^+, t), \delta(t)) = \min\{\delta(t) D_1(0^-, t), S_2(0^+, t)\}; \tag{5.6b}$$

$$q = f_3(D_1(0^-, t), S_2(0^+, t), \delta(t)) = \min\{D_1(0^-, t), \delta(t) S_2(0^+, t)\}. \tag{5.6c}$$

From the above equations, we find that the discrete control is applied to both the upstream demand and the downstream supply in Equation (5.6a), to the upstream demand only in Equation (5.6b), and to the downstream supply only in Equation (5.6c), respectively.

Theorem 5.1. *The three forms of discrete signal control in Equation (5.6) are equivalent in the LWR model, and thus, it doesn't matter where to put $\delta(t)$.*

Proof: During the effective green time period, i.e., $t \in [nT, nT + \eta T)$ for $n = 0, 1, 2, ...$, we have

$$\begin{aligned} f_1(D_1(0^-, t), S_2(0^+, t), \delta(t)) &= 1 \times \min\{D_1(0^-, t), S_2(0^+, t)\} \\ &= \min\{D_1(0^-, t), S_2(0^+, t)\}; \end{aligned} \tag{5.7a}$$

$$\begin{aligned} f_2(D_1(0^-, t), S_2(0^+, t), \delta(t)) &= \min\{1 \times D_1(0^-, t), S_2(0^+, t)\} \\ &= \min\{D_1(0^-, t), S_2(0^+, t)\}; \end{aligned} \tag{5.7b}$$

$$\begin{aligned} f_3(D_1(0^-, t), S_2(0^+, t), \delta(t)) &= \min\{D_1(0^-, t), 1 \times S_2(0^+, t)\} \\ &= \min\{D_1(0^-, t), S_2(0^+, t)\}. \end{aligned} \tag{5.7c}$$

But during the red time period, i.e., $t \in [nT + \eta T, (n+1)T)$ for $n = 0, 1, 2, ...$, we have

$$f_1(D_1(0^-, t), S_2(0^+, t), \delta(t)) = 0 \times \min\{D_1(0^-, t), S_2(0^+, t)\} = 0; \tag{5.8a}$$

$$f_2(D_1(0^-, t), S_2(0^+, t), \delta(t)) = \min\{0 \times D_1(0^-, t), S_2(0^+, t)\} = 0; \tag{5.8b}$$

$$f_3(D_1(0^-, t), S_2(0^+, t), \delta(t)) = \min\{D_1(0^-, t), 0 \times S_2(0^+, t)\} = 0. \tag{5.8c}$$

Therefore, the three forms $f_i(D_1(0^-, t), S_2(0^+, t), \delta(t))$, $i \in \{1, 2, 3\}$, are equivalent to each other in the LWR model. ■

5.3 Continuous approximate models and their invariant forms

5.3.1 Continuous approximate models

According to [70], when a parameter in a system equation is a T-periodic function in t, we can simplify the system dynamics by averaging the function over T. Since $\delta(t)$ in Equation (5.6) is a T-periodic function, its average can be calculated as

$$\bar{\delta} = \frac{1}{T} \int_0^T \delta(s) ds = \eta. \tag{5.9}$$

Therefore, the continuous approximate models for Equation (5.6) can be formulated as

$$q = F_1(D_1(0^-, t), S_2(0^+, t), \eta) = \eta \min\{D_1(0^-, t), S_2(0^+, t)\}; \tag{5.10a}$$

$$q = F_2(D_1(0^-, t), S_2(0^+, t), \eta) = \min\{\eta D_1(0^-, t), S_2(0^+, t)\}; \tag{5.10b}$$

$$q = F_3(D_1(0^-, t), S_2(0^+, t), \eta) = \min\{D_1(0^-, t), \eta S_2(0^+, t)\}. \tag{5.10c}$$

With Equation (5.10), the signalized road link is changed into a regular road link with a different flux function $q = F_i(D_1(0^-, t), S_2(0^+, t), \eta)$, $i \in \{1, 2, 3\}$, at $x = 0$. Here, functions like $q = F_i(D_1(0^-, t), S_2(0^+, t), \eta)$ are considered as local flux functions since they only use local demand and supply information to determine the junction flux.

5.3.2 Derivation of invariant forms

If initial conditions (Equation (5.4)) and the junction flux function (Equation (5.10)) are given, we can have three types of traffic states on the road link if it is infinitely long [48]:

- Initial states: $U_1 = (D_1, S_1)$ and $U_2 = (D_2, S_2)$;
- Stationary states: $U_1^- = (D_1^-, S_1^-)$ and $U_2^+ = (D_2^+, S_2^+)$;
- Interior states: $U_1(0^-, t) = (D_1(0^-, t), S_1(0^-, t))$ and $U_2(0^+, t) = (D_2(0^+, t), S_2(0^+, t))$.

The locations of these traffic states are provided in Figure 5.1. Note that the interior states take infinitesimal space in the LWR model and only take one cell in the cell transmission model (CTM) simulations [9]. Correspondingly, we have three types of Riemann problems arising at the signalized road link:

- Type I: the Riemann problem between U_1 and U_1^-, or between U_2 and U_2^+;
- Type II: the Riemann problem between $U_1(0^-, t)$ and U_1^-, or between $U_2(0^+, t)$ and U_2^+;
- Type III: the Riemann problem between $U_1(0^-, t)$ and $U_2(0^+, t)$.

Here, the Riemann problems are solved in the supply-demand framework in [48] with the entropy conditions in Equation (5.10), and then, possible stationary and interior states are obtained.

Lemma 5.1. *With the entropy condition in Equation (5.10a) applied at the signalized junction, stationary and interior states can take the following values:*

(1) When $\min\{D_1, S_2\} > \eta \min\{C_1, C_2\}$, $U_1^- = U_1(0^-, t) = (C_1, \eta \min\{C_1, C_2\})$, *and* $U_2^+ = U_2(0^+, t) = (\eta \min\{C_1, C_2\}, C_2)$.

(2) When $D_1 < S_2$ *and* $D_1 \leq \eta \min\{C_1, C_2\}$, $U_1^- = (D_1, C_1)$, $U_1(0^-, t) = (D_1/\eta, C_1)$, *and* $U_2^+ = U_2(0^+, t) = (D_1, C_2)$.

(3) When $D_1 > S_2$ *and* $S_2 \leq \eta \min\{C_1, C_2\}$, $U_1^- = U_1(0^-, t) = (C_1, S_2)$, $U_2^+ = (C_2, S_2)$, *and* $U_2(0^+, t) = (C_2, S_2/\eta)$.

(4) When $S_2 = D_1$ *and* $S_2 \leq \eta \min\{C_1, C_2\}$, $U_1^- = (D_1, C_1)$, *and* $U_2^+ = (C_2, S_2)$.

(a) If $U_2(0^+, t) = (C_2, S_2/\eta)$, $U_1(0^-, t) = (D_1(0^-, t), S_1(0^-, t))$ *with* $S_1(0^-, t) \geq D_1$ *and* $D_1(0^-, t) \geq D_1/\eta$.

(b) If $U_1(0^-, t) = (D_1/\eta, C_1)$, $U_2(0^+, t) = (D_2(0^+, t), S_2(0^+, t))$ *with* $S_2(0^+, t) \geq S_2/\eta$ *and* $D_2(0^+, t) \geq S_2$.

The proof is provided in Appendix C.

On the signalized road link, the junction flux can be calculated from the stationary states. Then according to Lemma 5.1, we have the following theorem.

Theorem 5.2. *With the entropy condition in Equation (5.10a) applied at the signalized junction, the junction flux can take the following values:*

(1) When $\min\{D_1, S_2\} > \eta \min\{C_1, C_2\}$, $q = \eta \min\{C_1, C_2\}$.

(2) When $D_1 \leq \min\{S_2, \eta \min\{C_1, C_2\}\}$, $q = D_1$.

(3) When $S_2 \leq \min\{D_1, \eta \min\{C_1, C_2\}\}$, $q = S_2$.

Therefore, the continuous approximate model can be written as

$$q = \hat{F}_1(D_1, S_2, \eta) = \min\{D_1, S_2, \eta C_1, \eta C_2\}. \tag{5.11}$$

The proof is simple and thus omitted here.

We find that in order to determine the junction flux, global information such as the initial conditions in Equation (5.4) is used in Equation (5.11). Therefore, functions like Equation (5.11) are considered as global flux functions.

Definition 5.1. *For a global flux function $\hat{F}(D_1, S_2, \eta)$, if the same global form can be derived from its local from $F(D_1(0^-, t), S_2(0^+, t), \eta)$ by solving the Riemann problems arising at the signalized road link, $\hat{F}(D_1, S_2, \eta)$ is called invariant. Otherwise, it is non-invariant.*

Corollary 5.1. *The continuous approximate model in Equation (5.11) is invariant.*

Proof: If we apply the following entropy condition

$$q = \hat{F}_1'(D_1(0^-, t), S_2(0^+, t), \eta) = \min\{D_1(0^-, t), S_2(0^+, t), \eta C_1, \eta C_2\}, \tag{5.12}$$

at the signalized junction, we can derive the same continuous approximate model in Equation (5.11). Therefore, Equation (5.11) is invariant. ■

Theorem 5.3. *With the entropy conditions in Equations (5.10b) and (5.10c) at the signalized junction, we can derive the following invariant continuous approximate models.*

$$\textit{For Equation (5.10b):} \qquad q = \hat{F}_2(D_1, S_2, \eta) = \min\{D_1, S_2, \eta C_1\}; \tag{5.13a}$$

$$\textit{For Equation (5.10c):} \qquad q = \hat{F}_3(D_1, S_2, \eta) = \min\{D_1, S_2, \eta C_2\}. \tag{5.13b}$$

The proof is similar to that in Lemma 5.1 and thus omitted here.

Corollary 5.2. *For the following three continuous approximate models, they are non-invariant and their invariant forms are in Equations (5.11) and (5.13).*

$$q = \tilde{F}_1(D_1, S_2, \eta) = \eta \min\{D_1, S_2\}; \tag{5.14a}$$

$$q = \tilde{F}_2(D_1, S_2, \eta) = \min\{\eta D_1, S_2\}; \tag{5.14b}$$

$$q = \tilde{F}_3(D_1, S_2, \eta) = \min\{D_1, \eta S_2\}. \tag{5.14c}$$

Proof: For continuous approximate models in Equation (5.14), their local flux functions are provided in Equation (5.10). From Theorems 5.2 and 5.3, the derived invariant forms are different from those in Equation (5.14), and therefore, the continuous approximate models in Equation (5.14) are non-invariant. ■

5.4 Properties of the invariant continuous approximate models

5.4.1 Under different capacity constraints

When the upstream and downstream capacities are the same, the continuous approximate models in Equations (5.11) and (5.13) are identical. However, they have different properties when the upstream and downstream capacities are different. At the signalized road link, we have the following cases of capacity combinations.

- Case 1: $C_1 < C_2$.

In this case, Equation (5.11) is the same as Equation (5.13a). In Figures 5.2(a) and 5.2(b), we provide the solutions of stationary states for the three invariant continuous approximate models with $C_1 < C_2$ in the $D_1 - S_2$ space. Red dots stand for initial states, while blue dots stand for stationary states. We find that when $D_1 \leq \eta C_1$ or $S_2 \leq \eta C_1$, the solutions of stationary states (or the approximated stationary junction flux) are the same for these three models. However, when both D_1 and S_2 are greater than ηC_1, the stationary states for the three models are different. It is found that the approximated stationary junction flux is bounded by the upstream capacity constraint ηC_1 for the models in Equations (5.11) and (5.13a), while it is bounded by $\min\{\eta C_2, C_1\}$ for the model in Equation (5.13b).

In the discrete signal control, when the downstream supply is high enough to accommodate all upstream vehicles during the effective green time period, the maximum junction flux is equal to the upstream capacity. But it reduces to zero when the traffic light turns red. Therefore, the maximum average junction flux can only be ηC_1. The approximated stationary junction flux by Equation (5.13b) is higher than this value, which means Equation (5.13b) fails to capture the upstream capacity constraint.

- Case 2: $C_1 > C_2$.

  In this case, Equation (5.11) is the same as Equation (5.13b). Similarly, we provide the solutions of stationary states for the three continuous approximate models with $C_2 < C_1$ in Figures 5.3(a) and 5.3(b). We find that these three models are the same when $D_1 \leq \eta C_2$ or $S_2 \leq \eta C_2$. However, they are different when both D_1 and S_2 are greater than ηC_2. In this case, the approximated stationary junction flux is bounded by $\min\{\eta C_1, C_2\}$ for the model in Equation (5.13a) and by the downstream capacity constraint ηC_2 for the models in Equations (5.11) and (5.13b).

  In the discrete signal control, when the upstream demand is high enough to fully use the effective green time in each cycle, the maximum junction flux is equal to the

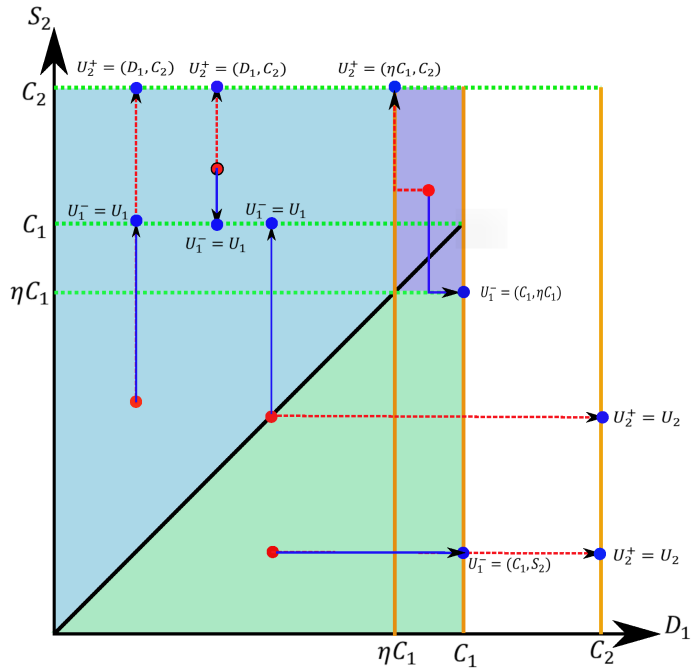

(a) $C_1 < C_2$ and $q = \min\{D_1, S_2, \eta C_1\}$

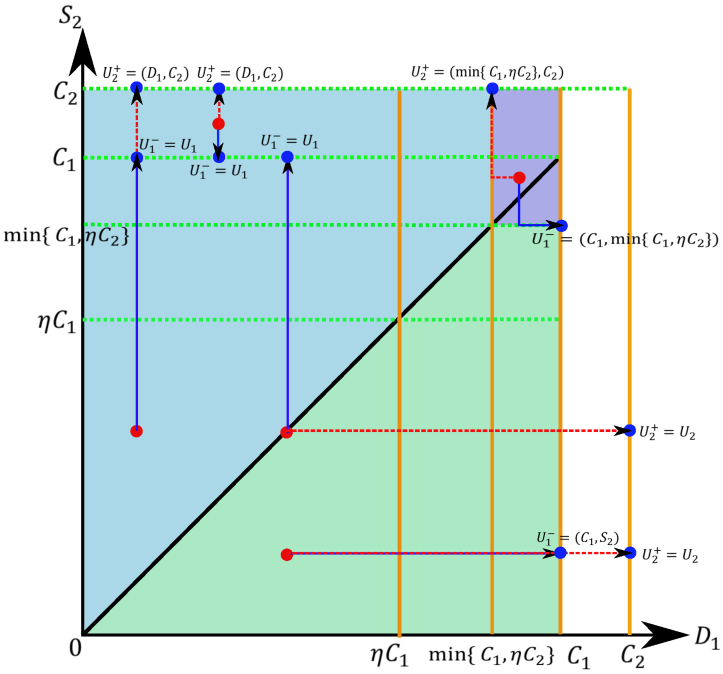

(b) $C_1 < C_2$ and $q = \min\{D_1, S_2, \eta C_2\}$

Figure 5.2: Solutions of stationary states for the three invariant continuous approximate models with $C_1 < C_2$

downstream capacity. Again, due to the red light, the junction flux is zero for $1-\eta$ of the cycle. Therefore, the maximum average junction flux can only be ηC_2. The approximated stationary junction flux by Equation (5.13a) is higher than this value, which means Equation (5.13a) fails to capture the downstream capacity constraint.

From the above analysis, we find that only the invariant continuous approximate model in Equation (5.11) can fully capture the capacity constraints at the signalized junction. Other invariant continuous approximate models fail to capture either the upstream (e.g., Equation (5.13b)) or the downstream (e.g., Equation (5.13a)) capacity constraint, and therefore, they should not be used when the capacities of the upstream and downstream links are different.

5.4.2 Multiple non-invariant forms

In [34], a continuous approximate model was proposed for a signalized merging junction with the consideration of effective supplies in the downstream. If one of the upstream links is empty and has zero demand, the signalized merging junction is changed into the signalized road link shown in Figure 5.1. Then the model in [34] is simplified as

$$q = \tilde{F}_4(D_1, S_2, \eta) = \min\{D_1, \eta S_2'\} = \min\{D_1, \eta S_2, \eta C_1\}. \tag{5.15}$$

Here, S_2' is the effective supply and defined as $S_2' = \min\{S_2, C_1\}$. Correspondingly, the entropy condition applied at the signalized junction is

$$q = F_4(D_1(0^-, t), S_2(0^+, t), \eta) = \min\{D_1(0^-, t), \eta S_2(0^+, t), \eta C_1\}. \tag{5.16}$$

Then we can have the following theorem.

Theorem 5.4. *The continuous approximate model in Equation (5.15) is non-invariant but*

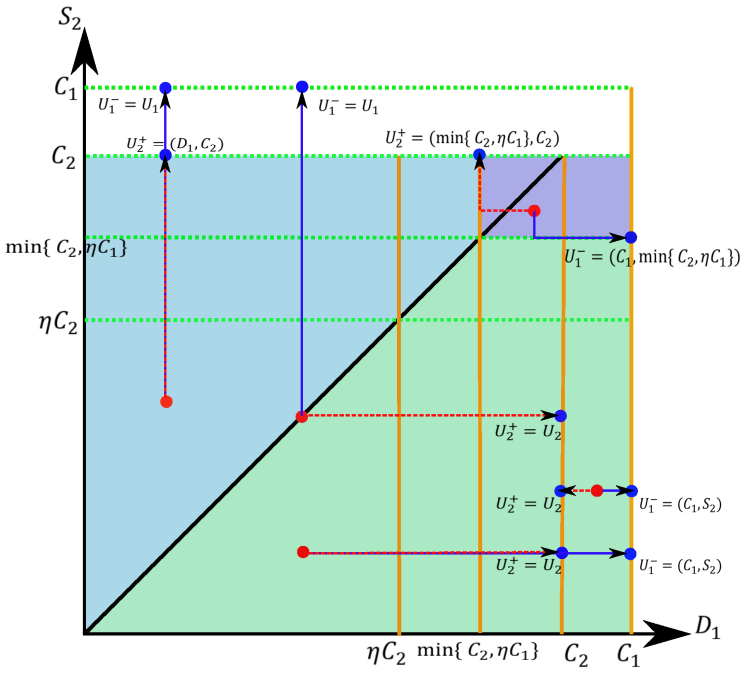

(a) $C_1 > C_2$ and $q = \min\{D_1, S_2, \eta C_1\}$

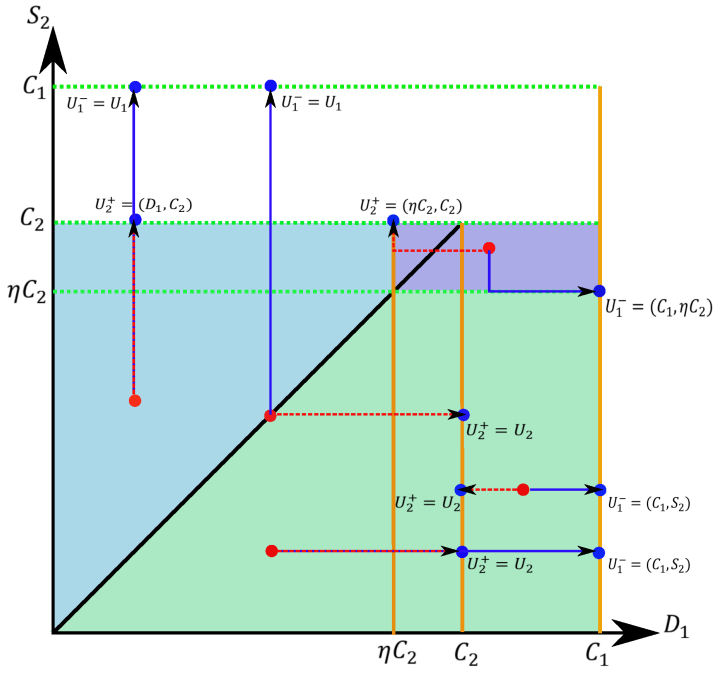

(b) $C_1 > C_2$ and $q = \min\{D_1, S_2, \eta C_2\}$

Figure 5.3: Solutions of stationary states for the three invariant continuous approximate models with $C_1 > C_2$.

has the same invariant form in Equation (5.11). That means different non-invariant continuous approximate models can have the same invariant form.

Proof: With the entropy function in Equation (5.16) applied at the signalized junction, we can get the following stationary and interior states:

(1) When $\min\{D_1, S_2\} > \eta \min\{C_1, C_2\}$, $U_1^- = U_1(0^-, t) = (C_1, \eta \min\{C_1, C_2\})$, and $U_2^+ = U_2(0^+, t) = (\eta \min\{C_1, C_2\}, C_2)$.

(2) When $D_1 < S_2$ and $D_1 \leq \eta \min\{C_1, C_2\}$, $U_1^- = U_1(0^-, t) = (D_1, C_1)$, and $U_2^+ = U_2(0^+, t) = (D_1, C_2)$.

(3) When $D_1 > S_2$ and $S_2 \leq \eta \min\{C_1, C_2\}$, $U_1^- = U_1(0^-, t) = (C_1, S_2)$, $U_2^+ = (C_2, S_2)$, and $U_2(0^+, t) = (C_2, S_2/\eta)$.

(4) When $S_2 = D_1$ and $S_2 \leq \eta \min\{C_1, C_2\}$, $U_1^- = (D_1, C_1)$, and $U_2^+ = (C_2, S_2)$.

   (a) If $U_2(0^+, t) = (C_2, S_2/\eta)$, $U_1(0^-, t) = (D_1(0^-, t), S_1(0^-, t))$ with $S_1(0^-, t) \geq D_1$ and $D_1(0^-, t) \geq D_1$.

   (b) If $U_1(0^-, t) = (D_1, C_1)$, $U_2(0^+, t) = (D_2(0^+, t), S_2(0^+, t))$ with $S_2(0^+, t) \geq S_2/\eta$ and $D_2(0^+, t) \geq S_2$.

   (c) If $D_1 = S_2 = \eta C_1$, $U_1(0^-, t) = (D_1(0^-, t), S_1(0^-, t))$ with $S_1(0^-, t) \geq D_1$ and $D_1(0^-, t) \geq D_1$; $U_2(0^+, t) = (D_2(0^+, t), S_2(0^+, t))$ with $S_2(0^+, t) \geq S_2/\eta$ and $D_2(0^+, t) \geq S_2$.

Based on the stationary states, we can easily derive the invariant continuous approximate model which is the same as Equation (5.11). Even though Equations (5.14a) and (5.15) are two different non-invariant continuous approximate models, they have the same invariant form (Equation (5.11)). ■

5.5 Approximation accuracy in a signalized ring road

In this section, we analyze the approximation accuracy of the invariant continuous approximate model (Equation (5.11)) under different cycle lengths, initial densities, and fundamental diagrams. Here we consider a signalized ring road which is formed by connecting the downstream exit with the upstream entrance in Figure 5.1. At the signalized junction, the downstream part is labeled as 0 while the upstream part is labeled as L, where L is the length of the ring. The ring road is a one-lane roadway with a triangular fundamental diagram, i.e., $q = Q_t(k) = \min\{v_f k, w(k_j - k)\}$. Initially, vehicles are uniformly distributed along the ring.

5.5.1 Impacts of initial densities and cycle lengths

With the discrete signal control at the junction, it is hard to obtain analytical solutions of traffic stationary states. Therefore, CTM simulations [9] are used. We set the ring to be 1 mile long, i.e., $L = 1$ mile, and equally divide it into 150 cells. The free-flow speed v_f, the shock-wave speed w, and the jam density k_j are set to be 60 mph, 15 mph, and 150 vpm, respectively, and therefore, the capacity C is 1800 vph. The effective green time is $\eta = 0.5$. The updating time step Δt is 0.4s, and the total simulation time is 2 hours, which is considered long enough to allow traffic to reach a stationary state.

In Figure 5.4, junction fluxes with the discrete signal control are provided as solid blue lines. The cycle length is the same, which is $T = 60$s, but the initial densities are different. From the figure, periodic patterns in the junction fluxes can be observed under different initial densities, which indicates traffic in the signalized ring road is in stationary states [43]. Therefore, average junction fluxes are obtained by averaging the periodic ones over the last four cycles and provided as dashed-dotted blue lines in the figure.

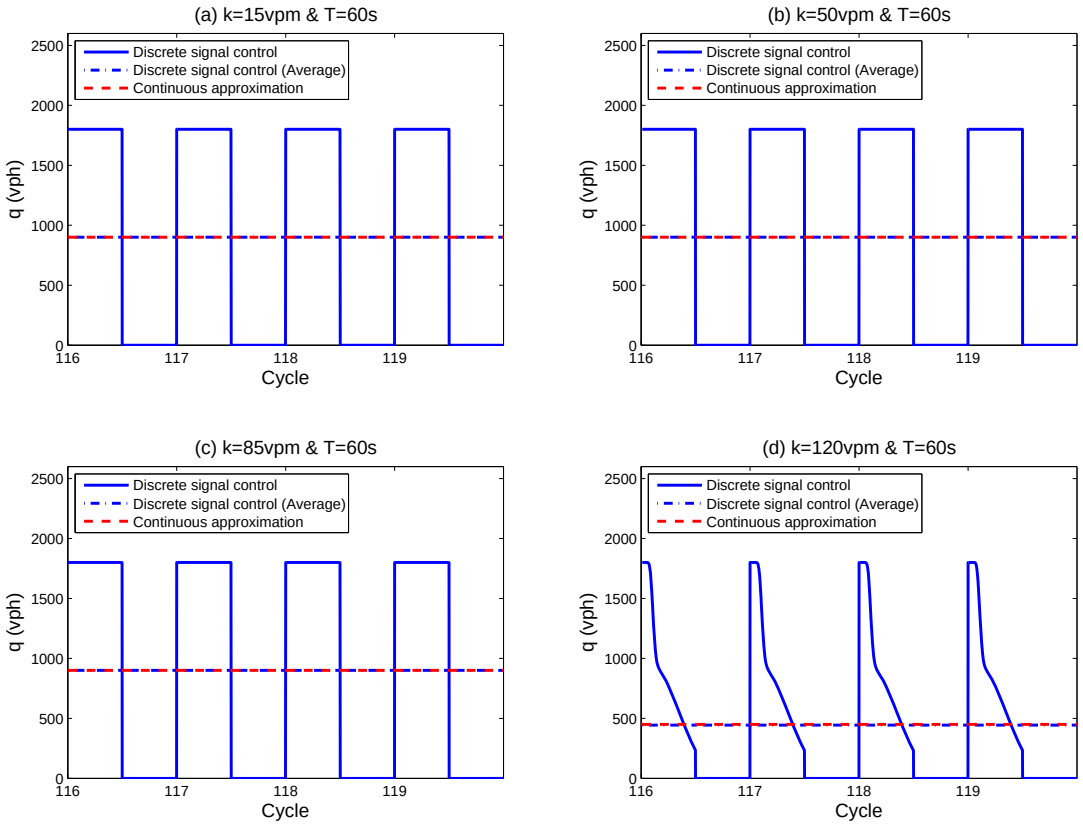

Figure 5.4: Junction fluxes with the same cycle length but different initial densities.

However, with the invariant continuous approximate model in Equation (5.11), it is possible to analytically derive possible stationary states under different initial densities. According to [44], there exist three types of stationary states on a road link: strictly under critical (SUC), over critical (OC), and zero-speed shock wave (ZS). When $C_1 = C_2 = C$, the entropy condition (Equation 5.12) at the signalized junction is now changed to $q = \min\{D(L,t), S(0,t), \eta C\}$. Then we have the following stationary states in the signalized ring road:

(1) If $q = D(L,t)$, only SUC stationary states can exist. That means $U = (D(x,t), S(x,t)) = (D(L,t), C)$ for $x \in [0, L]$.

(2) If $q = S(0,t)$, only OC stationary states can exist. That means $U = (D(x,t), S(x,t)) = (C, S(0,t))$ for $x \in [0, L]$.

(3) If $q = \eta C$, SUC, OC, and ZS stationary states can exist. When SUC stationary states exist, we have $U = (D(x,t), S(x,t)) = (\eta C, C)$ for $x \in [0, L]$; when OC stationary states exist, we have $U = (D(x,t), S(x,t)) = (C, \eta C)$ for $x \in [0, L]$; when ZS stationary states exist, we have $U = (D(x,t), S(x,t)) = (\eta C, C)$ for $x \in [0, \alpha L]$, and $U = (D(x,t), S(x,t)) = (C, \eta C)$ for $x \in (\alpha L, L]$, where $\alpha \in (0, 1)$.

We provide the derived junction fluxes with the invariant continuous approximate model as dashed red lines in Figure 5.4. From the figure, we find that under our current settings, the derived flow-rates with the invariant continuous approximate model are the same as the average ones with the discrete signal control.

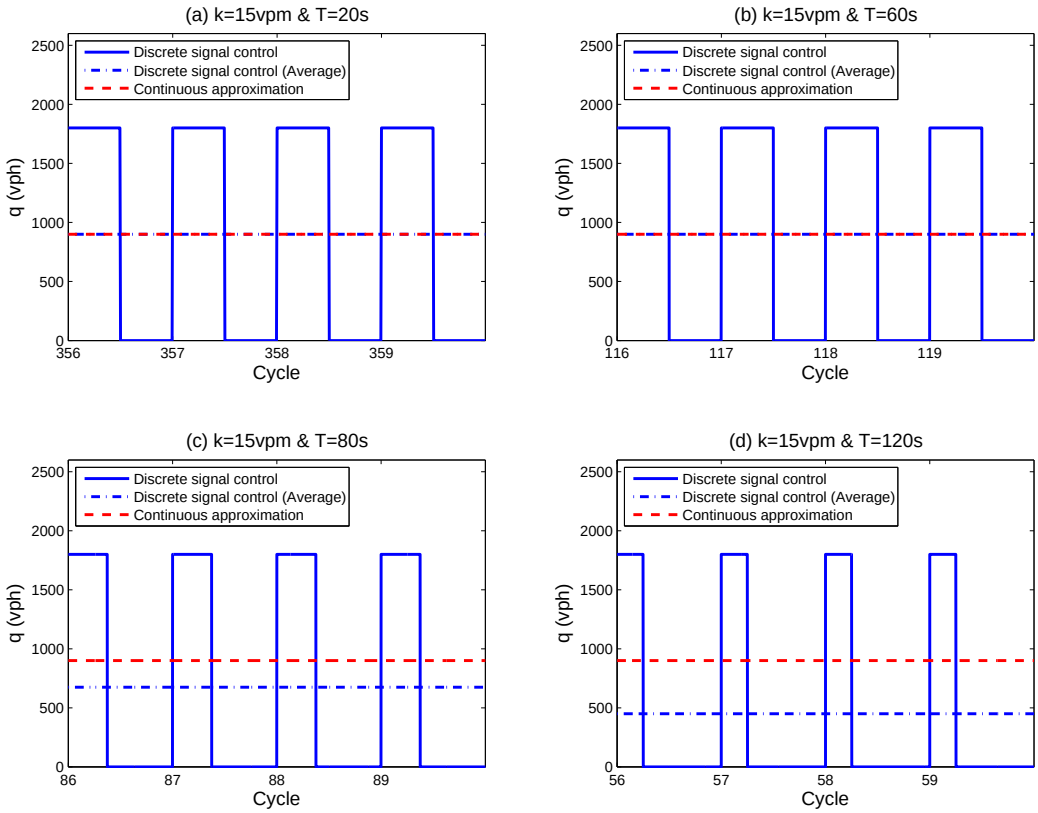

Figure 5.5: Junction fluxes with the same initial density but different cycle lengths.

Given the same initial density, e.g., $k = 15$vpm, but different cycle lengths, the junction fluxes and their averages obtained from the discrete signal control are provided in Figure 5.5. Also, the junction fluxes derived from the invariant continuous approximate model

under the same settings are provided in the same figure. We find that with the same initial density, the differences between the junction fluxes obtained from the invariant continuous approximate model and the ones from the discrete signal control gradually increase as the cycle length increases. We further verify that similar patterns can be found with other initial densities, which indicates the approximation accuracy is impacted by the cycle lengths: long cycle lengths can reduce the approximation accuracy.

5.5.2 Differences in the macroscopic fundamental diagram

The macroscopic fundamental diagram [27] with the discrete signal control in Equation (5.6) is provided as circles in Figure 5.6(a). In the simulations, the cycle length varies from 4s to 720s with $\eta = 0.5$. According to the simulation results, we have the following observations: (i) consistent with Figure 5.5, for one average network density, the average junction flux can take different values, which is related to the cycle lengths; (ii) the average junction fluxes are inside the shaded region formed by $Q_t(k)$, $\eta Q_t(k)$, and ηC, which is also shown in Figure 5.6(a). The derived MFD with the invariant continuous approximate model (Equation (5.11)) is shown as the blue solid line in Figure 5.6(a). From the figure, we find that the average junction fluxes derived from the invariant continuous approximate model are on the upper bound of the MFD with the discrete signal control.

Furthermore, we analyze the property of the invariant continuous approximate model with a strictly concave traffic flow fundamental diagram, e.g., Greenshields' fundamental diagram [32]. In Greenshields' fundamental diagram, i.e., $q = Q_g(k) = v_f k(1 - k/k_j)$, the free-flow speed is $v_f = 60$ mph, and the jam density is $k_j = 150$ vpm. The cycle length ranges from 4s to 360s. In Figure 5.6(b), we provide the MFDs with both the discrete signal control and the invariant continuous approximate model. From the figure, we find that the invariant continuous approximate model is not sensitive to the type of fundamental diagrams since

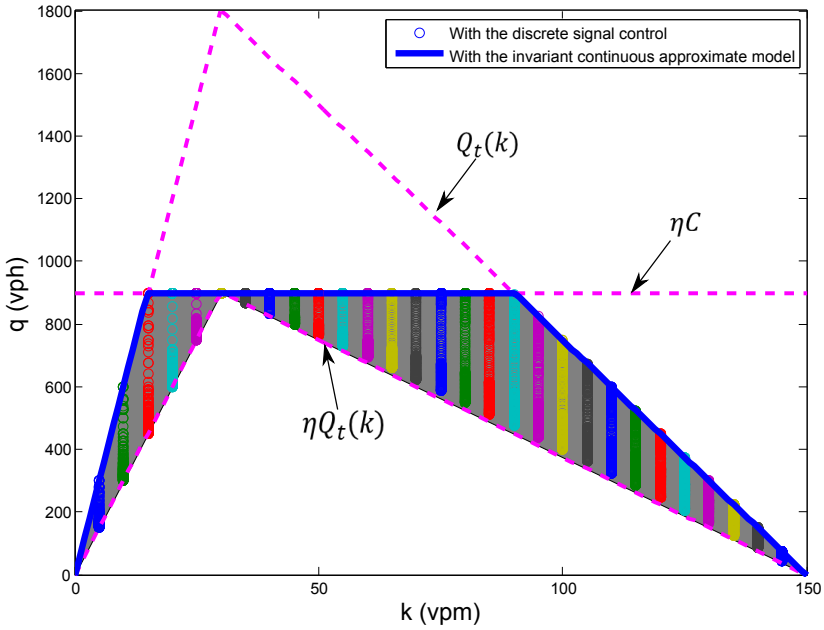

(a) With the triangular fundamental diagram

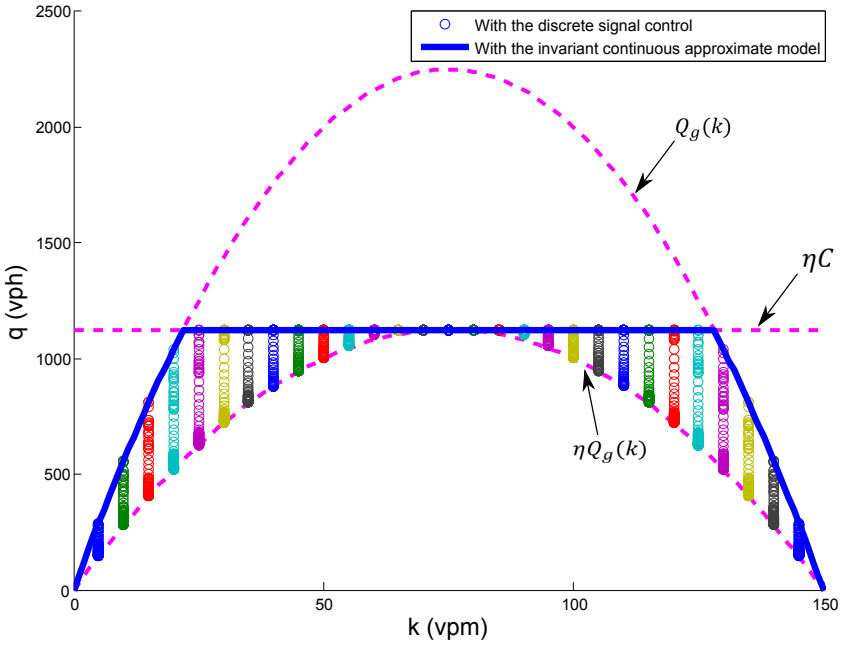

(b) With Greenshields' fundamental diagram

Figure 5.6: Macroscopic fundamental diagrams of the signalized ring road.

similar patterns as those in Figures 5.6(a) can be observed.

5.6 Importance of invariant continuous approximate models in the link transmission model

In [47], continuous formulations of the link transmission model (LTM) [78] were provided. It was shown that when traffic is stationary, the demand and supply of link a can be determined by the flow-rate q_a and the congested portion β_a in the downstream part of the link, which are provided below:

$$D_a = \min\{q_a + H(\beta_a(1 - \frac{q_a}{C_a})k_{a,j}L_a), C_a\}, \tag{5.17a}$$

$$S_a = \min\{q_a + H((1 - \beta_a)(1 - \frac{q_a}{C_a})k_{a,j}L_a), C_a\}, \tag{5.17b}$$

where L_a is the length of link a, and the indicator function $H(y)$ for $y \geq 0$ is defined as

$$H(y) = \lim_{\Delta t \to 0^+} \frac{y}{\Delta t} = \begin{cases} 0, & y = 0; \\ +\infty, & y > 0. \end{cases} \tag{5.18}$$

Theorem 5.5. *For the signalized road link in Figure 5.1, the non-invariant continuous approximate model in Equation (5.14a) can not be used in LTM since the traffic statics problem does not have a solution under certain traffic conditions.*

Proof: Let's consider the case with the origin demand $D_1(-L_1, t) = C_1$ and the destination supply $S_2(L_2, t) < \eta \min\{C_1, C_2\}$. When the network reaches a stationary state, we have $U_1^- = (D_1^-, S_1^-)$ and $U_2^+ = (D_2^+, S_2^+)$ inside the two links. At the downstream end of link 2, we have

$$q_2 = \min\{D_2^+, S_2(L_2, t)\} = \min\{q_2 + H(\beta_2(1 - \frac{q_2}{C_2})k_{2,j}L_2), S_2(L_2, t)\}. \tag{5.19}$$

Since $q_2 < C_2$, we have $q_2 = S_2(L_2, t)$ if $\beta_2 > 0$, and $q_2 \leq S_2(L_2, t)$ if $\beta_2 = 0$. At the upstream

entrance of link 1, we have

$$q_1 = \min\{D_1(-L_1, t), S_1^-\} = \min\{C_1, q_1 + H((1-\beta_1)(1-\frac{q_1}{C_1})k_{a,j}L_1)\}. \tag{5.20}$$

Then we have $(1-\beta_1)(1-\frac{q_1}{C_1}) = 0$, which leads to $q_1 \leq C_1$ and $D_1^- = C_1$.

At the junction, we use the non-invariant continuous approximate model in Equation (5.14a):

$$q_1 = q_2 = \eta \min\{D_1^-, S_2^+\} = \eta \min\{C_1, S_2^+\}. \tag{5.21}$$

If $\beta_2 < 1$, $S_2^+ = C_2$, which leads to $q_2 = \eta \min\{C_2, C_1\} > S_2(L_2, t)$ and contradicts $q_2 \leq S_2(L_2, t)$. If $\beta_2 = 1$, we have $S_2^+ = q_2 = S_2(L_2, t)$ and $q_2 = \eta S_2^+$, which is impossible. Therefore, with the non-invariant continuous approximate model in Equation (5.14a), the traffic statics problem does not have a solution in the link transmission model under the boundary condition $D_1(-L_1, t) = C_1$ and $S_2(L_2, t) < \eta \min\{C_1, C_2\}$. ■

Theorem 5.6. *With the invariant continuous approximate model in Equation (5.11) applied at the junction, the traffic statics problem in LTM has the same solutions of stationary states as those in Theorem 5.2.*

Proof: At the downstream end of link 2, we have

$$q_2 = \min\{D_2^+, S_2(L_2, t)\} = \min\{q_2 + H(\beta_2(1-\frac{q_2}{C_2})k_{2,j}L_2), S_2(L_2, t)\}. \tag{5.22}$$

At the upstream entrance of link 1, we have

$$q_1 = \min\{D_1(-L_1, t), S_1^-\} = \min\{D_1(-L_1, t), q_1 + H((1-\beta_1)(1-\frac{q_1}{C_1})k_{a,j}L_1)\}. \tag{5.23}$$

At the junction, we have

$$q_1 = q_2 = \min\{D_1^-, S_2^+, \eta C_1, \eta C_2\}. \tag{5.24}$$

Then we have the following possible stationary states:

(1) $\min\{D_1(-L_1, t), S_2(L_2, t)\} > \eta \min\{C_1, C_2\}$. It is impossible to have $\beta_1 < 1$ since it leads to $q_1 = D_1(-L_1, t) > \eta \min\{C_1, C_2\}$ and contradicts $q_1 \leq \min\{\eta C_1, \eta C_2\}$. It is also impossible to have $\beta_2 > 0$ since it leads to $q_2 = S_2(L_2, t) > \eta \min\{C_1, C_2\}$ and contradicts $q_2 \leq \min\{\eta C_1, \eta C_2\}$. Therefore, we have $\beta_1 = 1$ and $\beta_2 = 0$, which leads to $D_1^- = C_1$ and $S_2^+ = C_2$. In this case, $q_1 = q_2 = \min\{\eta C_1, \eta C_2\}$.

(2) $D_1(-L_1, t) < S_2(L_2, t)$ and $D_1(-L_1, t) \leq \eta \min\{C_1, C_2\}$. It is impossible to have $\beta_2 > 0$ since it leads to $q_2 = S_2(L_2, t) > D_1(-L_1, t)$ and contradicts $q_2 = q_1 \leq D_1(-L_1, t)$. Therefore, $\beta_2 = 0$, $S_2^+ = C_2$, and $q_1 = q_2 = \min\{D_1^-, \eta C_1, \eta C_2\}$. When $\beta_1 > 0$, we have $D_1^- = C_1$ and $q_1 = \min\{\eta C_1, \eta C_2\} \geq D_1(-L_1, t)$. Since $q_1 \leq D_1(-L_1, t)$, we have $q_1 = q_2 = \min\{\eta C_1, \eta C_2\} = D_1(-L_1, t)$ when $\beta_1 > 0$. When $\beta_1 = 0$, we have $S_1^- = C_1$ and $D_1^- = q_1$, and thus $q_1 = q_2 = D_1(-L_1, t)$.

(3) $D_1(-L_1, t) > S_2(L_2, t)$ and $S_2(L_2, t) \leq \eta \min\{C_1, C_2\}$. It is impossible to have $\beta_1 < 1$ since it leads to $q_1 = D_1(-L_1, t) > S_2(L_2, t)$ and contradicts $q_1 = q_2 \leq S_2(L_2, t)$. Therefore, $\beta_1 = 1$, $D_1^- = C_1$, and $q_1 = q_2 = \min\{S_2^+, \eta C_1, \eta C_2\}$. When $\beta_2 < 1$, we have $S_2^+ = C_2$ and $q_2 = \min\{\eta C_1, \eta C_2\} \geq S_2(L_2, t)$. Since $q_2 \leq S_2(L_2, t)$, we have $q_1 = q_2 = \min\{\eta C_1, \eta C_2\} = S_2(L_2, t)$ when $\beta_2 < 1$. When $\beta_2 = 1$, we have $D_2^+ = C_2$ and $S_2^+ = q_2$, and thus $q_1 = q_2 = S_2(L_2, t)$.

(4) $D_1(-L_1, t) = S_2(L_2, t) \leq \eta \min\{C_1, C_2\}$. When $\beta_1 > 0$ and $\beta_2 < 1$, we have $D_1^- = C_1$, $S_2^+ = C_2$ and $q_1 = \min\{\eta C_1, \eta C_2\}$, which leads to $q_1 = q_2 = \min\{\eta C_1, \eta C_2\} = D_1(-L_1, t) = S_2(L_2, t)$. When $\beta_1 > 0$ and $\beta_2 = 1$, we have $D_1^- = C_1$, $D_2^+ = C_2$, $S_2^+ = q_2$, which leads to $q_1 = q_2 = S_2(L_2, t) = D_1(-L_1, t) \leq \min\{\eta C_1, \eta C_2\}$. When

$\beta_1 = 0$ and $\beta_2 < 1$, we have $D_1^- = q_1$, $S_1^- = C_1$, and $S_2^+ = C_2$, which leads to $q_1 = q_2 = S_2(L_2, t) = D_1(-L_1, t) \leq \min\{\eta C_1, \eta C_2\}$. When $\beta_1 = 0$ and $\beta_2 = 1$, we have $D_1^- = q_1$, $S_1^- = C_1$, $D_2^+ = C_2$, $S_2^+ = q_2$, which leads to $q_1 = q_2 = S_2(L_2, t) = D_1(-L_1, t) \leq \min\{\eta C_1, \eta C_2\}$.

From the above analysis, we find that junction fluxes at stationary states exist under various traffic conditions and are the same as those in Theorem 5.2. ■

5.7 Conclusions

In this chapter, we provided a systematic and comprehensive study on deriving invariant continuous approximate models for a signalized road link and analyzing their properties under different capacity constraints, traffic conditions, fundamental diagrams, and traffic flow models. We first proposed three forms of discrete signal control at the signalized road link and derived their invariant continuous approximate models by averaging the periodic control parameter over time and solving the Riemann problems in the supply-demand framework [48]. We analyzed the properties of these three invariant continuous approximate models and showed that only one of them can fully capture the capacity constraints at the signalized junction. We also showed that multiple non-invariant continuous approximate models can have the same invariant form. Using CTM simulations in a signalized ring road, we demonstrated the invariant continuous approximate model is a good approximation to the discrete signal control even under different fundamental diagrams. But we also showed that long cycle lengths will reduce the approximation accuracy. In addition, we proved that non-invariant continuous approximate models can not be used in the link transmission model since they can yield no solution to the traffic statics problem under certain traffic conditions. But with the invariant continuous approximate model, the derived junction fluxes under stationary state conditions are the same as those in the LWR model.

Chapter 6

Simulation studies on the traffic statics and dynamics in a signalized grid network

6.1 Introduction

In previous chapters, traffic statics and dynamics have been comprehensively studied in a signalized double-ring network using the kinematic wave approach in Chapter 3 and the Poincaré map approach in Chapter 4. However, it is still unclear about the static and dynamic properties of traffic flow in more general signalized networks, such as a signalized grid network. Also it is unclear about whether the analytical insights obtained for double-ring networks can apply to more general networks or not. In this chapter, we want to fill this gap.

Different from the signalized double-ring network, traffic statics and dynamics in the signalized grid network are more complicated since it involves more signalized junctions, more

route choices, and more complicated demand patterns. It is hard to apply the Poincaré map approach in Chapter 4 to the signalized grid network since it is unclear how to define the Poincaré maps and where to put the Poincaré sections. It is also not suitable to apply the kinematic wave mode to the signalized grid network since complicated shock and rarefaction waves can exist inside a link and it will take a long time for the network to reach a stationary state in simulations. Therefore, the link queue model in [43] is used to study the static and dynamic properties of traffic flow in the signalized grid network. Similar to Chapter 3, we are going to verify the existence of periodic traffic patterns (i.e., stationary states) and study the impacts of signal settings and route choice behaviors on the average network flow-rates as well as the MFDs.

The rest of this chapter is organized as follows. In Section 6.2, we provide a link queue formulation to the traffic dynamics in a signalized grid network. In Section 6.3, we demonstrate the existence of stationary states under different retaining ratios and initial densities. In Section 6.4, we show the impacts of retaining ratios and cycle lengths on the average network flow-rates. We also provide the shapes of the MFDs under different retaining ratios and cycle lengths. In Section 6.5, we provide the impacts of random retaining ratios on the stationary states and thus the MFDs. In Section 6.6, we summarize our research findings.

6.2 Formulation of traffic dynamics in a signalized grid network

In Figure 6.1, a signalized 6×6 grid network is provided. There are 72 one-way links and 36 intersections in the network. The links are divided into two families: the ones in the East-West direction are in one family while those in the North-South direction are in the other family. In order to maintain the same number of vehicles inside the network,

exiting vehicles are immediately added into the network from their corresponding upstream entrances, and therefore, the signalized grid network is changed into a closed network with periodic boundary conditions.

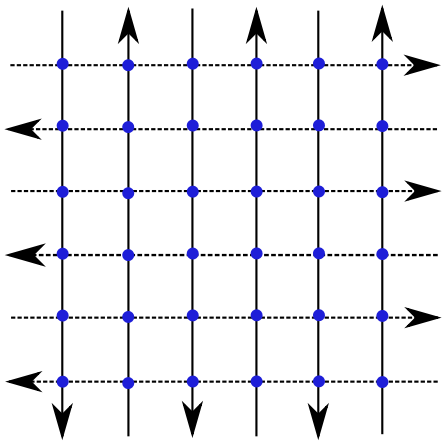

Figure 6.1: A signalized 6×6 grid network.

Similar to Chapter 4.2.1, traffic dynamics in the signalized grid network are formulated as follows:

- At each intersection, it contains one upstream link and one downstream link from each of the two families. The upstream and the downstream links in the East-West direction are denoted as h_u and h_d, respectively, while the ones in the North-South direction are denoted as v_u and v_d, respectively. In each cycle, without loss of generality, we assign phase 1 to vehicles on link h_u and phase 2 to those on link v_u. We assume all intersections have the same cycle length T and the same lost time Δ for each phase. The green ratio is denoted as π_1 for phase 1 and π_2 for phase 2. We further assume the yellow and all red period in each phase is the same as the lost time, and therefore, the effective green time is $\pi_1 T$ for phase 1 and $\pi_2 T$ for phase 2, and $(\pi_1 + \pi_2)T = T - 2\Delta$. Then the signal control at intersection j can be described using the following indicator

functions:

$$\delta_1(t;T,\Delta,\pi_1) = \begin{cases} 1, & t \in [nT, nT+\pi_1 T), \\ 0, & \text{otherwise}, \end{cases} \qquad n \in \mathbb{N}_0 \tag{6.1a}$$

$$\delta_2(t;T,\Delta,\pi_1) = \begin{cases} 1, & t \in [nT+\Delta+\pi_1 T, (n+1)T-\Delta), \\ 0, & \text{otherwise}, \end{cases} \qquad n \in \mathbb{N}_0 \tag{6.1b}$$

where $\mathbb{N}_0 = \{0, 1, 2, 3, ...\}$.

The retaining ratio is denoted as $\xi_1(t) \in (0,1)$ for vehicles from link h_u to link h_d and $\xi_2(t) \in (0,1)$ for those from link v_u to link v_d. That is to say, the turning ratio is $1-\xi_1(t)$ for vehicles from link h_u to link v_d and $1-\xi_2(t)$ for those from link v_u to link h_d. Then the out-fluxes $g_{h_u}(t)$, $g_{v_u}(t)$, and the in-fluxes $f_{h_d}(t)$, $f_{v_d}(t)$ can be calculated as

$$g_{h_u}(t) = \delta_1(t) \min\{D_{h_u}(t), \frac{S_{h_d}(t)}{\xi_1(t)}, \frac{S_{v_d}(t)}{1-\xi_1(t)}\}, \tag{6.2a}$$

$$g_{v_u}(t) = \delta_2(t) \min\{D_{v_u}(t), \frac{S_{v_d}(t)}{\xi_2(t)}, \frac{S_{h_d}(t)}{1-\xi_2(t)}\}, \tag{6.2b}$$

$$f_{h_d}(t) = g_{h_u}(t)\xi_1(t) + g_{v_u}(t)(1-\xi_2(t)), \tag{6.2c}$$

$$f_{v_d}(t) = g_{h_u}(t)(1-\xi_1(t)) + g_{v_u}(t)\xi_2(t), \tag{6.2d}$$

where $D_{h_u}(t)$ and $D_{v_u}(t)$ are the demands of the upstream links h_u and v_u, respectively, and $S_{h_d}(t)$ and $S_{v_d}(t)$ are the supplies of the downstream links h_d and v_d, respectively. The demands and supplies can be calculated using Equation (4.1) in Chapter 4.

- For link i, the average link density $k_i(t)$ is the only stable variable. Traffic dynamics on link i can be described using the following equation:

$$\frac{dk_i(t)}{dt} = \frac{1}{L}(f_i(t) - g_i(t)). \tag{6.3}$$

With Equations (6.1) to (6.3), the system dynamics of the signalized grid network are complete: the in-/out-fluxes of each link can be calculated using Equations (6.1) and (6.2), and the density of each link can be updated using Equation (6.3).

6.3 Existence of traffic stationary states

In this section, we are going to verify the existence of stationary states in the signalized grid network. For simplicity, we have the following homogeneous settings: (i) all links have the same lengths, e.g., $L = 0.25$ miles, and the same time-and-location independent triangular traffic flow fundamental diagram with $v_f = 60$ mph, $k_c = 30$ vpm, and $k_j = 150$ vpm; (ii) at all intersections, the retaining ratios are the same and time independent, i.e., $\xi_1(t) = \xi_2(t) = \xi$; (iii) at all intersection, the lost times and offsets are zero, and the effective green times are the same for the two incoming approaches, i.e., $\pi_1 = \pi_2 = \pi = 0.5$; (iv) initially, the densities are the same among the links belonging to the same family, e.g., $k_1(0)$ for the East-West links and $k_2(0)$ for the North-South links. For the LQM simulations in this section, the cycle length is $T = 30$s. The updating time step is $\Delta t = 0.05$s. The total simulation time is 10 hours, which is considered to be long enough for the signalized grid network to reach a stationary state. To calculate the asymptotic average network flow-rate, the following equation is used:

$$q(t) = \frac{\sum_{i=1}^{n} \hat{g}_i(t)}{n} = \frac{\sum_{i=1}^{n} \int_{s=t-T}^{t} g_i(s)ds}{nT}, \tag{6.4}$$

where n is the total number of regular links in the signalized grid network.

6.3.1 With large retaining ratios

In this subsection, the retaining ratio is $\xi_1 = \xi_2 = 0.6$. With initial densities $k_1(0) = k_2(0) = 25$ vpm, the distribution of link densities at the last cycle is provided in Figure 6.2(a). From the figure, we find that the densities of the links in the same family are the same and very close to those in the other family. In Figure 6.2(b), we provide the evolution pattern of the average network flow-rate in the grid network. We find that the average network flow-rate reaches a constant value after 0.1 hour, which shows the signalized grid network has reached a stationary state.

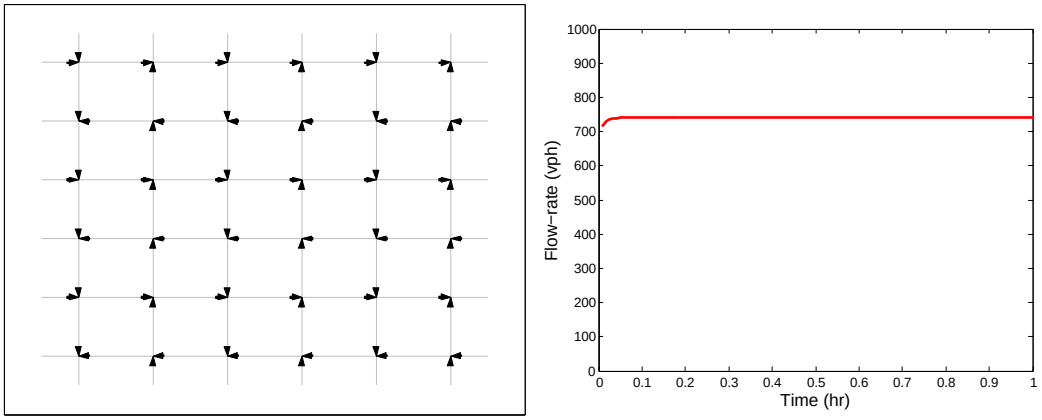

(a) Density distribution (b) Average flow-rate

Figure 6.2: The distribution of link densities at the last cycle and the evolution pattern of the average network flow-rate with $k_1(0) = k_2(0) = 25$ vpm and $\xi = 0.6$.

When the average network density increases to a certain value, the traffic patterns are different. In Figure 6.3, we provide the distributions of link densities at the last cycle and the evolution patterns of the average network flow-rate under the same average network density but different initial densities. As shown in Figures 6.3(a) and 6.3(b), starting with $k_1(0) = 20$ vpm and $k_2(0) = 100$ vpm, traffic is more congested in the North-South links when the network reaches a stationary state. However, as shown in Figures 6.3(c) and 6.3(d), densities are more uniformly distributed among the links of the two families when the initial densities are $k_1(0) = 60$ vpm and $k_2(0) = 60$ vpm. The average network flow-rate

is the highest, which is half of the link capacity. Furthermore, as shown in Figure 6.3(e), if the initial densities are $k_1(0) = 100$ vpm and $k_2(0) = 20$ vpm, the density distribution is different: the East-West links are more congested when the network reaches a stationary state. From Figure 6.3(f), the average network flow-rate is the same as that in Figure 6.3(b) when the network reaches a stationary state. The simulation results show that when the average network density reaches a certain value, multivaluedness in the flow-density relation exists: for the same average network density, we can have different average network flow-rates, which is consistent with the finding in the signalized double-ring network.

When the average network density is greater than half of the jam density, the traffic pattern is also different. In Figure 6.4, we provide the distribution of link densities at the last cycle and the evolution pattern of the average network flow-rate with initial densities $k_1(0) = k_2(0) = 120$ vpm. We find that the grid network is finally gridlocked in the North-South links and the average network flow-rate reduces to zero. Such a gridlock pattern is also consistent with that in the signalized double-ring network. Note that in the signalized double-ring network, there exists an unstable stationary state with a more symmetric density distribution and a higher average network flow-rate. But it is hard to find such a stationary state in the signalized grid network using simulations since it is unstable.

6.3.2 With small retaining ratios

In this subsection, the retaining ratio is $\xi_1 = \xi_2 = 0.4$. We provide the distribution of link densities at the last cycle and the evolution pattern of the average network flow-rate in Figure 6.5 when initial densities are $k_1(0) = k_2(0) = 25$ vpm. From the figure, we find that when the network reaches a stationary state, the links have relatively the same densities, which is similar to Figure 6.2.

However, it is a different case when the average network density reaches a certain value, e.g.,

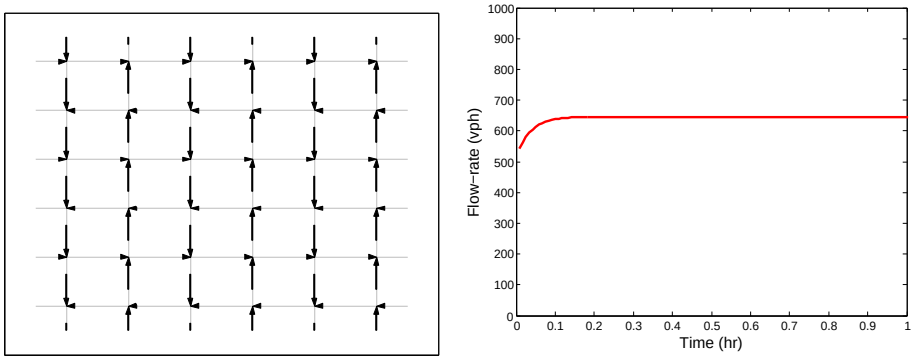

(a) $(k_1(0), k_2(0))$ =(20,100) vpm (b) $(k_1(0), k_2(0))$ =(20,100) vpm

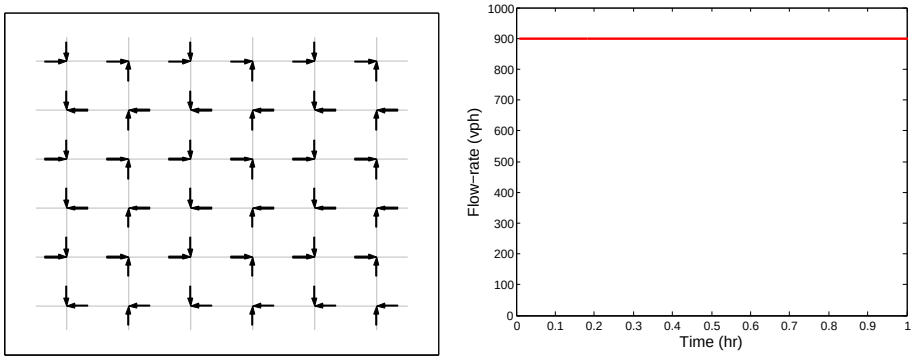

(c) $(k_1(0), k_2(0))$ =(60,60) vpm (d) $(k_1(0), k_2(0))$ =(60,60) vpm

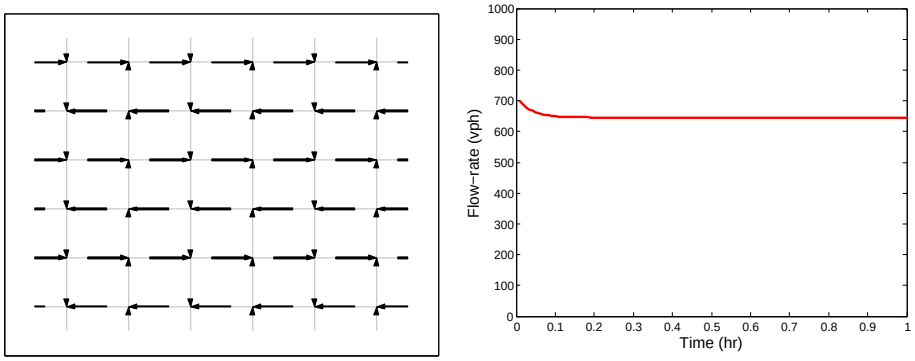

(e) $(k_1(0), k_2(0))$ =(100,20) vpm (f) $(k_1(0), k_2(0))$ =(100,20) vpm

Figure 6.3: Distributions of link densities at the last cycle (left) and evolution patterns of the average network flow-rate (right) with $k = 60$ vpm and $\xi = 0.6$.

$k = 60$ vpm. In Figure 6.6, we provide the distributions of link densities at the last cycle and the evolution patterns of the average network flow-rate under the same average network density but different initial densities. Different from Figure 6.3, when $\xi = 0.4$, densities are relatively uniformly distributed among the links even starting with different initial densities.

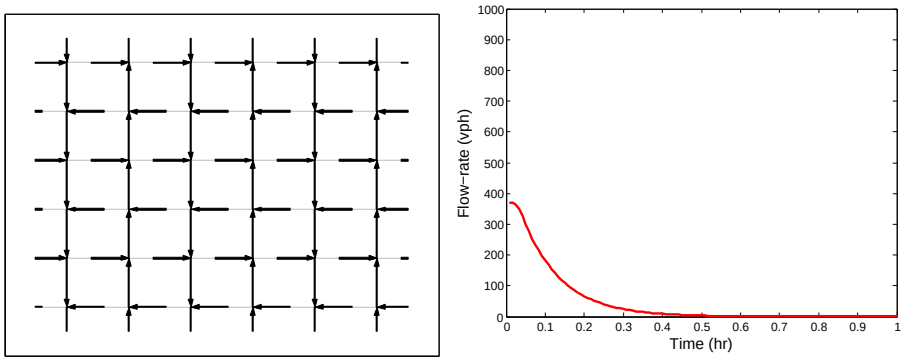

(a) Density distribution (b) Average flow-rate

Figure 6.4: The distribution of link densities at the last cycle (left) and the evolution pattern of the average network flow-rate (right) with $k_1(0) = k_2(0) = 120$ vpm and $\xi = 0.6$.

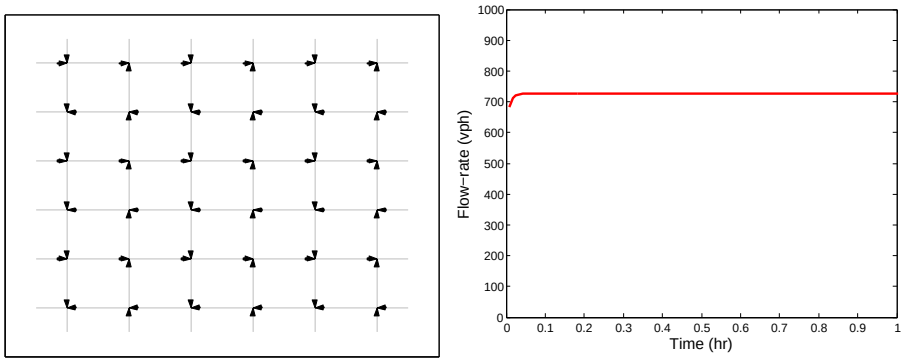

(a) Density distribution (b) Average flow-rate

Figure 6.5: The distribution of link densities at the last cycle (left) and the evolution pattern of the average network flow-rate (right) with $k_1(0) = k_2(0) = 25$ vpm and $\xi = 0.4$.

The average network flow-rates for the three cases in Figure 6.6 are the same, which is half of the link capacity. The simulation results show that with lower retaining ratios, the grid network can have higher average network flow-rates and more symmetric density distributions, which is consistent with that in the signalized double-ring network.

When the average network density is greater than half of the jam density, the traffic pattern is also different with $\xi = 0.4$. In Figure 6.7, we provide the distribution of link densities at the last cycle and the evolution pattern of the average network flow-rate with initial densities $k_1(0) = k_2(0) = 120$ vpm. We find that the signalized grid network is not gridlocked with low retaining ratios. Compared with Figure 6.4, the density distribution is more symmetric

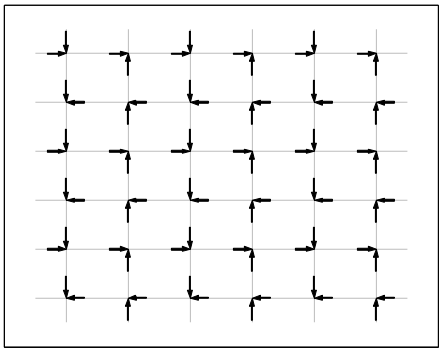

(a) $(k_1(0), k_2(0))$ =(20,100) vpm

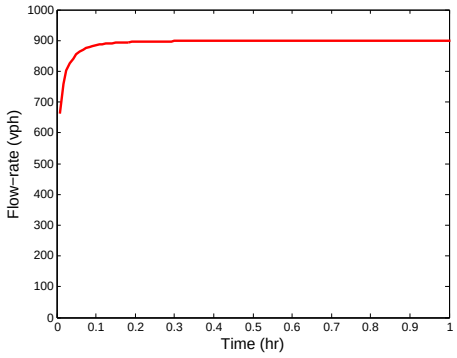

(b) $(k_1(0), k_2(0))$ =(20,100) vpm

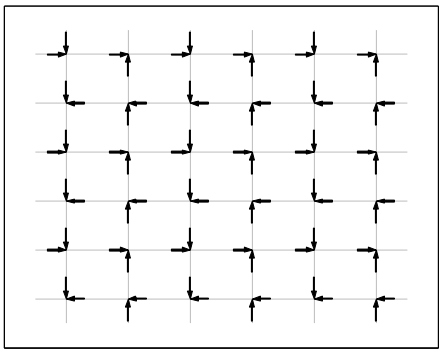

(c) $(k_1(0), k_2(0))$ =(60,60) vpm

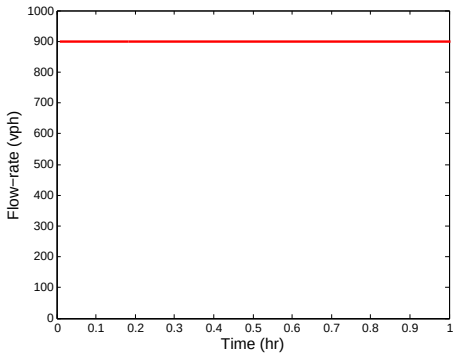

(d) $(k_1(0), k_2(0))$ =(60,60) vpm

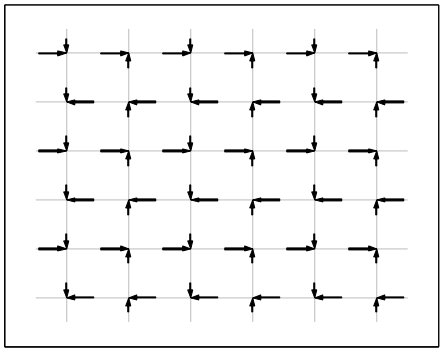

(e) $(k_1(0), k_2(0))$ =(100,20) vpm

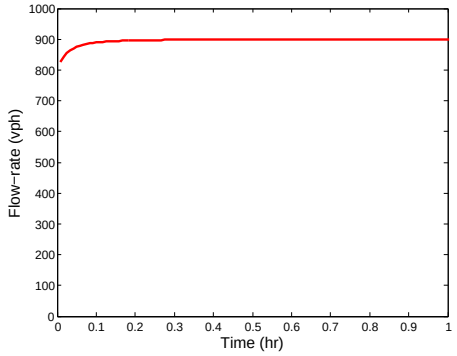

(f) $(k_1(0), k_2(0))$ =(100,20) vpm

Figure 6.6: Distributions of link densities at the last cycle (left) and evolution patterns of the average network flow-rate (right) with $k = 60$ vpm and $\xi = 0.4$.

among the links and the average network flow-rate is higher, which is also consistent with that in the signalized double-ring network.

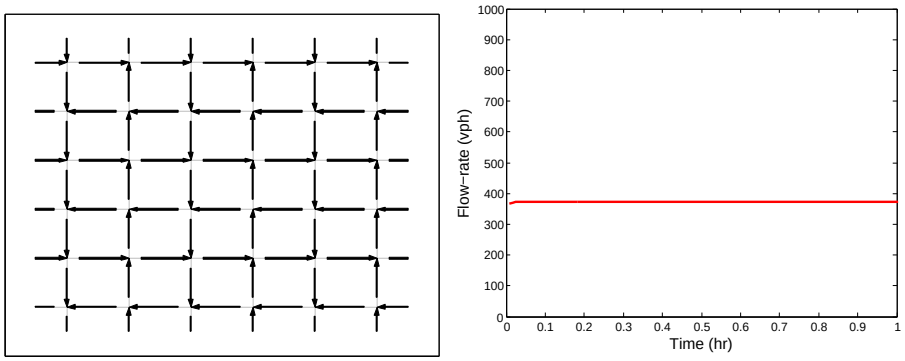

(a) Density distribution (b) Average flow-rate

Figure 6.7: The distribution of link densities at the last cycle (left) and the evolution pattern of the average network flow-rate (right) with $k_1(0) = k_2(0) = 120$ vpm and $\xi = 0.4$.

6.4 Impacts of cycle lengths and retaining ratios and macroscopic fundamental diagrams

6.4.1 Impacts of cycle lengths and retaining ratios

In this subsection, we analyze the impacts of cycle lengths and retaining ratios on the average network flow-rates in the signalized grid network. In Figure 6.8, we provide the average network flow-rates with a constant retaining ratio $\xi = 0.85$ but different cycle lengths and average network densities. From the figure, we find that the relation between the cycle length and the average network flow-rate is quite complicated under different average network densities. With a low average network density, e.g., $k = 15$ vpm, the average network flow-rate decreases with the cycle length. However, with a medium average network density, e.g., $k = 50$ vpm, the average network flow-rate increases with the cycle length. When the average network density is greater than half of the jam density, the average network flow-rate is always zero, which is shown in Figures 6.8 (c) and (d).

In Figure 6.9, we provide the average network flow-rates with a constant cycle length $T =$ 100s but different retaining ratios and average network densities. From the figure, we find

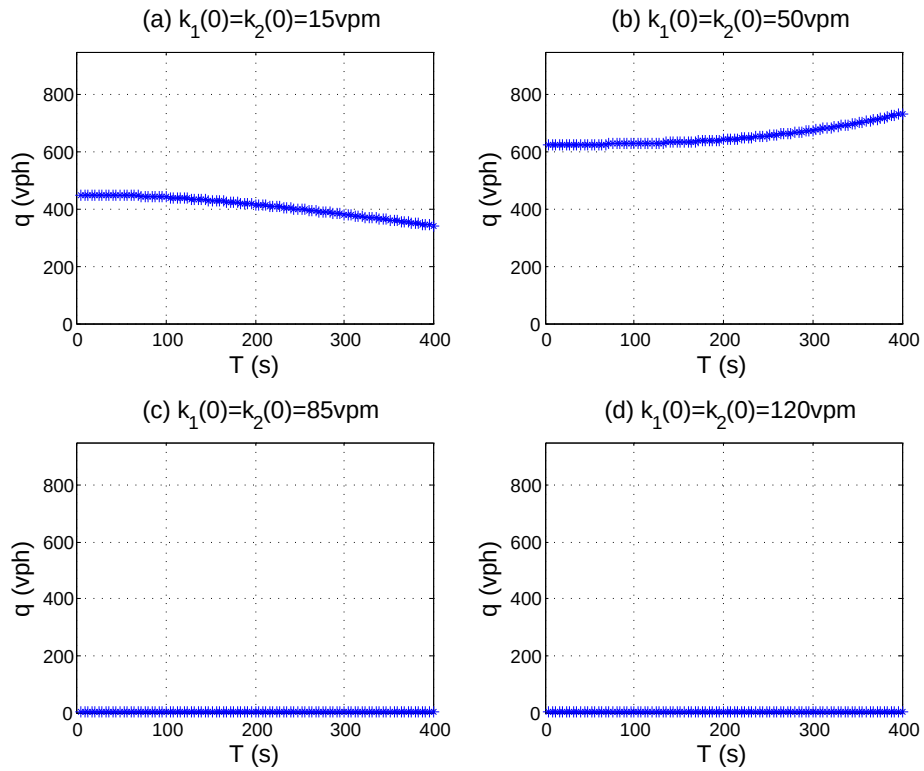

Figure 6.8: Impacts of the cycle length T on the average network flow-rate q with a constant retaining ratio $\xi = 0.85$.

that different retaining ratios can also lead to different average network flow-rates even with the same initial densities. When the retaining ratio is low, e.g. $\xi < 0.5$, the average network flow-rate increases with the retaining ratio. However, with medium or high average network densities, when the retaining ratio is high, i.e., $\xi > 0.5$, the average network flow-rate decreases or even converges to zero as the retaining ratio increases, which can be observed from Figures 6.9 (b) to (d).

6.4.2 Macroscopic fundamental diagrams

In Figure 6.10, we provide the MFDs under different combinations of cycle lengths and retaining ratios. In Figures 6.10(a) and 6.10(c), MFDs are provided when $\xi = 0.6$ but $T = 30$s and 120s, respectively. From the figures, we have the following findings: (i) with

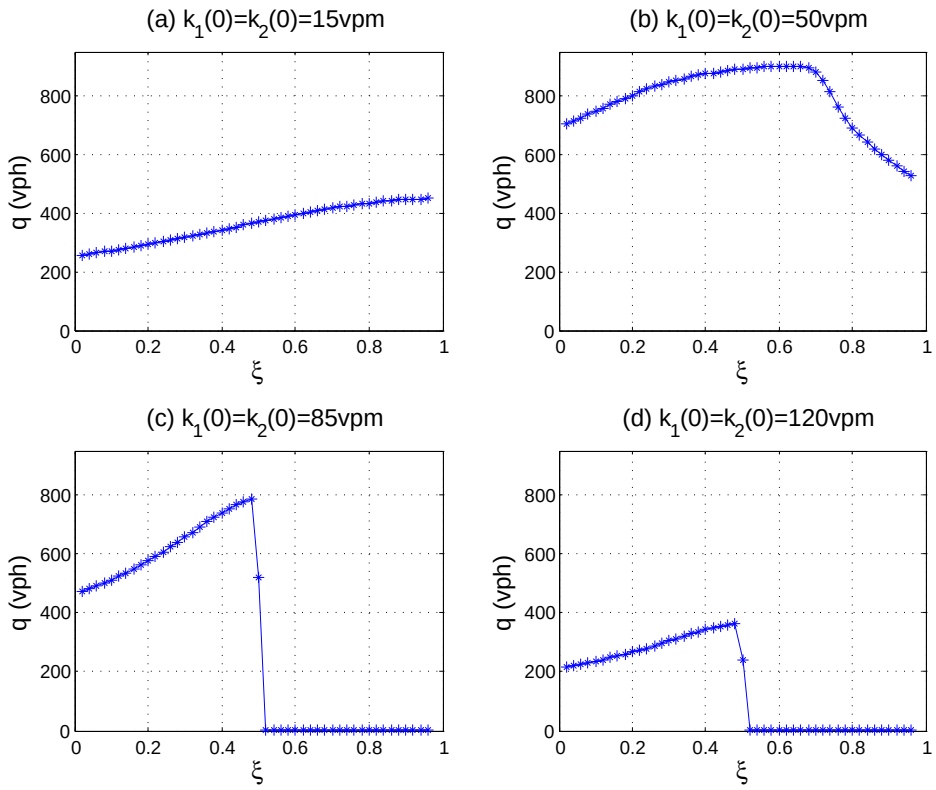

Figure 6.9: Impacts of the retaining ratio ξ on the average network flow-rate q with a constant cycle length $T = 100$s.

large retaining ratios, multivaluedness exists in the network flow-density relation and the network will get gridlocked when the average network density is higher than half of the jam density; (ii) the shapes of the MFDs are similar to that in Figure 4.3(a), but the unstable branch is not observed in the simulations; (iii) with longer cycle lengths, the average network flow-rates are harder to sustain at the highest value, which is half of the link capacity.

In Figures 6.10(b) and 6.10(d), MFDs are provided when $\xi = 0.4$ but $T = 30$s and 120s, respectively. From the figures, we have the following findings: (i) with low retaining ratios, the grid network won't get gridlocked unless it initially is; (ii) the multivaluedness disappears for the densities lower than half of the jam density, and the average network flow-rates are higher; (iii) with longer cycle lengths, the average network flow-rates are harder to sustain at the highest value and systematically lower than or equal to those with shorter cycle lengths. The MFDs are similar to those in Figure 4.3(b).

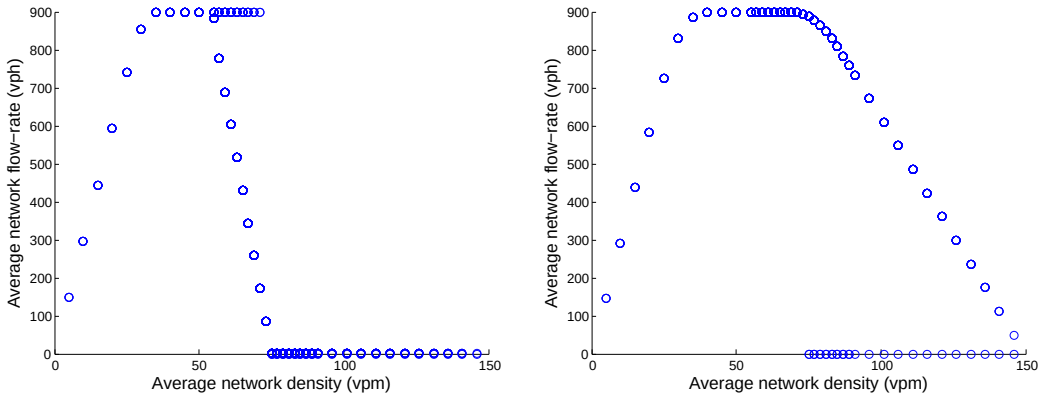

(a) $T = 30$s and $\xi = 0.6$

(b) $T = 30$s and $\xi = 0.4$

(c) $T = 120$s and $\xi = 0.6$

(d) $T = 120$s and $\xi = 0.4$

Figure 6.10: Macroscopic fundamental diagrams in the signalized grid network with different cycle lengths and retaining ratios.

According to the MFDs in Figure 6.10, we can find that lower retaining ratios can help the signalized grid network have higher average network flow-rates, which is consistent with that in the signalized double-ring network.

6.5 Impact of random retaining ratios

In our previous analysis, we have a set of homogeneous settings such as the same signal settings and the same retaining ratios at all intersections. But in reality, retaining ratios at an intersection are changing from time to time. Therefore, in this section we relax such a

homogeneous assumption and consider the retaining ratios at an intersection are random. In our simulation, the retaining ratios are different from cycle to cycle but the same within the cycle. At the beginning of each cycle, retaining ratios can pick any values within the interval $[\bar{\xi} - 0.05, \bar{\xi} + 0.05]$, where $\bar{\xi}$ is the average retaining ratio over time and the same for all intersections.

6.5.1 On the stationary states

In Figure 6.11, we provide the distributions of link densities at the last cycle and the evolution patterns of the average network flow-rate under different initial densities with retaining ratios $\xi \in [0.55, 0.65]$. From Figures 6.11(a) and 6.11(b), we find that when the average network density is low, e.g., $k = 20$ vpm, the signalized grid network is hard to get gridlocked. However, with medium or high average network densities, traffic inside the signalized grid network will finally converge to gridlock, which can be observed from Figures 6.11(c) to 6.11(f). In addition, when the retaining ratios are constant, the signalized grid network is not gridlocked with $k = 60$ vpm. But as shown in Figures 6.11(c) and 6.11(d), the network is finally gridlocked when randomness exists in the retaining ratios.

In Figure 6.12, we provide the distributions of link densities at the last cycle and the evolution patterns of the average network flow-rate under different initial densities with retaining ratios $\xi \in [0.35, 0.45]$. Similar to the case with $\xi \in [0.55, 0.65]$, we find that the signalized grid network is hard to get gridlocked when the average network density is low, which can be observed from Figures 6.12(a) and 6.12(b). In our previous analysis, with small and constant retaining ratios, the signalized grid network won't get gridlocked unless it initially is. However, similar to the case with $\xi \in [0.55, 0.65]$, the signalized grid network will get gridlocked with lower retaining ratios when randomness exists in the retaining ratios, which is shown in Figures 6.12(c) to 6.12(f).

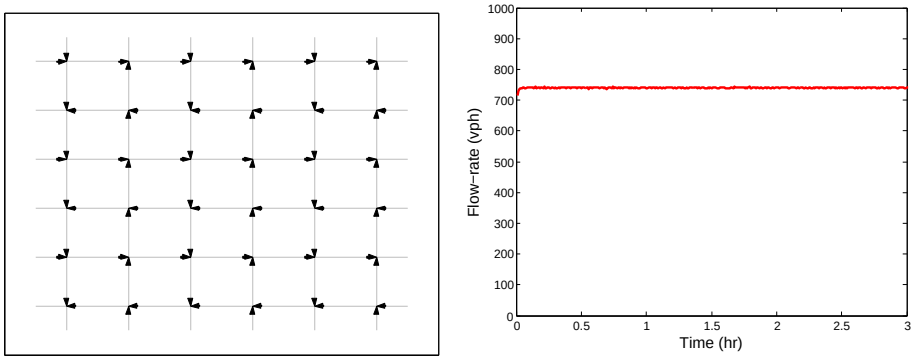

(a) $(k_1(0), k_2(0))$ =(25,25) vpm (b) $(k_1(0), k_2(0))$ =(25,25) vpm

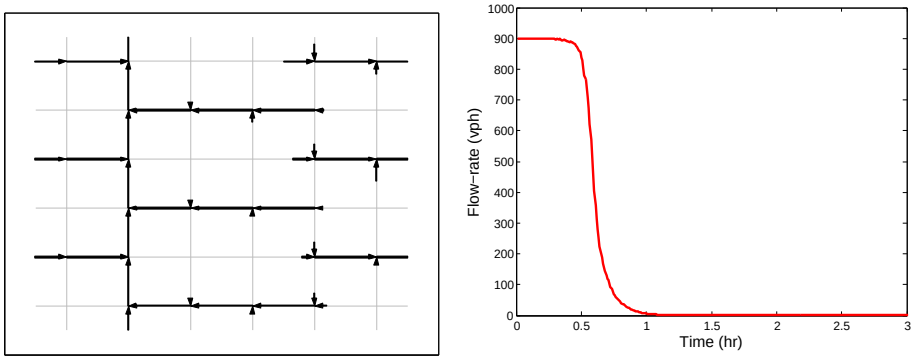

(c) $(k_1(0), k_2(0))$ =(60,60) vpm (d) $(k_1(0), k_2(0))$ =(60,60) vpm

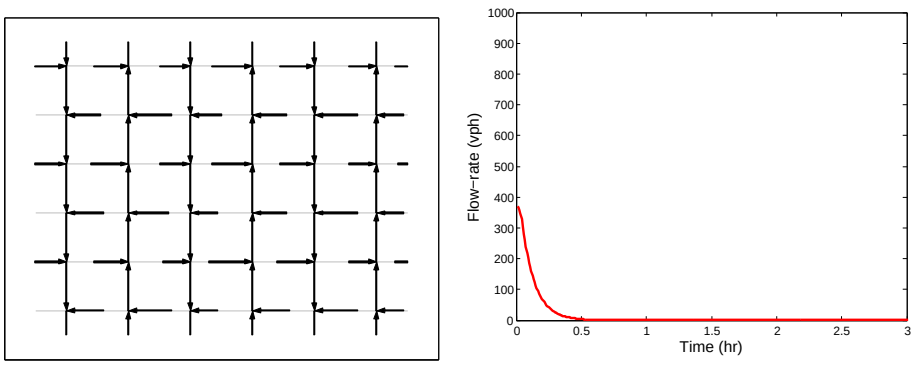

(e) $(k_1(0), k_2(0))$ =(120,120) vpm (f) $(k_1(0), k_2(0))$ =(120,120) vpm

Figure 6.11: Distributions of link densities at the last cycle (left) and evolution patterns of the average network flow-rate (right) with random retaining ratios $\xi \in [0.55, 0.65]$.

6.5.2 On the macroscopic fundamental diagram

In Figure 6.13, we provide the network flow-density relations in the signalized grid network after 10-hour simulations under different combinations of cycle lengths and retaining ratios. From the figure, we find that the network flow-density relations are similar to each other

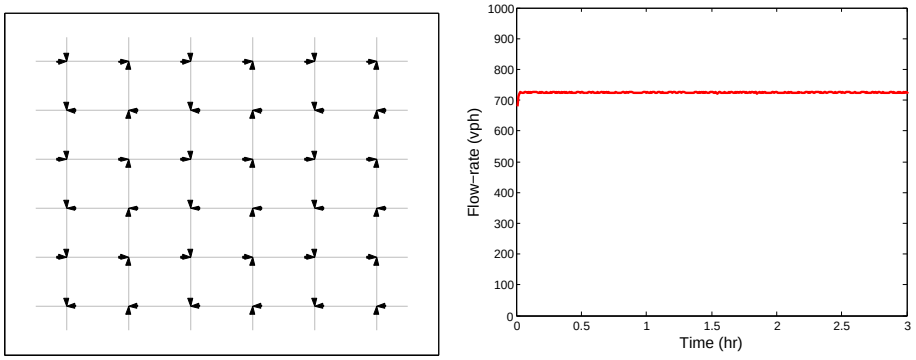

(a) $(k_1(0), k_2(0))$ =(25,25) vpm (b) $(k_1(0), k_2(0))$ =(25,25) vpm

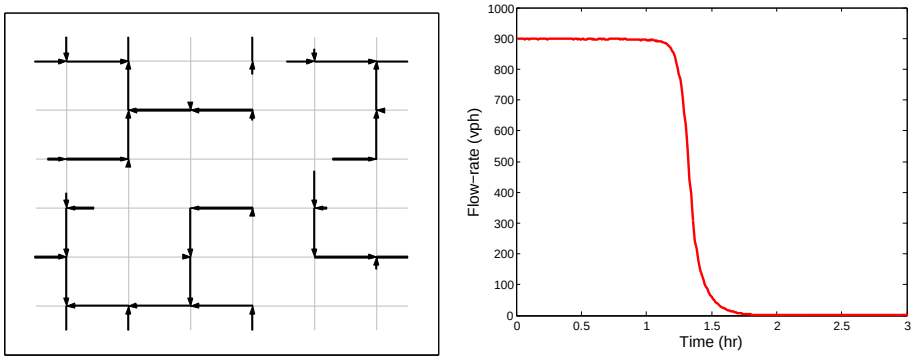

(c) $(k_1(0), k_2(0))$ =(60,60) vpm (d) $(k_1(0), k_2(0))$ =(60,60) vpm

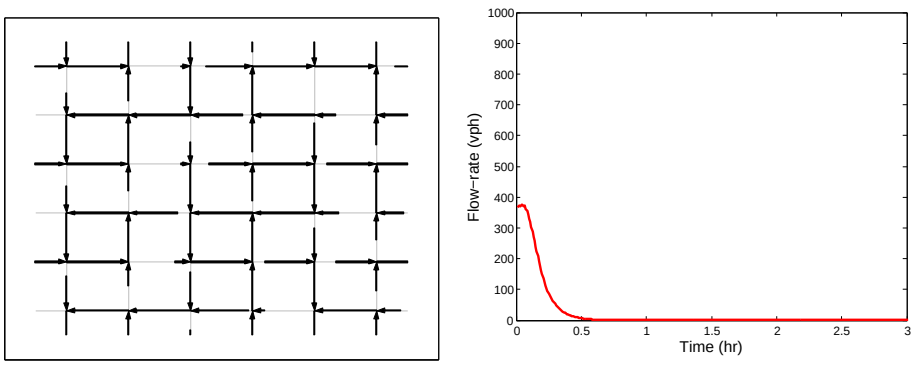

(e) $(k_1(0), k_2(0))$ =(120,120) vpm (f) $(k_1(0), k_2(0))$ =(120,120) vpm

Figure 6.12: Distributions of link densities at the last cycle (left) and evolution patterns of the average network flow-rate (right) with random retaining ratios $\xi \in [0.35, 0.45]$.

even the cycle lengths or retaining ratios are different. With randomness in the retaining ratios, the signalized grid network will get gridlocked even with small retaining ratios, which is shown in Figures 6.13(b) and 6.13(d). Note that it is normal to observe transitional points in the network flow-density relation in Figure 6.13(a) since the retaining ratios are random

and the signalized grid network may not converge to near-stationary states at the end of the simulations. Comparing 6.13(a) with 6.13(c) or 6.13(b) with 6.13(d), we find that: (i) it is harder for the signalized grid network to maintain higher average network flow-rates with longer cycle lengths; (ii) with shorter cycle lengths, the signalized grid network tends to get gridlocked at lower average network densities.

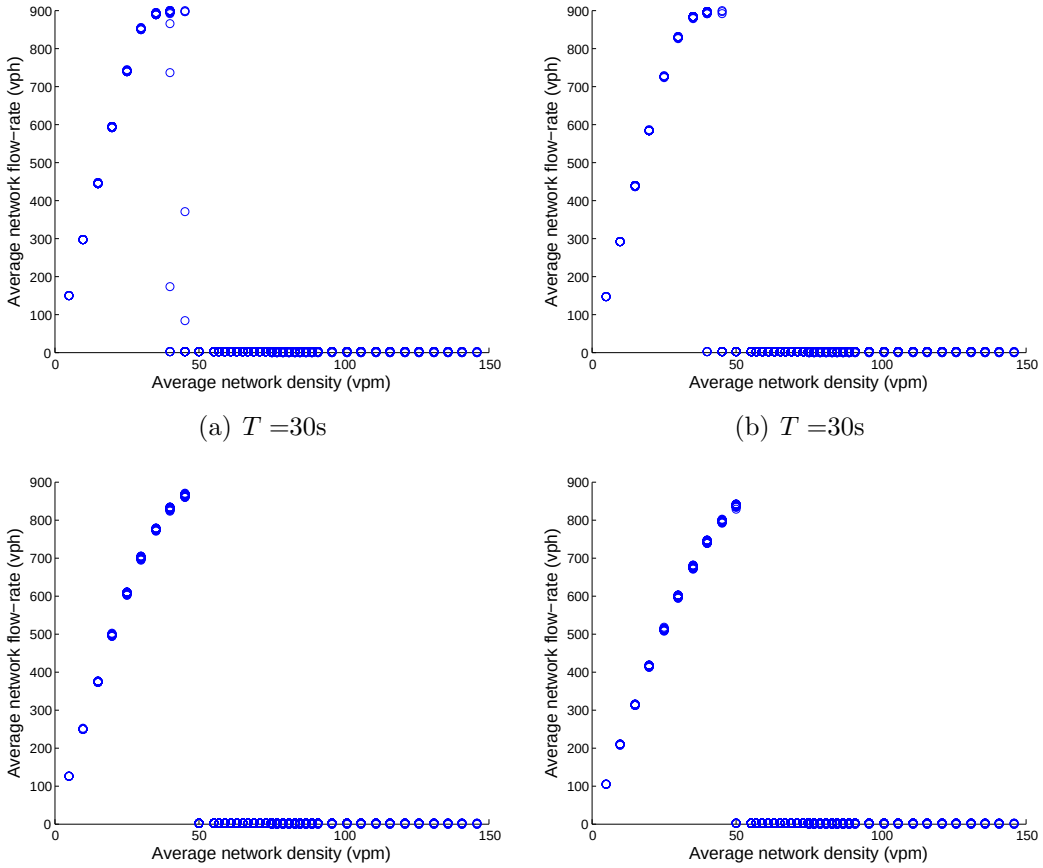

(a) T =30s (b) T =30s

(c) T =120s (d) T =120s

Figure 6.13: Network flow-density relations in the signalized grid network after 10-hour simulations with random retaining ratios $\xi \in$[0.55,0.65] in (a) and (c), and $\xi \in$[0.35,0.45] in (b) and (d).

6.6 Conclusions

In this chapter, traffic dynamics in a signalized grid network were formulated using the link queue model [43]. Under homogeneous settings, such as the same retaining ratios, signal settings, and link lengths, simulation results showed that stationary states with periodic traffic patterns exist in the signalized grid network and are very consistent with those in the signalized double-ring network. Impacts of cycle lengths and retaining ratios on the average network flow-rates were analyzed, and it was found that different cycle lengths and retaining ratios can lead to different average network flow-rates even under the same initial densities. MFDs under different combinations of cycle lengths and retaining ratios were also provided using simulations. It was found that the shapes of the MFDs are similar to those in the signalized double-ring network. In addition, when the retaining ratios are random, it was found that the traffic patterns in the signalized grid network are fundamentally different: the signalized grid network will get gridlocked at lower average network densities regardless of the retaining ratios.

Chapter 7

Conclusions

7.1 Summary

In transportation engineering, effective and efficient control and management strategies are needed to improve the network performance, e.g., to improve the average network flow-rate. However, in this dissertation, we have shown that a fundamental understanding in the static and dynamic properties of urban traffic is necessary since even with the same average network density, different combinations of signal settings, route choice behaviors, and demand patterns can lead to different average network flow-rates.

Instead of tackling large urban networks, we mainly focused on the signalized double-ring network in this dissertation. In Chapter 3, we formulated the traffic dynamics in the signalized double-ring network using a kinematic wave approach [54, 68]. Due to infinitely many state variables on the two links, traffic statics and dynamics are very difficult to solve analytically, and thus, CTM simulations [9, 10] were used. In order to obtain analytical results, in Chapter 4, the link queue model in [43] was used to aggregate the traffic dynamics at the link level. With the triangular traffic flow fundamental diagram [33], the signalized double-

ring network is formulated as a switched affine system. Since periodic density evolution orbits exist in the switched affine system, the Poincaré map approach was used to study the stationary states and their stability properties and relations to cycle lengths, route choice behaviors, and demand patterns.

Due to the existence of periodic signal control at the junction, traffic dynamics in the signalized double-ring network are still very complicated to solve. Therefore, we further extended our studies to derive invariant continuous approximate models at signalized junctions. In Chapter 5, we derived invariant continuous approximate models for a signalized road link by averaging the periodic signal control parameter at the junction over time and solving the Riemann problems in the supply-demand framework [48]. We then analyzed the properties of the derived invariant continuous approximate models under different capacity constraints, traffic conditions, fundamental diagrams, and traffic flow models.

Furthermore, in Chapter 6 we studied the traffic statics and dynamics in a signalized grid network using simulations in the link queue model.

Through this dissertation research, we have the following findings:

(1) Periodic traffic patterns in junction fluxes and density distributions exist in the signalized double-ring network and are defined as stationary states.

(2) There can be a single, multiple, or infinitely many stationary states with the same average network density. Stationary states can be Lyapunov stable, asymptotically stable, or unstable.

(3) Stationary states are closely related to cycle lengths, route choice behaviors, and initial densities. With high retaining ratios, traffic tends to get gridlocked when the network average density is greater than or equal to $k_j/2$. But with low retaining ratios, traffic tends to be more symmetrically distributed over the two rings and won't get gridlocked

unless it initially is.

(4) The average network flow-rate in the macroscopic fundamental diagram can be written as a function of the average network density, the green ratio, and the retaining ratio in the signalized double-ring network. Gridlock times can be analytically calculated when the cycle lengths are small.

(5) Only one of the three derived invariant continuous approximate models can fully capture the capacity constraints at the signalized road link. The other two fail to capture either the upstream or the downstream capacity constraint. Multiple non-invariant continuous approximate models can have the same invariant form.

(6) The invariant continuous approximate model is a good approximation to the discrete signal control at the road link. But cycle lengths can reduce the approximation accuracy.

(7) Non-invariant continuous approximate models can not be used in the link transmission model [78, 47] since there is no solution to the traffic statics problem under certain boundary conditions.

(8) Under homogeneous settings of link lengths, fundamental diagrams, signal settings, and route choice behaviors, traffic statics and dynamics in a signalized grid network are similar to those in the signalized double-ring network.

7.2 Future research directions

In the future, we will continue our work in the following three directions:

(1) Development of effective and efficient signal control and evacuation schemes.

We find that when the retaining ratios at the signalized junction are high, traffic in the

signalized double-ring network will get gridlocked when the average network density is greater than or equal to $k_j/2$. Such a gridlock state is asymptotically stable. However, we also find that for the same average network density, there exists an unstable stationary state with a more symmetric density distribution and a higher average junction flux. To improve the network performance and avoid the occurrence of gridlock, we are interested in developing new signal control strategies that can adaptively change the effective green times and retaining ratios at the signalized junction. In addition, we are also interested in developing new evacuation schemes to regulate traffic movements at the intersections when accidents and disasters happen.

(2) Development of invariant continuous approximate models for more complicated signalized junctions.

Our current study is limited to a signalized road link. But the supply-demand framework [48] can be applied to more complicated signalized junctions, such as the signalized merging and general junctions. However, we also expect the derivation is more complicated since merging and diverging behaviors should be taken into account at these junctions. The combinations of traffic conditions are also more than those in the signalized road link. Fortunately, a complete set of invariant models have been developed for uninterrupted junctions in [48, 41, 46, 42]. Insights from these studies are definitely very helpful in developing invariant continuous approximate models for more general signalized junctions. In addition, for network simulations, different traffic flow models such as CTM [9, 10], LQM [43], and LTM [78, 47] can be used. Therefore, we need to thoroughly analyze the properties of the derived invariant continuous approximate models in these traffic flow models.

(3) Analytical and simulation studies on large-scale urban networks.

In this dissertation, we have studied the static and dynamic properties of traffic flow in the signalized grid network using LQM simulations. In the future, it is possible for us

to study the static and dynamic properties using another link-based mode, the LTM in [78, 47]. It is also possible for us to obtain some analytical results on large-scale urban networks using the link-based traffic flow models and the invariant continuous approximate models developed for the signalized junctions. When the settings in the grid network are not homogeneous, e.g., with random retaining ratios at the signalized junctions, traffic dynamics are fundamentally different from those with homogeneous settings. Therefore, we are also interested in studying the traffic statics and dynamics in the signalized grid network with inhomogeneous settings of link lengths, signal settings, route choice behaviors, and demand patterns.

Bibliography

[1] R. E. Allsop. Delay-minimizing settings for fixed-time traffic signals at a single road junction. *IMA Journal of Applied Mathematics*, 8(2):164–185, 1971.

[2] R. E. Allsop. SIGSET: a computer program for calculating traffic signal settings. *Traffic Engineering & Control*, 1971.

[3] R. E. Allsop. Estimating the traffic capacity of a signalized road junction. *Transportation Research*, 6(3):245–255, 1972.

[4] R. E. Allsop. SIGCAP: A computer program for assessing the traffic capacity of signal-controlled road junctions. *Traffic Engineering & Control*, 17(Analytic), 1976.

[5] M. Bando, K. Hasebe, K. Nakanishi, A. Nakayama, A. Shibata, and Y. Sugiyama. Phenomenological study of dynamical model of traffic flow. *Journal de Physique I*, 5(11):1389–1399, 1995.

[6] C. Buisson and C. Ladier. Exploring the impact of homogeneity of traffic measurements on the existence of macroscopic fundamental diagrams. *Transportation Research Record: Journal of the Transportation Research Board*, 2124:127–136, 2009.

[7] J. D. Castillo and F. Benitez. On the functional form of the speed-density relationship II: empirical investigation. *Transportation Research Part B: Methodological*, 29(5):391–406, 1995.

[8] R. Courant, K. Friedrichs, and H. Lewy. Über die partiellen differenzengleichungen der mathematischen physik. *Mathematische Annalen*, 100(1):32–74, 1928.

[9] C. F. Daganzo. The cell transmission model: A dynamic representation of highway traffic consistent with the hydrodynamic theory. *Transportation Research Part B*, 28(4):269–287, 1994.

[10] C. F. Daganzo. The cell transmission model, part II: network traffic. *Transportation Research Part B*, 29(2):79–93, 1995.

[11] C. F. Daganzo, V. V. Gayah, and E. J. Gonzales. Macroscopic relations of urban traffic variables: Bifurcations, multivaluedness and instability. *Transportation Research Part B*, 45(1):278–288, 2011.

[12] C. F. Daganzo and N. Geroliminis. An analytical approximation for the macroscopic fundamental diagram of urban traffic. *Transportation Research Part B*, 42(9):771–781, 2008.

[13] G. D'ans and D. Gazis. Optimal control of oversaturated store-and-forward transportation networks. *Transportation Science*, 10(1):1–19, 1976.

[14] L. De la Breteque and R. Jezequel. Adaptive control at an isolated intersection-a comparative study of some algorithms. *Traffic Engineering & Control*, 20(7), 1979.

[15] J. Drake, J. Schofer, and A. May. A statistical analysis of speed-density hypotheses. in vehicular traffic science. In *Proceedings of the Third International Symposium on the Theory of Traffic Flow*, 1967.

[16] N. Duncan. A further look at speed/flow/concentration. *Traffic Engineering and Control*, 20(10), 1979.

[17] A. El Aroudi, M. Debbat, and L. Martinez-Salamero. Poincaré maps modeling and local orbital stability analysis of discontinuous piecewise affine periodically driven systems. *Nonlinear dynamics*, 50(3):431–445, 2007.

[18] B. Engquist and S. Osher. One-sided difference schemes and transonic flow. *Proceedings of the National Academy of Sciences*, 77(6):3071–3074, 1980.

[19] J. F. Epperson. *An introduction to numerical methods and analysis*. John Wiley & Sons, 2014.

[20] N. Farhi, M. Goursat, and J. Quadrat. The traffic phases of road networks. *Transportation Research Part C*, 19(1):85–102, 2011.

[21] N. H. Gartner. OPAC: A demand-responsive strategy for traffic signal control. *Transportation Research Record*, (906), 1983.

[22] N. H. Gartner, S. F. Assman, F. Lasaga, and D. L. Hou. A multi-band approach to arterial traffic signal optimization. *Transportation Research Part B*, 25(1):55–74, 1991.

[23] V. Gayah and C. Daganzo. Effects of turning maneuvers and route choice on a simple network. *Transportation Research Record: Journal of the Transportation Research Board*, 2249:15–19, 2011.

[24] V. V. Gayah and C. F. Daganzo. Clockwise hysteresis loops in the macroscopic fundamental diagram: An effect of network instability. *Transportation Research Part B*, 45(4):643–655, 2011.

[25] D. C. Gazis. Optimum control of a system of oversaturated intersections. *Operations Research*, 12(6):815–831, 1964.

[26] D. C. Gazis and R. B. Potts. The oversaturated intersection. Technical report, 1963.

[27] N. Geroliminis and C. F. Daganzo. Existence of urban-scale macroscopic fundamental diagrams: Some experimental findings. *Transportation Research Part B*, 42(9):759–770, 2008.

[28] N. Geroliminis and J. Sun. Properties of a well-defined macroscopic fundamental diagram for urban traffic. *Transportation Research Part B*, 45(3):605–617, 2011.

[29] J. Godfrey. The mechanism of a road network. *Traffic Engineering and Control*, 8(8), 1969.

[30] S. K. Godunov. A difference method for numerical calculation of discontinuous solutions of the equations of hydrodynamics. *Matematicheskii Sbornik*, 89(3):271–306, 1959.

[31] H. Greenberg. An analysis of traffic flow. *Operations research*, 7(1):79–85, 1959.

[32] B. D. Greenshields, J. Bibbins, W. Channing, and H. Miller. A study of traffic capacity. In *Highway research board proceedings*, 1935.

[33] R. Haberman. *Mathematical models*. SIAM, 1977.

[34] K. Han, V. V. Gayah, B. Piccoli, T. L. Friesz, and T. Yao. On the continuum approximation of the on-and-off signal control on dynamic traffic networks. *Transportation Research Part B: Methodological*, 61:73–97, 2014.

[35] D. Helbing. Derivation of a fundamental diagram for urban traffic flow. *The European Physical Journal B*, 70(2):229–241, 2009.

[36] R. Herman and I. Prigogine. A two-fluid approach to town traffic. *Science*, 204:148–151, 1979.

[37] P. Hunt, D. Robertson, R. Bretherton, and M. Royle. The SCOOT on-line traffic signal optimisation technique. *Traffic Engineering & Control*, 23(4), 1982.

[38] P. Hunt, D. Robertson, R. Bretherton, and R. Winton. SCOOT-a traffic responsive method of coordinating signals. Technical report, 1981.

[39] G. Improta and G. Cantarella. Control system design for an individual signalized junction. *Transportation Research Part B*, 18(2):147–167, 1984.

[40] Y. Ji, W. Daamen, S. Hoogendoorn, S. Hoogendoorn-Lanser, and X. Qian. Investigating the shape of the macroscopic fundamental diagram using simulation data. *Transportation Research Record: Journal of the Transportation Research Board*, 2161:40–48, 2010.

[41] W.-L. Jin. Continuous kinematic wave models of merging traffic flow. *Transportation research part B: methodological*, 44(8):1084–1103, 2010.

[42] W.-L. Jin. A kinematic wave theory of multi-commodity network traffic flow. *Transportation Research Part B: Methodological*, 46(8):1000–1022, 2012.

[43] W.-L. Jin. A link queue model of network traffic flow. *arXiv preprint arXiv:1209.2361*, 2012.

[44] W.-L. Jin. The traffic statics problem in a road network. *Transportation Research Part B*, 46(10):1360–1373, 2012.

[45] W.-L. Jin. Stability and bifurcation in network traffic flow: A poincaré map approach. *Transportation Research Part B: Methodological*, 57:191–208, 2013.

[46] W.-L. Jin. Analysis of kinematic waves arising in diverging traffic flow models. *Transportation Science*, 2014.

[47] W.-L. Jin. Continuous formulations and analytical properties of the link transmission model. *arXiv preprint arXiv:1405.7080*, 2014.

[48] W.-L. Jin, L. Chen, and E. G. Puckett. Supply-demand diagrams and a new framework for analyzing the inhomogeneous lighthill-whitham-richards model. In *Transportation and Traffic Theory 2009: Golden Jubilee*, pages 603–635. Springer, 2009.

[49] W.-L. Jin, Q.-J. Gan, and V. V. Gayah. A kinematic wave approach to traffic statics and dynamics in a double-ring network. *Transportation Research Part B: Methodological*, 57:114–131, 2013.

[50] W.-L. Jin and H. M. Zhang. On the distribution schemes for determining flows through a merge. *Transportation Research Part B: Methodological*, 37(6):521–540, 2003.

[51] V. Knoop, S. Hoogendoorn, and J. W. Van Lint. Routing strategies based on macroscopic fundamental diagram. *Transportation Research Record: Journal of the Transportation Research Board*, 2315:1–10, 2012.

[52] J. La Salle. The stability of dynamical systems. 1976.

[53] J. Lebacque. The godunov scheme and what it means for first order traffic flow models. In *Internaional symposium on transportation and traffic theory*, pages 647–677, 1996.

[54] M. Lighthill and G. Whitham. On kinematic waves. II. a theory of traffic flow on long crowded roads. *Proceedings of the Royal Society of London. Series A. Mathematical and Physical Sciences*, 229(1178):317–345, 1955.

[55] J. D. Little. The synchronization of traffic signals by mixed-integer linear programming. *Operations Research*, 14(4):568–594, 1966.

[56] H. K. Lo. A novel traffic signal control formulation. *Transportation Research Part A*, 33(6):433–448, 1999.

[57] H. K. Lo, E. Chang, and Y. C. Chan. Dynamic network traffic control. *Transportation Research Part A*, 35(8):721–744, 2001.

[58] H. Mahmassani, J. Williams, and R. Herman. Investigation of network-level traffic flow relationships: Some simulation results. Technical report, 1984.

[59] A. J. Miller. A computer control system for traffic networks. 1963.

[60] A. J. Miller. Settings for fixed-cycle traffic signals. *Operations Research*, pages 373–386, 1963.

[61] K. Moskowitz. Discussion of freeway level of service as influenced by volume and capacity characteristics by DR Drew and CJ Keese. *Highway Research Record*, 99:43–44, 1965.

[62] G. Newell. A simplified car-following theory: a lower order model. *Transportation Research Part B: Methodological*, 36(3):195–205, 2002.

[63] G. F. Newell. Nonlinear effects in the dynamics of car following. *Operations Research*, 9(2):209–229, 1961.

[64] P. Olszewski, H. Fan, and Y. Tan. Area-wide traffic speed-flow model for the singapore cbd. *Transportation Research Part A*, 29:273–281, 1995.

[65] M. Papageorgiou, C. Diakaki, V. Dinopoulou, A. Kotsialos, and Y. Wang. Review of road traffic control strategies. *Proceedings of the IEEE*, 91(12):2043–2067, 2003.

[66] L. Pipes. An operational analysis of traffic dynamics. *Journal of applied physics*, 24(3):274–281, 1953.

[67] L. Pipes. Car following models and the fundamental diagram of road traffic. *Transportation Research*, 1(1):21–29, 1967.

[68] P. Richards. Shock waves on the highway. *Operations research*, pages 42–51, 1956.

[69] D. I. Robertson. "TRANSYT"method for area traffic control. *Traffic Engineering & Control*, 11(6), 1969.

[70] J. J. A. Sanders, F. Verhulst, and J. A. Murdock. *Averaging methods in nonlinear dynamical systems*, volume 59. Springer, 2007.

[71] D. Schrank, B. Eisele, and T. Lomax. TTI 's 2012 urban mobility report. *Texas A&M Transportation Institute. The Texas A&M University System*, 2012.

[72] P. Sorensen, M. Wachs, E. Y. Min, A. Kofner, and L. Ecola. *Moving Los Angeles: Short-term policy options for improving transportation*. RAND Corporation, 2008.

[73] Z. Sun and S. S. Ge. *Stability theory of switched dynamical systems*. Springer, 2011.

[74] G. Teschl. *Ordinary differential equations and dynamical systems*, volume 140. American Mathematical Soc., 2012.

[75] F. V. Webster. Traffic signal settings. Technical report, 1958.

[76] S. Wiggins, S. Wiggins, and M. Golubitsky. *Introduction to applied nonlinear dynamical systems and chaos*, volume 2. Springer, 1990.

[77] X. Wu, H. X. Liu, and N. Geroliminis. An empirical analysis on the arterial fundamental diagram. *Transportation Research Part B*, 45(1):255–266, 2011.

[78] I. Yperman. The link transmission model for dynamic network loading. *PhD dissertation*, 2007.

Appendices

A Approximation of average network flow-rates

The stationary states are provided in Table 4.3 under different retaining ratios. For $\xi > 0.5$, the possible combinations of regions having stationary states are: $(1,5)$, $(1,7)$, $(2,6)$, $(4,7)$, $(3,5)$, $(3,7)$, and $(3,8)$. For regions $(4,7)$ and $(3,8)$, the stationary states are gridlock states, and therefore, the average network average flow-rates are zero. For the rest of the regions, we can approximate the average network flow-rate using Equation (4.13).

(1) For regions $(1,5)$, the fixed point is $k_1^* = \frac{2k}{1+e^{-\gamma_1 \pi T}}$. Starting with $k_1(nT) = k_1^*$, we can get $k_1(nT + \pi T) = k_1(nT)e^{-\gamma_1 \pi T}$. Since ring 1 is uncongested, $g_1(k_1) = v_f k_1$. Therefore, the average network flow-rate is

$$q(k) \approx \pi \frac{g_1(k_1^*) + g_1(k_1(nT + \pi T))}{2} = \frac{1}{2}\pi v_f (k_1^* + k_1(nT + \pi T)) = \frac{1}{2}\pi v_f 2k \frac{1+e^{-\gamma_1 \pi T}}{1+e^{-\gamma_1 \pi T}} = \pi v_f k. \tag{A.1}$$

(2) For regions $(1,7)$, the fixed point is $k_1^* = \frac{(k_j - 2k)(e^{\gamma_5 \pi T} - 1)}{1 - e^{(\gamma_5 - \gamma_1)\pi T}}$. Starting with $k_1(nT) = k_1^*$, we can get $k_1(nT + \pi T) = k_1(nT)e^{-\gamma_1 \pi T}$. Since ring 1 is uncongested, $g_1(k_1) = v_f k_1$. In addition, since T is small, $-\gamma_1 \pi T$, $\gamma_5 \pi T$, and $(\gamma_5 - \gamma_1)\pi T$ are also small. Therefore,

the average network flow-rate is

$$\begin{aligned} q(k) &\approx \tfrac{1}{2}\pi v_f(k_1^* + k_1(nT+\pi T)) = \tfrac{1}{2}\pi v_f(k_j - 2k)\tfrac{(e^{\gamma_5\pi T}-1)(1+e^{-\gamma_1\pi T})}{1-e^{(\gamma_5-\gamma_1)\pi T}} \\ &\approx \tfrac{1}{2}\pi v_f(k_j-2k)\tfrac{\gamma_5\pi T(2-\gamma_1\pi T)}{(\gamma_1-\gamma_5)\pi T} \approx \pi C\tfrac{(k_j-2k)}{\xi(k_j-k_c)-k_c}. \end{aligned} \tag{A.2}$$

(3) For regions $(2,6)$, the fixed point is $k_1^* = k_1(t)$. In this combination of regions, the out-fluxes are restricted by the capacity. Therefore, the average network flow-rate is

$$q(k) \approx \pi\frac{g_1(k_1^*) + g_1(k_1(nT+\pi T))}{2} = \pi C. \tag{A.3}$$

(4) For regions $(3,5)$, the fixed point is $k_1^* = \frac{2k(1-e^{-\gamma_4\pi T})-k_j(e^{\gamma_2\pi T}-1)e^{-\gamma_4\pi T}}{1-e^{(\gamma_2-\gamma_4)\pi T}}$. Starting with $k_1(nT) = k_1^*$, we can get $k_1(nT+\pi T) = k_j(1-e^{\gamma_2\pi T})+k_1(nT)e^{\gamma_2\pi T}$. In this combination of regions, the out-flux is governed by the supply in link 1, i.e., $g_1(k_1) = \frac{S_1(k_1)}{\xi} = \frac{C(k_j-k_1)}{\xi(k_j-k_c)}$. Therefore, the average network flow-rate is

$$\begin{aligned} q(k) &\approx \pi C\tfrac{2k_j-(k_j(1-e^{\gamma_2\pi T})+k_1^*(1+e^{\gamma_2\pi T}))}{2\xi(k_j-k_c)} \approx \pi C\tfrac{2k_j-2\frac{2k*\gamma_4-k_j*\gamma_2}{\gamma_4-\gamma_2}}{2\xi(k_j-k_c)} \\ &= \pi C\tfrac{(k_j-2k)\frac{\gamma_4}{\gamma_4-\gamma_2}}{\xi(k_j-k_c)} = \pi C\tfrac{(k_j-2k)}{\xi(k_j-k_c)-k_c}. \end{aligned} \tag{A.4}$$

(5) For regions $(3,7)$, the fixed point is $k_1^* = \frac{2k+k_j(e^{\gamma_2\pi T}-1)}{e^{\gamma_2\pi T}+1}$. Starting with $k_1(nT) = k_1^*$, we can get $k_1(nT+\pi T) = k_j(1-e^{\gamma_2\pi T})+k_1(nT)e^{\gamma_2\pi T}$. In this combination of regions, the out-flux is governed by the supply in link 1, i.e., $g_1(k_1) = \frac{S_1(k_1)}{\xi} = \frac{C(k_j-k_1)}{\xi(k_j-k_c)}$. Therefore, the average network flow-rate is

$$\begin{aligned} q(k) &\approx \pi C\tfrac{2k_j-(k_j(1-e^{\gamma_2\pi T})+k_1^*(1+e^{\gamma_2\pi T}))}{2\xi(k_j-k_c)} = \pi C\tfrac{2k_j-(k_j(1-e^{\gamma_2\pi T})+2k+k_j(e^{\gamma_2\pi T}-1))}{2\xi(k_j-k_c)} \\ &= \pi C\tfrac{k_j-k}{\xi(k_j-k_c)}. \end{aligned} \tag{A.5}$$

Based on the average network flow-rates calculated above, the macroscopic fundamental diagram for the signalized double-ring network with $0.5 < \xi < 1$ can be easily derived and thus omitted here. ■

B Algorithm of finding stationary states

Inputs: k, T, Δ, ξ, and $\Phi(k_1)$

Initialization: vector of stationary states, i.e., SS=[]; minimum value of k_1, i.e., $k_{1,min} = \max\{2k - k_j, 0\}$; maximum value of k_1, i.e., $k_{1,max} = \min\{2k, k_j\}$; the threshold of k_1, i.e., e_k; searching step, i,e., Δk; maximum number of iterations, i.e., n_{max}

For $k_1 = k_{1,min} : \Delta k : k_{1,max}$

Set $k_1^0 = k_1$ and calculate $\Phi(k_1^0)$

If $\Phi(k_1^0) == 0$

k_1^0 is a root, and add it to SS

Else

Set $k_1^1 = Pk_1^0$ and calculate $\Phi(k_1^1)$

For n=1 : n_{max}

If $|k_1^1 - k_1^0| < e_k$ **or** $\Phi(k_1^1) == 0$, add k_1^1 to SS and break

$k_1^{tmp} = k_1^1 - \Phi(k_1^1)[\frac{k_1^1 - k_1^0}{\Phi(k_1^1) - \Phi(k_1^0)}]$, and calculate $\Phi(k_1^{tmp})$

$k_1^0 = k_1^1$ and $\Phi(k_1^0) = \Phi(k_1^1)$

$k_1^1 = k_1^{tmp}$ and $\Phi(k_1^1) = \Phi(k_1^{tmp})$

End for

End if

End for

C Proof of Lemma 5.1

We denote $q(U_1^-)$ and $q(U_2^+)$ as the fluxes for the Riemann problems of Type I, $q_1(0^-,t)$ and $q_2(0^+,t)$ as the fluxes for the Riemann problems of Type II, and q as the flux for the Riemann problem of Type III. According to the traffic conservation, we have the following equation

$$q = q_1(0^-,t) = q_2(0^+,t) = q(U_1^-) = q(U_2^+) \tag{C.6}$$

To determine the stationary and interior states arising at the signalized road link, we use the admissible conditions in Section 4 in [48]. After solving the Riemann problems with the entropy condition $q = \eta \min\{D_1(0^-,t), S_2(0^+,t)\}$ applied at the signalized junction, we can have the following combinations of stationary and interior states:

(1) When $D_1 < S_2 \le C_2$, we have $U_2^+ = U_2(0^+,t) = (D_2^+, C_2)$ since the downstream link is SUC, which leads to $q = \eta \min\{D_1(0^-,t), C_2\}$.

   (a) If the upstream link is SOC, i.e., $U_1^- = U_1(0^-,t) = (C_1, S_1^-)$, we can have $q = S_1^- = D_2^+ = \eta \min\{C_1, C_2\}$, and $D_1 > \eta \min\{C_1, C_2\}$.

   (b) If the upstream link is UC, i.e., $D_1 \le S_1^- = C_1$, we have $U_1^- = (D_1, C_1)$ and $U_1(0^-,t) = (D_1(0^-,t), S_1(0^-,t))$ with $S_1(0^-,t) \ge D_1^- = D_1$. Therefore, we have $q = D_2^+ = D_1 = \eta \min\{D_1(0^-,t), C_2\}$, which leads to $D_1(0^-,t) = D_1/\eta$ and $S_1(0^-,t) = C_1$. Since $D_1(0^-,t) \le C_1$, we have $D_1 \le \eta \min\{C_1, C_2\}$.

(2) When $S_2 < D_1 \le C_1$, the upstream link is SOC. Thus we have $U_1^- = U_1(0^-,t) = (C_1, S_1^-)$, which leads to $q = \eta \min\{C_1, S_2(0^+,t)\}$.

   (a) If the downstream link is SUC, i.e., $U_2^+ = U_2(0^+,t) = (D_2^+, C_2)$, we have $q = D_2^+ = S_1^- = \eta \min\{C_1, C_2\}$. In this case, $S_2 > \eta \min\{C_1, C_2\}$.

(b) If the downstream link is OC, $U_2^+ = (C_2, S_2)$ and $U_2(0^+, t) = (D_2(0^+, t), S_2(0^+, t))$ with $D_2(0^+, t) \geq S_2$. Thus we have $q = S_2 = S_1^- = \eta \min\{C_1, S_2(0^+, t)\}$, which leads to $S_2(0^+, t) = S_2/\eta$ and $D_2(0^+, t) = C_2$. Since $S_2(0^+, t) \leq C_2$, we can have $S_2 \leq \eta \min\{C_1, C_2\}$.

(3) When $D_1 = S_2$, we have $U_2^+ = U_2(0^+, t) = (D_2^+, C_2)$ if the downstream link is SUC, which leads to $q = \eta \min\{D_1(0^-, t), C_2\}$ and $S_2 > D_2^+$.

(a) If the upstream link is SOC, i.e., $U_1^- = U_1(0^-, t) = (C_1, S_1^-)$, then $q = S_1^- = D_2^+ = \eta \min\{C_1, C_2\}$. In this case, we have $D_1 = S_2 > \eta \min\{C_1, C_2\}$.

(b) If the upstream link is UC, i.e., $D_1 \leq S_1^-$, we have $U_1^- = (D_1, C_1)$, which leads to $U_1(0^-, t) = (D_1(0^-, t), S_1(0^-, t))$ with $S_1(0^-, t) \geq D_1^-$. Since $q(U_1^-) = D_1$, we have $q = q(U_1^-) = D_1$, which leads to $D_2^+ = D_1$. But it is impossible since $S_2 > D_2^+ = D_1$, which contradicts $D_1 = S_2$.

If the downstream link is OC, $U_2^+ = (C_2, S_2)$, and $U_2(0^+, t) = (D_2(0^+, t), S_2(0^+, t))$ with $D_2(0^+, t) \geq S_2$. Then we have $q = \eta \min\{D_1(0^-, t), S_2(0^+, t)\}$.

(c) If the upstream link is SOC, i.e., $U_1^- = U_1(0^-, t) = (C_1, S_1^-)$, then $q = S_1^- = S_2$, and $D_1 > S_1^-$. But it is impossible since we have $D_1 > S_2$, which contradicts $D_1 = S_2$.

(d) If the upstream link is UC, i.e., $D_1 \leq S_1^-$, we have $U_1^- = (D_1, C_1)$, which leads to $U_1(0^-, t) = (D_1(0^-, t), S_1(0^-, t))$ with $S_1(0^-, t) \geq D_1^-$. Because $q(U_1^-) = D_1$ and $q(U_2^+) = S_2$, we have $q = D_1 = S_2$. If $q = \eta D_1(0^-, t)$, we have $S_1(0^-, t) = C_1$ and $\eta S_2(0^+, t) \geq S_2$. If $q = \eta S_2(0^+, t)$, we have $D_2(0^+, t) = C_2$ and $\eta D_1(0^-, t) \geq D_1$. Since $D_1(0^-, t) \leq C_1$ and $S_2(0^+, t) \leq C_2$, we have $D_1 = S_2 \leq \eta \min\{C_1, C_2\}$.

■